New capabilities of the Notch signaling pathway

Thesis by

Nagarajan Nandagopal

In Partial Fulfillment of the Requirements for the degree of

Doctor of Philosophy

CALIFORNIA INSTITUTE OF TECHNOLOGY

Pasadena, California

2018

(Defended 2 Oct 2017)

Nagarajan Nandagopal
ORCID: 0000-0002-0469-6549

Dedicated to my grandfather, my namesake

Acknowledgements

This thesis is essentially an abbreviated and stoically-presented account of my wonderful scientific journey over the past seven years. The journey has been full of joys and disappointments, frustrations (often followed by fulminations), delights, and detours. And many many lattés. This travelogue would be incomplete without mention of the many people who have made the journey special, who have been responsible for the happy moments, and helped me get through the sad ones. One could not have asked for a wiser, nicer, more supportive or visionary guide on this journey of discovery than Michael Elowitz. I have learned much these past years, and much of it I have learned from him. Leah Santat has been a pillar of support, both technical and moral, a bundle of cheerful determination, and a dear friend. The work presented here is built on the shoulders of the Delta force: David Sprinzak, Lauren LeBon, and Amit Lakhanpal. Members of my thesis committee, Rob Phillips, Lea Goentoro, and Marianne Bronner, have been there when I have needed them the most, providing invaluable advice and guidance, without ever getting in the way. Joe Levine, Adam Shai, Naeem Husain, John Yong, and Fred Tan have all been fellow travelers at various points on this journey, and their companionship has magnified the best parts of the journey and diminished the worst. In addition to providing a much needed outlet for shooting the s-, the Sons of S (Joe L, Jon Young, Fred T) supplied endless needlessly intense shenanigans and the Crossfit Crew (Joe L, John Yong, Joe Markson, Kirsten Frieda) supplied much not-so-silent judgment, for which I think I am grateful. Labowitz has been the best ship to take this journey on, and I have delighted in the company and thrived on the support of its members through the years. And finally, this trip (as in, ‘so trippy!’, or ‘he’s trippin’) would have been altogether something else without my dear Elizabeth Jensen, and would not have been possible at all but for my brother Anand, and my parents Ganesa Nandagopal and Vijaya Sarada. For that, and for more than can be put into words, thank you.

Abstract

Animal cells use a conserved repertoire of signaling pathways to exchange information during and after development. The constituent molecules of these pathways and their individual interactions are now well-characterized. However, it is becoming clear that pathways often possess unexpected signal-processing capabilities, which are typically collective, systems-level, features. Recent work shows that these capabilities are best investigated using quantitative, single-cell, dynamic analyses of pathway behavior. Here, we used this approach to study Notch signaling pathway, which is widely utilized for juxtacrine signaling during the development and maintenance of most tissues. Our work reveals two new capabilities of this pathway. First, the receptor Notch1 is capable of discriminating between two similar ligands, Dll1 and Dll4, and can use this ability to enact ligand-specific developmental programs. To enable this, the pathway encodes ligand identity in the dynamics of Notch1 signaling, and later decodes it for controlling gene expression. We show that dynamic encoding by Dll1 and Dll4 results from different requirements for ligand-receptor clustering during activation. Second, the pathway is capable of cell-autonomous signaling (*cis*-activation). This mode of signaling is general to multiple ligand-receptor combinations, and possesses many attributes of intercellular signaling. We show that *cis*-activation occurs in natural stem-cell contexts, where it could be important for self-renewal and prevents premature differentiation. These new capabilities of this central signaling pathway have implications for understanding the role of Notch in development and homeostasis, diagnosing and treating its misregulation in disease, and controlling it for tissue engineering and regeneration.

Published Content and Contributions

Antebi, Y.E., Nandagopal, N., and Elowitz, M.B. (2017). An operational view of intercellular signaling pathways. Current Opinion in Systems Biology *1*, 16–24. doi: 10.1016/j.coisb.2016.12.003

Nandagopal N. participated in the conceptualization and writing of the manuscript.

Table of Contents

List of Figures

Chapter 1. Introduction

1.1 Deciphering the genetic plan: from molecules to systems

We are essentially physical manifestations of the information contained in our DNA. The genome is often described as a blueprint for constructing each multicellular organism during development, regulating its growth, and controlling its behavior. The 'coiled spring' (Bier) is a useful metaphor for describing the developmental process; in this view, the information packed into genetic material is equivalent to the potential of a coiled spring, and the developmental processes beginning at fertilization are equivalent to the controlled uncoiling of this spring, the regulated unleashing of genetic (and epigenetic) information. A fundamental goal of biology is to understand how this information is encoded in DNA, how it is decoded and executed in a controlled manner during and after development, and how it is altered by evolution.

As a blueprint, however, the genome is unlike any other. It provides not only instructions for carrying out the various processes involved in development and growth, but also directly templates the machinery - molecules such as proteins and RNA - that implement these instructions. An important insight of the molecular biology era was the realization that these two aspects are linked; proteins and RNA templated by DNA embody genetic information, because their sequences, and thus structures, control their functions. Ideas such as the 'one gene-one enzyme' hypothesis (Beadle and Tatum, 1941), which suggested that each protein controls one step in a series of reactions that results in a given trait, laid the foundations for the reductionist viewpoint of molecular biology, which posited that once we understood the structure of each protein and its specific function, we would

essentially be able to piece together organismal development and physiology, like assembling a jigsaw puzzle.

Consequently, a large part of the biological effort over the past decades has been devoted to dissecting "molecular anatomy" (Jacob, 1994) - characterizing the sequences of molecules, their structures, their modifications and their interactions. As a result of this endeavor, we now possess a detailed picture of hundreds of genes and their immediate functions - what they bind to, what they catalyze, what they cleave, etc. A sophisticated program of genetics, especially developmental genetics, has progressed in parallel, assigning developmental or physiological roles to genes by observing the phenotypic effects of mutating them.

What has become clear through this enormous - and essential - effort of cataloging and characterizing individual genes is that only rarely can a discrete biological function, such as the cell cycle or tissue patterning, be attributed to any one molecule (Alon, 2003; Hartwell et al., 1999). It is more often the case that functions arise from *interactions* among multiple molecules, which form networks that implement the dictates of the genome. That is, much of the information content of DNA is realized through such biological 'systems' of many interacting molecular components. It is therefore essential to study this layer of biological organization as it is the bridge between the individual gene and the cellular and tissue-level processes that it participates in.

Through the analysis of several biological systems, it has become clear that they can possess features or capabilities beyond those of the constituent components. Such capabilities are often abstract - amplification, error-minimization, robustness, multiplexing, etc. - and are a combined result of the properties of the molecular components and the way they are connected to each other, i.e. the wiring diagram of the system (Hartwell et al., 1999). In general, therefore, there are two questions one can ask about any biological system: first, what are capabilities of the system? For example, what does it use as input, and how is this input processed to produce the output? Second, given a set of processing abilities, how do the components and the set of interactions among them together confer these capabilities? Research focused on answering these questions in the context of various systems, such as gene regulatory networks, protein networks and, more recently, signal transduction networks, have yielded important insights into a diverse set of biological processes.

1.2 Intercellular signaling systems and their capabilities

Intercellular signaling pathways, which enable cell-cell communication in multicellular organisms, are examples of biological systems. Such pathways are typically composed of signaling ligands that engage receptors to control gene expression by regulating the levels or activity of transcription factors. Pathways also include a slew of regulatory proteins that are necessary for normal functioning.

There is a growing appreciation that such signaling pathways go beyond serving as simple relays that transmit the levels of extracellular stimuli into levels of intracellular component

activities (Antebi et al., 2017a). There are now several examples of signal processing and computation that these pathways are capable of, including 1. extracting specific features of the input like the rate of change of extracellular ligand (TGFβ, (Sorre et al., 2014)) or relative levels of multiple ligands (BMP (Antebi et al., 2017b)), 2. encoding ligand levels in dynamics (EGF (Albeck et al., 2013)) or fold-changes (Wnt (Goentoro and Kirschner, 2009; Goentoro et al., 2009)) of key intracellular components, and 3. amplifying signal in a tunable manner (MAPK pathways (O'Shaughnessy et al., 2011)). This type of understanding of pathway function typically has required quantitative and dynamic measurements of signaling at the single-cell level, coupled with mathematical modeling.

These discoveries have provided an *operational* understanding of these pathways, critical for understanding how and why particular pathways are used in specific contexts, for more precisely diagnosing problems with signaling behavior in diseases, and for manipulating these pathways for desired outcomes during tissue engineering or stem cell reprogramming (Antebi et al., 2017a). While significant progress has been made in recent years towards developing better systems-level understanding of signaling pathways, we have only scratched the surface in terms of characterizing the full repertoire of capabilities for the many signaling pathways used in organisms. One such pathway that remains poorly understood from a system-level perspective is the Notch pathway, which is central to many processes during development and homeostasis.

1.3 Brief history and overview of the Notch pathway

The Notch signaling pathway is one of the core signaling pathways in metazoans (Barolo and Posakony, 2002; Bray, 2016; Housden and Perrimon, 2014). It enables signaling between cells that are in direct contact with each other (juxtacrine signaling). It is used during the development and maintenance of nearly every tissue in the organism, including neural tissues such as the brain and spinal cord, blood, skin, heart, muscle, and intestines. Commensurate with its ubiquitous and central role in multiple contexts, its misregulation leads to a range of pathologies, including several cancers (Andersson and Lendahl, 2014).

The Notch gene locus was one of the first associated with a clear developmental phenotype in the mutational studies of T.H.Morgan and coworkers in *Drosophila melanogaster (Dexter, 1914)*, resulting in characteristic phenotypes such as notched wings and excessive neurogenesis. In fact, this discovery lent credence to the seminal idea that embryonic development was regulated by genes. Later, in the 1980s, this gene was cloned and sequenced (Artavanis-Tsakonas et al., 1983; Louvi and Artavanis-Tsakonas, 2006). This revealed that the protein product of this gene is a protein that contained a transmembrane domain and a large extracellular domain. Based on this finding it was hypothesized, with remarkable intuition, that the protein represented a key component of a cell-cell interaction machinery used during cell-fate specification (Wharton et al., 1985).

Indeed, since then it has become clear that the Notch gene encodes a transmembrane receptor that can be activated by a transmembrane ligand (Delta or Serrate in *Drosophila*) expressed on the surface of a neighboring cell. Ligand binding and consequent activation

of the receptor leads to release of the Notch intracellular domain (NICD), which translocates to the nucleus and binds to the CSL (CBF-1/Su(H)/Lag-1) complex to regulate gene expression in the signal-receiving cell. Activation of the receptor is preceded by the endocytosis of the ligand into the signal-sending cell (Bray, 2016; Weinmaster and Fischer, 2011). The extracellular domain of the receptor, which remains bound to the ligand, is *trans*-endocytosed into the sending cell during this process, a necessary prelude to the cleavage and release of the NICD. Besides the receptor and ligand, the pathway includes other proteins that are essential to the proper functioning of the pathway, such as glycosyltransferases that modify ligand-receptor interactions, ubiquitin ligases that regulate endocytosis and stability, proteases that control activity, and other proteins responsible for the complex regulation and trafficking of receptors and ligands.

1.4. Towards understanding the capabilities of the Notch pathway

Due to its overtly linear topology (ligand -> receptor -> NICD), presumed one-to-one interaction between ligands and receptors, and the lack of enzymatic steps or post-translational regulation (such as phosphorylation) during the signal relay from membrane to nucleus, there is a pervasive sense that signal transduction in the Notch pathway is 'simple' (Andersson et al., 2011; Bray, 2006; Louvi and Artavanis-Tsakonas, 2006). As a consequence, there has been little effort to look for processing behavior in the pathway using the quantitative, dynamic, single-cell approaches that have provided new insights regarding other pathways such as growth factor signaling, BMP, Wnt, and TGFβ (see above).

There are also some additional challenges to applying such approaches to the Notch pathway. In most of the other 'core' pathways, ligands are not cell-bound, and thus signaling in receiving cells can be activated and modulated using recombinant ligand molecules. On the other hand, a proper analysis of Notch signaling requires manipulation of both ligand-expressing sender cells and receiver cells, and the contacts between them. A second issue with measuring Notch signaling levels and dynamics is the instability of the Notch intracellular domain (NICD), the carrier of signaling information within the receiver cell (Housden et al., 2013; Ilagan et al., 2011). This makes it difficult to directly measure NICD at the single-cell level (for example, by fusing it to a fluorescent protein). Moreover, a lack of reporters that provide *bona fide*, high sensitivity readouts of NICD levels prevent measurement of its transcriptional activity, which can often serve as a proxy for signaling activity (Antebi et al., 2017b). Finally, a general problem with measuring input-output behavior of all pathways is the difficulty of maintaining the system at a 'steady-state'. The cellular milieu changes when pathways are activated, and many pathway components are under feedback control; since these factors influence the behavior of the pathway, the measured signal processing behavior of a pathway might change over time, because of the very attempt to measure it.

Our lab has previously developed a novel approach to study Notch signaling quantitatively in single cells. This approach tackles the issues mentioned above in two ways. First, Notch receptors and ligands are expressed in a cell-culture system to generate dedicated receiver and sender cell lines, respectively. Since these cells are more easily manipulated,

engineered, arranged, and imaged than *in vivo* tissue, this system offers significantly more control over pathway components and interactions than was previously possible. Second, pathway activity is measured using a chimeric Notch receptor that releases a long-lived transcription factor (Gal4) when activated. This provides the benefit of signal amplification - useful for measurements - while preserving the activation dynamics of the natural system. Previous work using this system have been successful, revealing new properties of the pathway, such as the ability to control signal direction (sending vs. receiving) by tuning the relative levels of ligands and receptors and, more generally, the 'signaling state' of the cell by controlling the identity of ligands and Fringe proteins co-expressed with the receptor (LeBon et al., 2014; Sprinzak et al., 2010).

As described in this thesis, this experimental platform, along with the general aspirational goal of understanding systems-level properties of the Notch signaling pathway through quantitative, single-cell analyses, has revealed two novel capabilities of this important pathway. The first, detailed in Chapter 2, is the ability of the pathway to encode ligand identity in dynamics of signaling, and to subsequently decode these dynamics to enact specific transcriptional and developmental programs. The second, described in Chapter 3, is prevalent and functional cell-autonomous (*cis*-) activation in cells co-expressing ligand and receptor, which could enable negative feedback and symmetry-breaking in several developmental contexts.

1.5. References

Albeck, J.G., Mills, G.B., and Brugge, J.S. (2013). Frequency-modulated pulses of ERK activity transmit quantitative proliferation signals. Mol. Cell *49*, 249–261.

Alon, U. (2003). Biological networks: the tinkerer as an engineer. Science *301*, 1866–1867.

Andersson, E.R., and Lendahl, U. (2014). Therapeutic modulation of Notch signalling [mdash] are we there yet? Nat. Rev. Drug Discov. *13*, 357–378.

Andersson, E.R., Sandberg, R., and Lendahl, U. (2011). Notch signaling: simplicity in design, versatility in function. Development *138*, 3593–3612.

Antebi, Y.E., Nandagopal, N., and Elowitz, M.B. (2017a). An operational view of intercellular signaling pathways. Current Opinion in Systems Biology *1*, 16–24.

Antebi, Y.E., Linton, J.M., Klumpe, H., Bintu, B., Gong, M., Su, C., McCardell, R., and Elowitz, M.B. (2017b). Combinatorial Signal Perception in the BMP Pathway. Cell *170*, 1184–1196.e24.

Artavanis-Tsakonas, S., Muskavitch, M.A., and Yedvobnick, B. (1983). Molecular cloning of Notch, a locus affecting neurogenesis in Drosophila melanogaster. Proc. Natl. Acad. Sci. U. S. A. *80*, 1977–1981.

Barolo, S., and Posakony, J.W. (2002). Three habits of highly effective signaling pathways: principles of transcriptional control by developmental cell signaling. Genes Dev. *16*, 1167–1181.

Beadle, G.W., and Tatum, E.L. (1941). Genetic Control of Biochemical Reactions in Neurospora. Proc. Natl. Acad. Sci. U. S. A. *27*, 499–506.

Bier, E. The coiled spring: How life begins. 2000. New York: Cold Spring Harbor *252*.

Bray, S.J. (2006). Notch signalling: a simple pathway becomes complex. Nat. Rev. Mol. Cell Biol. *7*, 678–689.

Bray, S.J. (2016). Notch signalling in context. Nat. Rev. Mol. Cell Biol. *17*, 722–735.

Dexter, J.S. (1914). The Analysis of a Case of Continuous Variation in Drosophila by a Study of Its Linkage Relations. Am. Nat. *48*, 712–758.

Goentoro, L., and Kirschner, M.W. (2009). Evidence that fold-change, and not absolute level, of beta-catenin dictates Wnt signaling. Mol. Cell *36*, 872–884.

Goentoro, L., Shoval, O., Kirschner, M.W., and Alon, U. (2009). The incoherent feedforward loop can provide fold-change detection in gene regulation. Mol. Cell *36*, 894–899.

Hartwell, L.H., Hopfield, J.J., Leibler, S., and Murray, A.W. (1999). From molecular to modular cell biology. Nature *402*, C47–C52.

Housden, B.E., and Perrimon, N. (2014). Spatial and temporal organization of signaling pathways. Trends Biochem. Sci. *39*, 457–464.

Housden, B.E., Fu, A.Q., Krejci, A., Bernard, F., Fischer, B., Tavaré, S., Russell, S., and Bray, S.J. (2013). Transcriptional dynamics elicited by a short pulse of notch activation involves feed-forward regulation by E(spl)/Hes genes. PLoS Genet. *9*, e1003162.

Ilagan, M.X.G., Lim, S., Fulbright, M., Piwnica-Worms, D., and Kopan, R. (2011). Real-time imaging of notch activation with a luciferase complementation-based reporter. Sci. Signal. *4*, rs7.

Jacob, F. (1994). The Possible and the Actual (Jessie and John Danz Lectures).

LeBon, L., Lee, T.V., Sprinzak, D., Jafar-Nejad, H., and Elowitz, M.B. (2014). Fringe proteins modulate Notch-ligand cis and trans interactions to specify signaling states. Elife *3*, e02950.

Louvi, A., and Artavanis-Tsakonas, S. (2006). Notch signalling in vertebrate neural development. Nat. Rev. Neurosci. *7*, 93–102.

O'Shaughnessy, E.C., Palani, S., Collins, J.J., and Sarkar, C.A. (2011). Tunable signal processing in synthetic MAP kinase cascades. Cell *144*, 119–131.

Sorre, B., Warmflash, A., Brivanlou, A.H., and Siggia, E.D. (2014). Encoding of temporal signals by the TGF-β pathway and implications for embryonic patterning. Dev. Cell *30*, 334–342.

Sprinzak, D., Lakhanpal, A., Lebon, L., Santat, L.A., Fontes, M.E., Anderson, G.A., Garcia-Ojalvo, J., and Elowitz, M.B. (2010). Cis-interactions between Notch and Delta generate mutually exclusive signalling states. Nature *465*, 86–90.

Weinmaster, G., and Fischer, J.A. (2011). Notch ligand ubiquitylation: what is it good for? Dev. Cell *21*, 134–144.

Wharton, K.A., Johansen, K.M., Xu, T., and Artavanis-Tsakonas, S. (1985). Nucleotide sequence from the neurogenic locus notch implies a gene product that shares homology with proteins containing EGF-like repeats. Cell *43*, 567–581.

Chapter 2. Dynamic encoding of ligand identity in the Notch pathway

Abstract

The Notch signaling pathway utilizes multiple ligands that interact promiscuously with Notch receptors, yet are deployed in distinct developmental and physiological contexts. Because the pathway provides no known mechanism by which signal-receiving cells might discern the identity of an activating ligand, it has remained unclear whether, and how, cells could adopt distinct gene expression programs or cell fates in response to signaling by different ligands. Here, we show that the Notch pathway uses dynamics to discriminate signaling by the closely related ligands Dll1 and Dll4 through a single receptor, Notch1. Using quantitative single-cell imaging in cell-culture, we find that Dll1 activates Notch1 in discrete, frequency-modulated pulses that preferentially regulate the Notch target gene Hes1. By contrast, Dll4 activates Notch1 in a sustained, amplitude-modulated manner that preferentially up-regulates the targets Hey1 and HeyL. Moreover, ligand discrimination affects fate determination *in vivo*. Ectopic expression of Dll1 in chick neural crest cells enhances myogenic differentiation in somites, while expression of Dll4 produces the opposite effect. Finally, using chimeric Dll ligands, we show that the dynamics of signaling are controlled by the ligand intracellular domains, which also influence patterns of receptor transendocytosis, suggesting a clustering-based model for dynamic signal encoding. Taken together, these data show that the Notch pathway uses dynamics to discriminate between different activating ligands, effectively establishing multiple channels of communication

through a single receptor. These results reveal unexpected capabilities of the Notch signaling pathway, with implications for diverse physiological, developmental, and disease processes.

2.1 Introduction

In metazoans, the Notch signaling pathway enables direct communication between neighboring cells. It plays critical roles in the development and maintenance of most tissues (Bray, 2016; Guruharsha et al., 2012), and its dysregulation has been implicated in a variety of diseases, making it an important therapeutic target (Andersson and Lendahl, 2014). In mammals, Notch signaling can be activated by four different transmembrane ligands: Dll1, Dll4, Jag1, and Jag2. When any of these ligands interact with Notch receptors expressed on the surface of neighboring receiver cells, they induce cleavage of the receptor. This releases the Notch intracellular domain (NICD), which translocates to the nucleus and, in complex with CSL/RBPjκ, activates Notch target genes (Figure 1A). In principle, different ligands could be used to activate distinct target programs, and thus constitute distinct "communication channels."

Figure 1.1

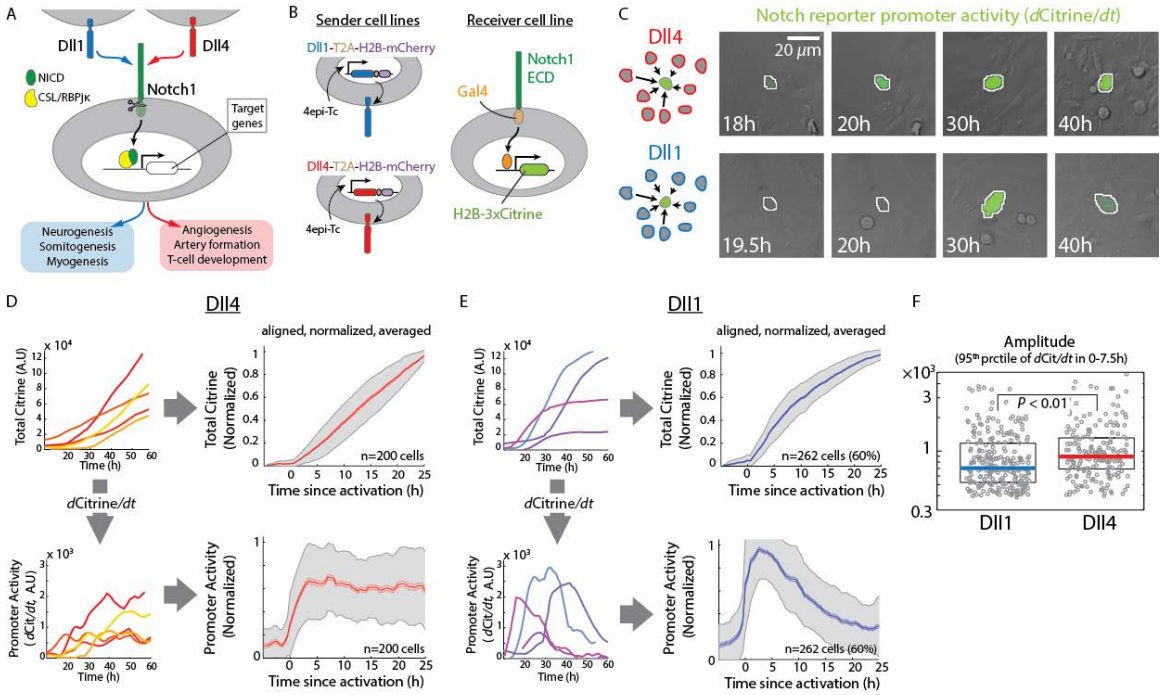

Dll1 and Dll4 activate Notch1 with pulsatile and sustained dynamics, respectively. A, Both Dll1 (blue) and Dll4 (red) activate the Notch1 receptor (green) to induce proteolytic release of the Notch intracellular domain (NICD), but are used in different biological contexts (blue and red boxes, *bottom*). The released NICD translocates to the nucleus and, in complex with CSL/RBPjκ (yellow), activates Notch target genes (white). **B**, *(Left)* Engineered CHO-K1 'sender' cell lines contain stably integrated constructs expressing Dll1 (blue) or Dll4 (red), each with a co-translational (T2A, brown) H2B-mCh readout (purple), from a 4epi-Tetracycline ('4epi-Tc') inducible promoter. *(Right)* 'Receiver' cells stably express a chimeric receptor combining the Notch1 extracellular domain ('Notch1ECD') with a Gal4 transcription factor (orange), which can activate a stably integrated fluorescent H2B-3xCitrine reporter gene (chartreuse). **C**, *(Left, schematics)* A minority of receiver cells (green) are co-cultured with an excess of either Dll1 (blue) or Dll4 (red) sender cells. *(Right)* Filmstrips showing representative sustained (upper panels, Dll4 senders) or pulsatile (lower panels, Dll1 senders) response of a single receiver cell (center, automatically segmented nucleus outlined in white). Grey channel shows DIC images of cells, while the rate of increase in Citrine fluorescence, scaled to 25%-75% of its total range, is indicated using green pseudo-coloring. Also see Supplementary Movie 1, 2. **D**, (*Left*) Representative traces showing total nuclear Citrine fluorescence levels (*top*) or corresponding derivatives of the total Citrine ('*d*Citrine/*d*t'), i.e. promoter activity (*bottom*), in individual receiver cells activated by Dll4. (*Right*) Average values of total fluorescence (*top*) and promoter activity (*bottom*) in receiver cells activated by Dll4. Solid traces represent medians, lighter shades indicate s.e.m, and gray shading indicates standard deviation. 'n' indicates number of traces included in the alignment. See Methods for alignment and normalization procedure. **E**, (*Left*) Corresponding plots (as in panel D) showing total nuclear Citrine fluorescence levels (*top*)

and promoter activity (*bottom*) in individual receiver cells in co-culture with Dll1. (*Right*) Average values of total fluorescence (*top*) and promoter activity (*bottom*) in receiver cells activated by Dll1. The percentage value ('60%') in the plots on *Right* indicates the fraction of receiver traces included in the alignment (Methods, see also Figure S1.2F). **F**, 95th percentile of (absolute, non-normalized) promoter activity values between 0 and 7.5h (after alignment) in the traces included in panel D and E. This time window is chosen to simultaneously estimate the promoter activity at the peak of Dll1 pulses and at steady-state levels of Dll4 signaling. Solid horizontal lines represent medians, while the boxes delineate 25th - 75th percentile values. *P*-value calculated by two-sided KS-test. **See also Figure S1.2, S2.**

Indeed, ligand-specific effects of Notch signaling have been observed in multiple contexts, and occur even with close paralogs like Dll1 and Dll4 (Figure 1A). For example, Dll4 is unable to replace Dll1 function in many tissues, leading to embryonic lethality in mice when knocked into the Dll1 locus (Preuße et al., 2015). Dll1 and Dll4 also have opposing effects on muscle differentiation: Dll1 expressed in the neural crest induces differentiation of muscle progenitors in somites (Rios et al., 2011), while Dll4 expressed in endothelial cells can revert this fate in committed skeletal myoblasts, diverting them to form pericytes instead (Cappellari et al., 2013). Puzzlingly, although Dll1 and Dll4 can behave differently under certain conditions, they appear to function interchangeably in others. For example, when overexpressed, both ligands promote T-cell differentiation of primary hematopoietic stem cells in culture, but appear to do so with different efficiencies (Mohtashami et al., 2010).

These observations provoke the question of how different ligands could induce different responses in signal-receiving cells, given that they all act through Notch receptor cleavage. One explanation could be differences in signaling strength. In fact, the Dll1 and Dll4

extracellular domains differ by more than 10-fold in their affinity for Notch (Andrawes et al., 2013). An additional possibility is that different ligands activate Notch with distinct dynamics. Cleaved NICD has a short half-life, enabling its concentration to respond rapidly to changes in Notch activation (Fryer et al., 2004; Housden et al., 2013; Ilagan et al., 2011). Similarly, the canonical Notch target gene Hes1 has short mRNA and protein half-lives and its levels oscillate in neurogenesis, somitogenesis, and other contexts (Kobayashi and Kageyama, 2014). While dynamics has been shown to play critical roles in other biological contexts (Purvis and Lahav, 2013), it has not been systematically investigated in the Notch pathway.

Here, by quantitatively analyzing the dynamics of Notch1 activation in individual cells, we show that Dll1 and Dll4 generate distinct patterns of direct target gene expression through an inherently dynamic mechanism. In this system, ligand identity is encoded in Notch1 activation dynamics. Specifically, Dll1 induces pulses of Notch activation, while Dll4 induces more sustained activity. These dynamics are in turn decoded to control relative levels of Hes1 and Hey1/L target gene expression. Notch activity in receiving cells is thus inherently multi-dimensional, possessing both an activation type (pulsatile or sustained) and an activation level. This ability to respond in a ligand-specific fashion enables signal sending cells to use different ligands to activate distinct Notch target programs in receiving cells, effectively increasing the number of different ‘channels’ of Notch pathway activity.

Results

2.2 Dll1 and Dll4 signal through Notch1 with different dynamics

In order to directly compare Notch1 signaling by Dll1 and Dll4 at the single cell level, we constructed 'sender' and 'receiver' cell lines in CHO-K1 cells (Figure 1B, Supplementary Table 1.1). Sender cells expressed either Dll1 or Dll4 along with a co-translational H2B-mCherry readout, under control of a promoter that is inducible by 4epi-Tetracycline (4epi-Tc) (LeBon et al., 2014; Sprinzak et al., 2010). We engineered receiver cells to express chimeric Notch1 receptors whose intracellular domain is replaced by the transcription factor Gal4 (Lecourtois and Schweisguth, 1998; Sprinzak et al., 2010; Struhl and Adachi, 1998), along with a Gal4-activated H2B-3xCitrine fluorescent protein reporter (Figure 1B). This 'diverted' reporter system enables readout of Notch activity without activation of endogenous Notch targets, avoiding potential complications due to downstream feedback interactions.

To compare signaling dynamics produced by the two ligands, we used time-lapse microscopy of sender-receiver co-cultures. In these experiments, a minority of receiver cells were co-cultured with an excess of either Dll1 or Dll4 sender cells, so that each receiver cell was in continuous contact with one or more sender cells (Figure 1C, Methods). Notch activation within the receiver cell was monitored by the rate of increase of fluorescence of the stable H2B-3xCitrine protein. This rate ('promoter activity') is controlled by the concentration of released Gal4, which in turn depends on Notch activation (Figure S1.2A, B). Briefly, we segmented nuclei of individual cells based on Citrine fluorescence, then extracted the total fluorescence within each nucleus at each timepoint, correcting for background fluorescence (see Methods). This generates a trajectory of total

fluorescence per cell over time. Notch activity can then be estimated from the time derivative of each fluorescent protein trace, computed by calculating the change in total nuclear fluorescence from one time point to the next (30 min apart).

Under these experimental conditions, Dll4-expressing sender cells activated receivers in a sustained fashion. After plating, individual receiver cells activated Citrine production and continued to actively produce Citrine for the duration of the experiment (~24h) (Figure 1C, D, Supplementary Movie 1). The sustained nature of Dll4 signaling was also reflected in the average response of these cells, obtained by normalizing each trace by its maximal level to extract the shape and aligning such normalized traces at the point of activation (Figure 1D, Methods).

In contrast, the same receiver cells activated in discrete, transient pulses in co-cultures with Dll1-expressing senders (Figure 1C, Supplementary Movie 2). In each pulse, the rate of Citrine production increased transiently, and then returned to baseline, displaying a characteristic shape (Figure 1D). Pulses occurred in an unsynchronized fashion, initiating at different times in different receiver cells, and could occur throughout the experiment (Figure S1.2C). Most cells under these conditions displayed a single pulse during the experiment (60% of traces), while two pulses could be detected in other traces (35%, Figure S1.2D, Supplementary Movie 3). These Dll1 pulses displayed peak amplitudes comparable to the amplitude observed during the corresponding period of Dll4 signaling (Figure 1E). These results indicate that Dll1 activates Notch1 through stochastic stereotyped pulses.

In order to better understand pulsatile Dll1 signaling dynamics, we first sought to estimate the duration of the underlying pulse of Notch activation, accounting for the half-lives of Gal4 protein and H2B-Citrine mRNA, which extend the duration of the observed reporter pulse. We computed values for these half-lives by analyzing the decay of Citrine production rate following inhibition of Notch signaling. For this experiment, cells were cultured on plate-bound recombinant Dll1 ligand (Sprinzak et al., 2010), which normally leads to continuous activation (Figure S1.2E). However, the pathway was blocked after 7h of activation by use of the γ-secretase inhibitor DAPT (Figure S1.2F). Using a simple mathematical model (Supplementary Information) to fit the resulting dynamics, we computed the half-lives of Gal4 protein (~4h, 95% CI [3.8h, 4h]) and H2B-3xCitrine mRNA (~3.4h, 95% CI [3.4h, 3.5h]), consistent with previously measured ranges in CHO-K1 cells (Bintu et al., 2016; Sprinzak et al., 2010). Together with the measured duration (~12h Full-Width at Half-Maximum, 'FWHM') and rise-time (~6h, 't_{rise}') of the Dll1-induced reporter activity pulses (Figure 1D), we computed an upper bound of ~1h on the duration of the underlying signaling events (Figure S1.2G, H). Simulations showed that pulses briefer than this would produce indistinguishable reporter dynamics (Figure S1.2I). As discussed more below, these brief pulses likely represent events in which multiple Notch receptors are activated (cleaved) simultaneously.

To better understand the difference in dynamics generated by the two ligands, we next asked whether the apparently sustained Dll4 signaling could be explained as a series of

Dll1-like pulses, possibly occurring at an elevated rate (Figure S1.2A). We computationally generated pulse trains composed of pulses with the same shape and amplitude distribution observed for Dll1 pulses (Supplementary Information, Figure S1.2B). We varied both the regularity of the pulses, using dynamic models ranging from periodic to Poisson distributed, as well as the pulse frequency (or mean interval between pulses) within each model, and analyzed the amplitude and temporal variability of the simulated pulse trains (Figure S1.2C, D). Higher pulse frequencies lead to greater pulse overlap, increasing signaling amplitude, while reducing the temporal variability of signaling (Figure S1.2E). Critically, tuning pulse frequency low enough to match the observed mean Dll4 signaling amplitude generated significantly greater temporal variability than observed experimentally (Figure S1.2E (inset), S2F). This analysis suggests that the observed sustained Dll4 signaling cannot be explained as a series of Dll1-like pulses. Furthermore, the difference in experimentally observed Dll1 and Dll4 dynamics was preserved even when the time resolution of the reporter was improved from 6h-12h (t_{rise} – FWHM, Figure S1G) to 2.5h-6h by destabilizing the Citrine mRNA (Figure S1.2G-I, see Methods). Taken together, these data and analysis strongly suggest that Dll1 and Dll4 activate Notch1 with distinct dynamics, Dll1 through brief pulses, and Dll4 in a sustained fashion. We note, however, that this does not rule out the possibility that Dll4 signaling originates from a series of smaller pulses (in the extreme limit, individual ligand-receptor activation events can be thought of as small, discrete “pulses”).

2.3 Dll1 levels modulate pulse frequency, while Dll4 levels modulate signaling amplitude

We next asked how the expression level of each ligand in the sender cell modulated signaling dynamics. To isolate signaling events produced by individual sender cells, we reversed the conditions of the assay, co-culturing an excess of receiver cells with a minority of sender cells (see Methods). We analyzed Dll1 senders across a >10-fold range of Dll1 expression levels (Figure S1.2J). Over this range, most receiver cells activated in pulses (Figure 1.2A, *bottom panels*, Supplementary Movie 4), which maintained the same stereotyped shape and duration (Figure 1.2B, *right panels*), and showed a 1.6-fold, increase in amplitude (Figure 1.2C, *right panels*). At the same time, we observed a stronger increase in the *number* of activated receiver cells with increasing Dll1 expression, reflecting an increase in pulse frequency (Figure 1.2D). Together, these results indicate that Dll1 expression levels modulate signaling predominantly through the frequency of stereotyped signaling pulses (Figure 1.2E, *left panel*).

Unlike Dll1, Dll4 showed sustained activation in the excess receiver assay across all levels of Dll4 expression analyzed (Figure 1.2A, B, *left panels,* Supplementary Movie 5, Figure S1.2K). We observed a systematic increase in peak (Figure 1.2C, *left panels*) and median (Figure S1.2L) signaling amplitude with increasing Dll4 expression level over a 10-fold range (Figure S1.2K). Together, these results indicate that Dll1 and Dll4 produce qualitatively different signaling dynamics across a broad range of expression and signaling levels, and modulate those dynamics in distinct ways, with Dll1 mainly controlling the frequency of stereotyped pulses, and Dll4 controlling the amplitude of sustained signaling (Figure 1.2E).

Figure 1.2

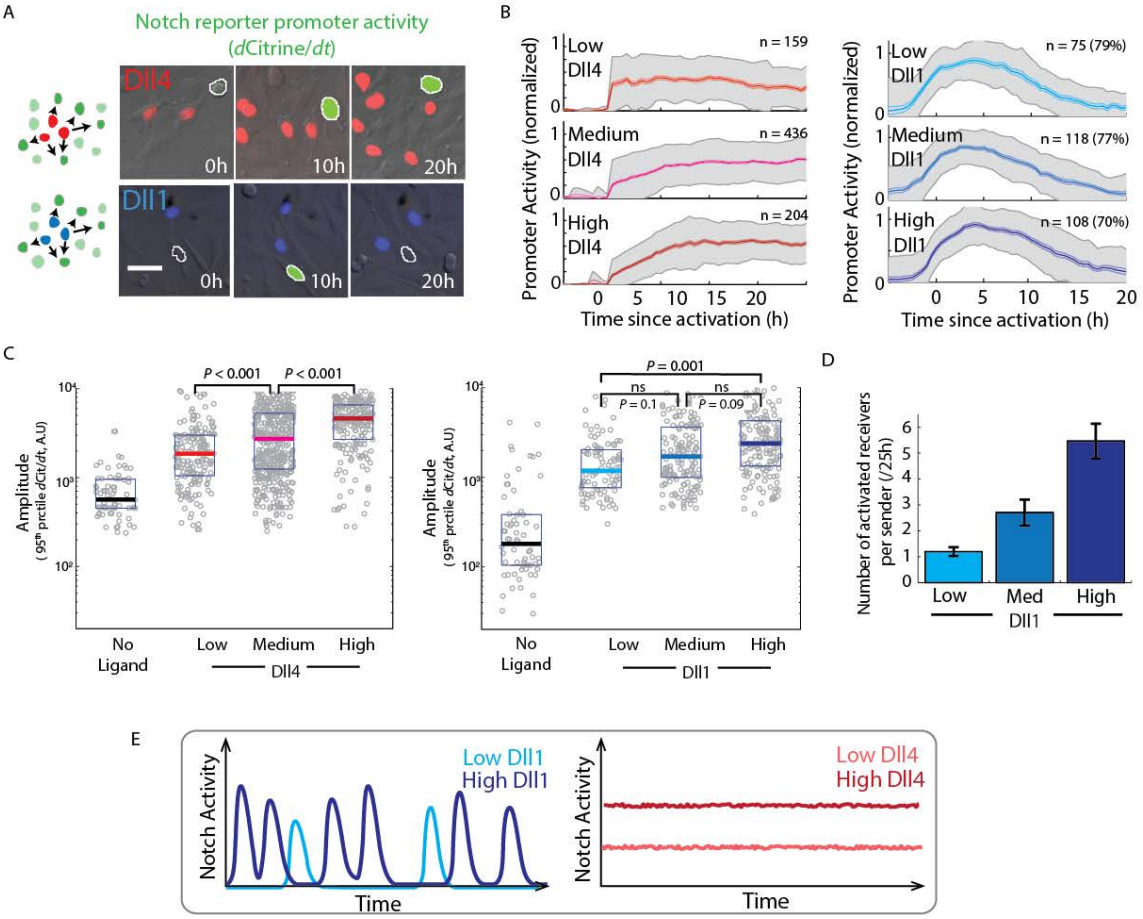

Differences in Dll1 and Dll4 dynamics are preserved across a range of ligand expression levels, and ligand-levels modulate these dynamics in different ways. A, (*Left*) Schematic of co-culture assay showing Dll1 (blue) or Dll4 (red) sender cells surrounded by receiver cells (green). (*Right*) Filmstrips showing sustained or pulsatile responses in a single receiver cell (green, automatically segmented nucleus outlined in white) neighboring either Dll4 (*Top,* nuclei pseudo-colored in red) or Dll1 (*Bottom,* nuclei pseudo-colored in blue) sender cells. The grey channel shows DIC images, in which other receiver cells can be seen. Intensity of green in the receiver cell indicates promoter activity scaled to 25%-75% of its range. See also Supplementary Movie 4, 5. **B**, Median response profiles in individual receiver cells co-cultured with sender cells expressing Low, Medium, or High levels of Dll4 (*Left*) or Dll1 (*Right*). (See Figure S1.2J, K for ligand expression levels in each group). Solid traces represent medians, light colored regions indicate s.e.m, gray shading indicates standard deviation. 'n' values indicate number of receiver cell responses included in the alignment. The percentage values in the Dll1 plots indicate the fraction of receiver traces included in the alignment (Methods). **C**, *(Left)* Comparison of maximal promoter activities (95th percentile of promoter activity values in each trace) in activated receiver cells adjacent to sender cells expressing no ligand (black), or Low (red), Medium (pink), or High (dark red) levels of Dll4 (same designations as used in panel B). *(Right)* Similar comparison for Dll1. Grey circles

represent individual responses, solid horizontal lines represent medians, while the boxes delineate 25th - 75th percentile values. *P*-values calculated by two-sided KS-test. ns, $P > 0.01$. **D**, Median values of the number of receiver cells activated by isolated Dll1 sender cells expressing Low, Medium, or High levels of co-translational H2B-mCherry, and their progeny during a 25h experiment, under excess receiver conditions. Error bars represent s.e.m. **E**, (*Schematic*) Summary of Dll1 and Dll4 modulation. Dll1 levels primarily control rate or frequency of stereotyped pulses, while Dll4 levels control amplitude of sustained signal. **See also Figure S1.2 (panels J-L).**

2.4 Pulsatile and continuous Notch signals can elicit distinct transcriptional responses

We next asked whether the different dynamics produced by Dll1 and Dll4 activation could regulate distinct sets of target genes, and thereby allow cells to discriminate between the ligands. To directly test the effect of NICD dynamics on target gene expression, we took advantage of the fact that truncated Notch1 receptors lacking most of their extracellular domain (N1ΔECD) are constitutively active, but can be inhibited by DAPT (Fortini et al., 1993; Kopan et al., 1996) (Figure 3A). Cells expressing N1ΔECD can therefore be activated for different durations and to varying levels by controlling DAPT concentration in the media for corresponding time intervals (see Methods).

We stably expressed N1ΔECD in C2C12 cells, where the binding of the NICD-CSL complex to target gene promoters has been previously characterized using CHIP-seq(Castel et al., 2013). Using RNA-seq (Methods), we identified genes that were up-regulated at early time points (1h or 6h) following Notch activation by DAPT removal (Figure S1.3A, B, Supplementary Table 1.2, 3). We focused specifically on putative direct Notch targets previously shown to bind the CSL-NICD complex in this cell line (Castel et al., 2013). Other genes that were activated were not considered for further analysis because they are not known Notch targets; several of these genes, such as *Dusp, Egr, Atf3, and Fos*

have been shown to be induced by growth factor signaling, suggesting that they could have induced by media change during DAPT removal (Allan et al., 2001; Gururajan et al., 2008; Kesarwani et al., 2017).

Figure 1.3

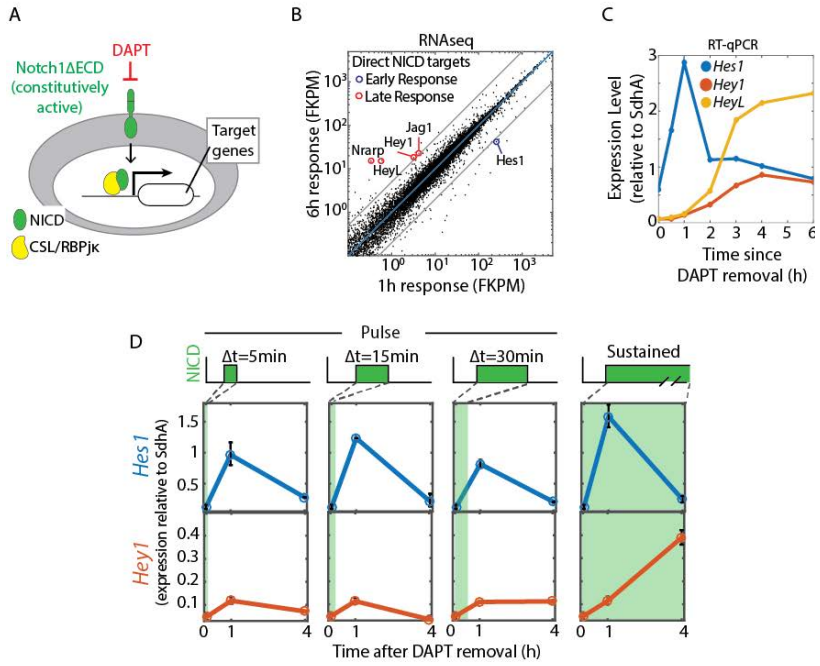

Pulsatile and sustained Notch activation can regulate different sets of target genes. A, C2C12 cells were engineered to expressed Notch1 receptors lacking the extracellular domain (N1ΔECD, green). This receptor is inactive in the presence of the γ-secretase inhibitor DAPT (red), but constitutively active when DAPT concentration is reduced in the culture medium. **B**, Comparison of transcript levels in C2C12-N1ΔECD cells, at 1h or 6h after DAPT removal. The blue line represents equal expression at 1h and 6h, and the grey lines represent 5-fold changes in either direction. Circled genes are putative direct Notch targets. The blue circle highlights target genes that are up-regulated >5-fold at 1h but not 6h, while red circles indicate target genes that are up-regulated >5-fold only after 6h. See also Figure S1.3 and Supplementary Table 1.2, 3. **C**, qPCR timecourse measurement of Hes1 (blue), Hey1 (orange), and HeyL (yellow) mRNA levels following complete DAPT removal at t = 0h. **D**, Duration dependence of Hes1 (blue) and Hey1 (orange) response to DAPT removal for 5 min, 15 min, or 30 min followed by replenishment ('Pulse'), or no replenishment until the 1h or 4h measurement ('Sustained'). Error bars represent S.E.M calculated from duplicate experiments. See also Figure S1.3.

Interestingly, even direct Notch target genes responded to activation of the pathway at different times (Figure 1.3B). Hes1, but not the other target genes, was rapidly activated,

showing strong (~10-fold) up-regulation by 1h (Figure 1.3B, Figure S1.3A, Supplementary Table 1.2). Other Notch targets such as Hey1, HeyL, Jag1, and Nrarp responded later, showing little change at 1h, but strong up-regulation by 6h (Figure 1.3B, Figure S1.3B, Supplementary Table 1.3). In order to follow the early and later response in finer detail, we carried out an RT-qPCR time-course measurement of Hes1, Hey1, and HeyL mRNA levels following DAPT removal (Figure 1.3C). Hes1 expression increased rapidly, within 30 min, and its levels peaked at 1h. By contrast, Hey1/L levels did not significantly increase until the end of the Hes1 activation pulse, at 2h, after which they continued to rise until reaching a steady state around 4h.

These results suggested the possibility that brief (<1h) pulses of Notch activation could selectively activate Hes1, with the other targets requiring longer durations of Notch signaling. To test this hypothesis, we used RT-qPCR to analyze the response of Hes1 and Hey1/L to varying durations and amplitudes of Notch activation (see Methods). We observed that Hes1 activation was relatively insensitive to the duration of Notch activation, and could be induced strongly by brief pulses (5min – 30min) and by sustained activation (Figure 1.3D). On the other hand, Hey1 and HeyL were more sensitive to duration, accumulating continuously as long as Notch activation was maintained (Figure 1.3D, Figure S1.3C).

In order to isolate the effects of signaling duration from those of signal amplitude, we compared Hey1/L expression at the same instantaneous NICD concentrations but after

different durations of NICD exposure (Figure S1.3D-G). Specifically, we compared a brief pulse of NICD generated by total DAPT removal for 15 min, with a longer (3h) duration of NICD activity generated by partial removal of DAPT to 0.3μM. These two perturbations produce the same final concentration of NICD but differ in the duration of NICD activity (Figure S1.3D, E). If NICD concentration alone controlled Hey1/L expression, then the two conditions should produce similar rates of Hey1/L synthesis (Figure S1.3F, *top*). By contrast, a requirement for sustained NICD activity would lead to a greater rate of Hey1/L expression in the prolonged case (Figure S1.3F, *bottom*). For each condition, we measured the increase of Hey1/L levels in a 30 minute window in order to quantify new Hey1/L expression at the corresponding time-point (Figure S1.3F). We observed increased Hey1/L expression only at the 3h time-point, indicating that an extended period of activity is required for efficient activation (Figure S1.3G). Higher NICD concentrations were not able to overcome the requirement for extended activation, as a 30 min pulse of total DAPT withdrawal, which produced higher NICD concentrations, did not increase Hey1/L expression (Figure S1.3D, G). NICD concentration did, however, affect the *maximum* induction levels of the Hes/Hey genes under sustained activation (Figure S1.3H). Finally, we note that the weakness of the Hey1/L response to brief activation pulses was not due to insufficient NICD, as the Notch1ΔECD system produces more NICD from DAPT withdrawal over 30 min than observed in Notch1-expressing receiver cells co-cultured with sender cells expressing maximal levels of Dll4 (Figure S1.3I). Together, these results indicate that pulsatile and sustained Notch dynamics are decoded into distinct gene

expression patterns, with Hes1 responding strongly even to brief pulses, and Hey1 and HeyL requiring sustained activation.

To gain insight into how decoding could occur, we built a simple mathematical model (see Supplementary Information) incorporating known features of the Hes and Hey transcription factors, including rapid turnover of Hes1 mRNA and protein, Hes1 negative autoregulation, and cross-repression of Hes1 and Hey1/L (Hirata et al., 2002; Fischer and Gessler, 2007; Heisig et al., 2012; Kobayashi and Kageyama, 2014). We first confirmed that our choice of biochemical parameters for Hes1 induction, turnover, and auto-repression permitted Hes1 oscillations (Figure S1.4A), which have previously been reported in several contexts including C2C12 cells (Hirata et al., 2002; Kobayashi and Kageyama, 2014). Further analysis of this model after inclusion of the Hey interactions (Figure S1.4B) showed that, in response to sustained Notch activation, Hes1 responds strongly at early times (< 1.5h), but Hey1 dominates after 1.5h, as observed experimentally (Figure 1.4c). In the simulation, Hes1 levels initially increase rapidly in response to Notch and suppress early accumulation of Hey1/L. However, Hes1 levels peak at ~1h and then decline due to negative autoregulation, permitting Hey1/L levels to increase and to then suppress subsequent Hes1 activation by Notch. Thus, this model is able to recapitulate the observed Hes/Hey dynamics, suggesting that decoding could arise from interactions between NICD, Hes1 and the Hey genes. We note that this NICD-Hes-Hey circuit essentially implements Incoherent Feed-Forward Logic (IFFL), which has been implicated in duration-sensing in other contexts.

2.5 Dll1 and Dll4 induce different gene responses

Based on the different responses of Hes1 and Hey1/L to Notch dynamics, we hypothesized that Dll1 signaling could activate Hes1 without significantly inducing the Hey genes, while Dll4 could more strongly upregulate Hey1/L, even at similar Hes1 induction levels. To test this hypothesis, we used a C2C12 cell line constitutively expressing wild-type Notch1, with its endogenous Notch2 knocked down by siRNA (see Methods). We first verified that the dynamic differences between Dll1 and Dll4 activation of Notch1 are preserved in this cell line, even at similar mean levels of Notch activity (Figure S1.4A-C). We then co-cultured this cell line with CHO-K1 cells expressing Dll1, Dll4, or no ligand, and measured Hes1, Hey1, and HeyL mRNA levels by RT-qPCR (Figure S1.4D, E). We found that for the same, reproducible, 1.6-fold upregulation in mean Hes1 levels, Dll4 induced ~3-5 fold more Hey1/L than Dll1 did (Figure S1.4E). This result is consistent with the different signaling dynamics of Dll1 and Dll4 inducing different Hes/Hey expression regimes. By contrast, sustained signaling levels (amplitudes) do influence the levels of both Hes and Hey1/L expression, but do so proportionately (Figure S1.3H), and therefore cannot explain the disproportionate induction of these gene sets by Dll1 and Dll4.

Further, we used a complementary imaging approach to analyze the effects of single (or few) sender cells on neighboring receivers, by using plating conditions that allowed the two cell types to contact each other predominantly along a linear interface (Figure S1.4F, Methods). Gene expression was analyzed by Hybridization Chain Reaction - Fluorescence *In Situ* Hybridization (HCR-FISH), which provides an amplified single-cell readout of specific mRNA levels (Choi et al., 2010, 2016) (Methods). In these experiments, we

similarly observed that Dll4 senders, but not Dll1 senders, strongly up-regulated Hey1/L in neighboring receiver cells (Figure S1.4G, H). Changes in Hes1 mRNA levels were more difficult to observe at the single cell level using this technique, due to the basal expression of Hes1 (Supplementary Table 1.2), and the stochastic, unsynchronized nature of Dll1 pulses. Nevertheless, these results further support the conclusion that Dll1 and Dll4 activate different Hes/Hey gene expression regimes, with Dll4 producing a higher expression of Hey1/L compared to Dll1 at similar Hes1 levels.

2.6 Dll1 and Dll4 direct opposite fates in vivo

We next sought to test the ability of Notch receiving cells to distinguish between Dll1 and Dll4 in the same *in vivo* context. To this end, we asked whether Notch1-expressing cells could carry out different developmental programs in response to each of the two ligands during embryonic myogenesis in chick somites. In the developing embryo, it has been shown that Dll1 expressed in migrating neural crest cells signals to Notch1 expressed in the dorsomedial lip (DML) of the neighboring somite. This interaction promotes differentiation of Pax7+ progenitor cells in the DML by up-regulating the muscle regulatory factors Myf5 and MyoD1, likely via Hes1(Rios et al., 2011) (Figure 1.4A). Consequently, overexpressing Dll1 in the neural crest up-regulates Hes1, Myf5, and MyoD1(Rios et al., 2011). Critically, in this system, transient activation of the Notch pathway enables normal muscle differentiation, while sustained activation inhibits this process (Rios et al., 2011).

Our results thus far suggest that transient and sustained Notch activation are intrinsic properties of the Dll1 and Dll4 ligands, respectively. Therefore, we predicted that the pulsatile dynamics of Dll1 would promote myogenic fate, while the sustained dynamics produced by Dll4 would inhibit myogenesis in the same cells. To test this possibility, we electroporated either Dll1 or Dll4 into the neural crest unilaterally in stage HH12-13 chick embryos, using the other side as a negative control(Elena de Bellard and Bronner-Fraser, 2005; Rios et al., 2011). 20h later, we measured expression levels of Notch targets (Hes1, Hey1, or HeyL) and MyoD1 in the adjacent somites using whole-mount HCR-FISH (Figure S1.5A, see Methods).

Consistent with previously published results, ectopic Dll1 expression in the neural crest systematically up-regulated Hes1 in the somite (Figure 1.4B-i, ii, quantification in Figure S1.5C), and frequently increased MyoD1 in adjacent somites (34% of somites, Figure 1.4B-iii, Table 1.1, Figure S1.5C) or maintained its levels (49% of somites, Table 1.1, Figure S1.5C). As expected, ectopic Dll1 expression did not significantly alter Hey1 levels (Figure 1.4C, S5C). On the other hand, ectopic Dll4 expression consistently increased Hey1 (Figure 1.4B - iv, v, Figure S1.5C) and HeyL (Figure S1.5B), in addition to Hes1 (Figure 1.4D, S5C). Importantly, Dll4 also strongly decreased MyoD1 in the majority of neighboring somites (65% of somites, Figure 1.4B-vi, Table 1.1, Figure S1.5C). Thus, Dll1 and Dll4 induced opposite effects on cell fate in the same Notch1-expressing somite cell population that received the signal. While a role for differences in signaling levels between the two ligands in this context cannot be directly excluded, it is striking that these

responses, observed in an *in vivo* context, matched the differences in dynamics and target specificity observed in cell culture systems.

Figure 1.4

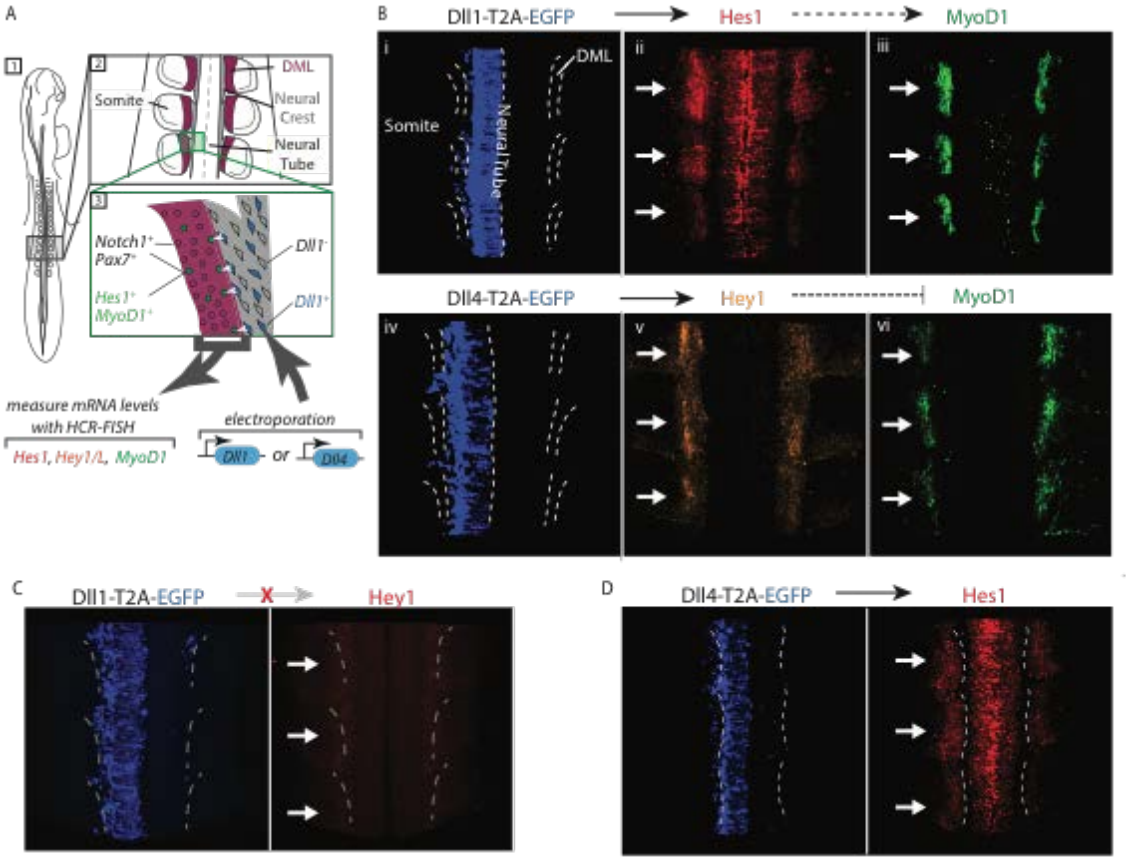

Dll1 expression in the chick neural crest promotes myogenesis, but Dll4 inhibits it. **A**, Developing chick embryo (dorsal view schematic). Dll1 (blue cells in 3) is expressed in a fraction of neural crest cells (grey, see 2, 3). These cells activate Notch1-expressing Pax7^{+} progenitor cells in the dorsomedial lip (DML, magenta) of the somite. When activated, these progenitor cells (green, 3) up-regulate Hes1 and the muscle regulatory gene MyoD1. **B-D,** Representative images showing effects of Dll1 or Dll4 electroporation into the neural crest, on Hes1, Hey1/L, and MyoD1 expression in the DML. White arrows indicate the somites on the electroporated side. The dotted lines indicate the DMLs of somites or the central line of the neural tube. **B,** (*Top*) CAG-Dll1-T2A-EGFP (i, blue), electroporated into the left side of the neural tube, is expressed in the neural tube and neural crest, resulting in up-regulation of Hes1 (ii, red) and MyoD1 (iii, green) in the somites on the electroporated (left) side compared to the right side, which serves as negative control. (*Bottom*) When CAG-Dll4-T2A-EGFP (iv, blue) is electroporated, Hey1 (v, red) is up-regulated on the electroporated side, and

MyoD1 (vi, green) expression is decreased. **C**, Dll1-T2A-EGFP (blue, *left*) electroporation does not affect expression of Hey1 (red, *right*) in adjacent somites. **D**, Dll4-T2A-EGFP (blue, *left*) electroporation increases expression of Hes1 (red, *right*) in adjacent somites. **See also Table 1.1 and Figure S1.5.**

Table 1.1

MyoD1 levels in somites on electroporated side relative to control side				
	# showing **Increase** (% of total)	# showing **No Change** (% of total)	# showing **Decrease** (% of total)	Total
Dll1	21 (34.4%)	**30 (49.1%)**	10 (16.3%)	61
Dll4	9 (14.8%)	12 (19.6%)	**40 (65.6%)**	61

Quantification of changes in MyoD1 expression in embryos electroporated with Dll1 (top row) **or Dll4** (bottom row)**.** For each treatment, 61 pairs of somites across 11 Dll1-expressing or 10 Dll4-expressing embryos were scored blindly for differences in HCR-FISH signal between the electroporated side and the control side (see Methods). Indicated are the number (and percentage) of somite pairs that show an increase (column 2) or decrease (column 4), or no change (column 3) in MyoD1 expression on the electroporated side. The number of somites corresponding to the most typical categorization in each case is highlighted.

2.7 Ligand intracellular domains influence dynamics through differences in transendocytosis

To gain insight into how Dll1 and Dll4 generate different Notch activation dynamics, we asked whether the type of dynamic behavior was determined by any particular domain of the ligand. Previous work demonstrated that the ligand extracellular domain (ECD) is responsible for receptor binding, while the intracellular domain (ICD) mediates transendocytosis of bound receptors, initiating the receptor cleavages required for activation (Chitnis, 2006; Weinmaster and Fischer, 2011). As shown above, plate-bound

recombinant Dll1ECD leads to sustained activation (Figure S1E), suggesting that the Dll1ECD does not by itself determine pulsatile signaling. We therefore constructed two chimeric Delta ligands, $Dll1_{ECD}$-$Dll4_{ICD}$ and $Dll4_{ECD}$-$Dll1_{ICD}$, by exchanging the ICDs of Dll1 and Dll4 (Methods), and stably expressed them in sender cell lines (as in Figure 1B), obtaining cell surface levels similar to those of their wild-type counterparts (Figure S1.5D, see Methods).

Figure 1.5

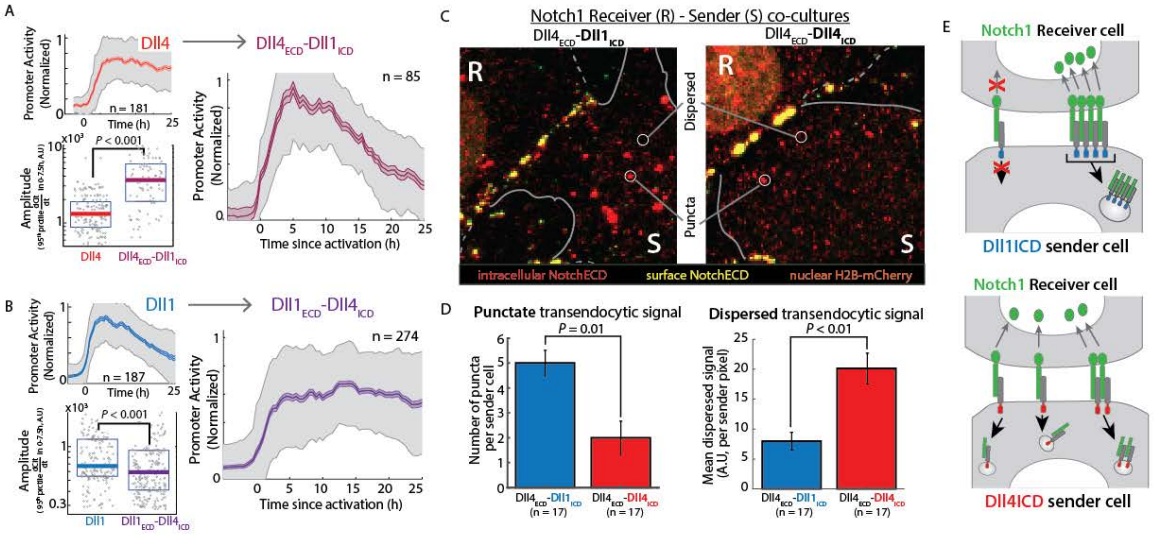

Ligand intracellular domains control dynamic signaling mode, and influence transendocytosis patterns. A, B, $Dll4_{ECD}$-$Dll1_{ICD}$ and $Dll1_{ECD}$-$Dll4_{ICD}$ were constructed by exchanging the intracellular domain (ICD) of Dll4 with that of Dll1. **A.** Median response profiles in activated receiver cells co-cultured with Dll4 sender cells (red, *top left)* or $Dll4_{ECD}$-$Dll1_{ICD}$ sender cells (magenta, *right*) under excess receiver conditions (as in Figure 1.2). Solid traces represent medians, lighter colored regions represent s.e.m., and grey shading represents standard deviation. 'n' represents number of cell traces included in the alignment. See Methods for alignment and normalization procedures. (*Bottom left*) 95th percentile of (absolute, non-normalized) promoter activity values between 0 and 7.5h (after alignment) in individual traces included in the averaging. Solid horizontal lines represent medians, while the boxes delineate 25th - 75th percentile values. *P*-value calculated by two-sided KS-test. **B,** Corresponding response profiles (*right, top left*) and amplitudes (*bottom left*) in activated receiver cells co-cultured with Dll1 sender cells (blue*)* or $Dll1_{ECD}$-$Dll4_{ICD}$ sender cells (purple) under excess sender conditions. **C,** Representative images of 'excess sender' co-cultures of receiver cells ('R') expressing full-length Notch1 and sender cells ('S')

expressing either $Dll4_{ECD}$-$Dll1_{ICD}$ (*left*) or Dll4 ('$Dll4_{ECD}$-$Dll4_{ICD}$', *right*), immunostained for Notch1ECD. Examples of dispersed, low intensity staining or higher-intensity puncta are indicated by the white circles. **D, (***Left*) Median values of number of puncta detected (see Methods) in Dll1ICD (blue) or Dll4ICD (red) sender cells neighboring receiver cells. (*Right*) Median values of the (background subtracted) mean pixel intensity of dispersed signal (see Methods) within Dll1ICD (blue) or Dll4ICD (red) sender cells that neighbor receiver cells. Error bars represent s.e.m. *P* value calculated using the two-sided *KS*-test. **E,** (*Schematic*) Proposed differences in the abilities of ligands containing the Dll1 (blue) and Dll4 (red) ICDs to initiate transendocytosis in different clustering states. **See also Figure S1.6.**

We first compared $Dll4_{ECD}$-$Dll1_{ICD}$ with Dll4 using the excess receiver co-culture assay. Unlike Dll4, the $Dll4_{ECD}$-$Dll1_{ICD}$ ligand generated pulsatile activation, showing that the Dll1 ICD can strongly alter the activation dynamics of the Dll4 ligand (Figure 1.5A). The amplitude of these pulses was ~3-fold *greater* than signaling amplitude generated by Dll4 at the highest expression levels analyzed here, suggesting that pulsatile $Dll4_{ECD}$-$Dll1_{ICD}$ dynamics could not be explained by a reduction in Dll4 signaling strength. In parallel, we compared Dll1 and a $Dll1_{ECD}$-$Dll4_{ICD}$ chimera using the excess sender co-culture assay. With this chimeric ligand, most signaling occurred in a sustained fashion, but at an amplitude slightly lower than the peak amplitude of Dll1 signaling (Figure 1.5B). This result indicates that the Dll4ICD can convert the dynamics of Dll1 to a more sustained behavior, even at comparable mean signaling strengths. Furthermore, consistent with the idea that dynamics strongly impact target gene expression, the $Dll1_{ECD}$-$Dll4_{ICD}$ chimeric ligand, like Dll4, produced more Hey1/L expression than Dll1 at a similar level of Hes1 activation (Figure S1.5E, *bottom panel inset*). Additionally, it was not possible to match Dll1-induced Hes/Hey gene expression levels by varying the expression level of the chimeric ligand (thus varying signal amplitude), suggesting that this ligand produces a qualitatively distinct Hes/Hey gene expression response compared to Dll1 (Figure S1.5E).

Together, these results indicate that the ligand ICD plays an important role in determining dynamic signaling mode of the ligand (pulsatile or sustained) and downstream gene expression.

How could ligand ICDs, functioning within sending cells, determine the dynamics of Notch activity in receiving cells? Based on previous work showing that the ligand ICD mediates receptor transendocytosis, we reasoned that the differences in dynamics between $Dll1_{ICD}$ and $Dll4_{ICD}$ ligands might reflect distinct modes of transendocytosis. We therefore compared transendocytosis in $Dll1_{ICD}$ and $Dll4_{ICD}$ sending cells, by immunostaining the Notch1ECD in sender-receiver co-cultures followed by confocal imaging (Figure S1.5F, see Methods).

We first compared Dll4 and $Dll4_{ECD}$-$Dll1_{ICD}$. At the interface between senders and receivers, we observed regions of intense Notch1ECD staining, which co-localized with ligand staining (Figure S1.6A). This is consistent with previous observations of Notch ligand-receptor 'clustering' at points of intercellular contacts(Bardot et al., 2005; Meloty-Kapella et al., 2012; Nichols et al., 2007). Within the sender cells, we observed two distinct types of staining for transendocytosed receptors: (1) dispersed, low-intensity staining that lacked apparent structure, and (2) discrete, high-intensity puncta that typically spanned >10 pixels (in three dimensions), possessed >100-fold higher cumulative intensities (Figure 1.5C, Figure S1.6D), and colocalized with the endocytosis marker Rab5 (Figure S1.6B).

The generally pulsatile Dll1 ICD was strongly associated with the punctate endocytosis patterns in a signaling context. $Dll4_{ECD}$-$Dll1_{ICD}$ senders adjacent to receivers showed a significant increase in the levels of punctate, but not dispersed, staining, relative to sender cells not adjacent to receivers (Figure S1.6C). Importantly, when compared at expression levels that produced similar Notch activity (Figure S1.6E), $Dll4_{ECD}$-$Dll1_{ICD}$ sender cells exhibited more puncta per cell compared to Dll4 senders (Figure 1.5D, *left*), and the wild-type Dll1 ligand also exhibited puncta (Figure S1.6F, G). Furthermore, the relative number of puncta per sender cell between $Dll4_{ECD}$-$Dll1_{ICD}$ and Dll1 (Figure S1.6G, *right*) was similar to the ratio of their pulse rates (Figure S1.6H), while dispersed staining levels were similar. These results show that pulsatile signaling correlates with the appearance of punctate transendocytosis patterns. By contrast, Dll4 sender cells showed elevated levels of dispersed staining relative to sender cells not adjacent to receivers (Figure S1.6C), and also relative to $Dll4_{ECD}$-$Dll1_{ICD}$ sender cells at the same mean signaling activity (Figure 1.5D, *right*), suggesting that dispersed staining reflects sustained signaling.

2.8 Dll1 and Dll4 intracellular domains show different sensitivities to ligand clustering

To directly test the effect of clustering on the ability of each ligand to transendocytose Notch receptors, we induced ligand clustering on the cell surface to different extents and analyzed the resulting effects on receptor transendocytosis. Adapting a previously developed assay (Meloty-Kapella et al., 2012), we pre-clustered Fc-tagged recombinant Notch1 extracellular domains ('NotchECD-Fc') with a polyclonal goat anti-Fc, and adsorbed these complexes onto Protein A-coated agarose beads. When added to sender cells, these beads induced ligand clustering on the cell surface through ligand-receptor

binding (Figure 1.6A). Bound ligands, in turn, subsequently transendocytosed NotchECD-Fc:anti-Fc complexes from the bead. Transendocytosis efficiency could then be estimated by calculating the ratio of internalized to surface-bound NotchECD-Fc (see Methods).

Due to the polyclonal nature of the anti-Fc antibody, different ratios of NotchECD-Fc to anti-Fc should induce different degrees of clustering (Figure S1.7A). Indeed, in a 'weakly-clustered' regime, ligand-bound receptors exhibited a relatively uniform distribution on the cell surface (Figure 1.6B, *left*, Figure S1.7B), which could be seen in representative line profiles (Figure S1.7C). By contrast, in a 'strongly-clustered' regime we observed stronger surface label peaks that were more sparsely distributed across the cell surface (Figure 1.6B, *right*, Figure S1.7D, E). Importantly, the regions of highest intensity in the strongly-clustered condition were both (a) systematically brighter than high intensity regions in the weakly-clustered condition, despite the lower NotchECD-Fc concentration (Figure S1.7F), and (b) separated by regions of nearly background level fluorescence (Figure S1.7E). This approach thus enables modulation of the surface ligand-receptor clustering state.

When strongly clustered, the two ICDs showed similar spatial distributions of transendocytic receptor staining (Figure 1.6C, *right*), and comparable, Mib1-dependent, transendocytosis efficiencies (Figure 1.6D, *right*, Figure S1.7G). However, in the weakly clustered regime, while staining became more dispersed for both ligands (Figure 1.6B, C, *left*), it showed a lower overall level for the Dll1 ICD compared to the Dll4 ICD (Figure

1.6D). Thus, the transendocytic abilities of the two ICDs differ in their sensitivity to ligand-receptor clustering.

These data together suggest a model for how different ligands could generate different Notch activity dynamics in signal receiving cells through differences in transendocytosis patterns. In this model, the Dll1 ICD preferentially activates in the context of a ligand-receptor cluster (Figure 1.5E, *top panel*). A typical signaling event would involve the simultaneous activation of multiple receptors by interacting ligands within a single cluster, thereby releasing multiple NICDs at the same time to generate a pulse of signaling in the receiving cell (Figure S1.6I). In the sending cell, these events would produce transendocytic vesicles containing many receptor ECDs (punctate staining). By contrast, while the Dll4 ICD can also form clusters (Figure 1.5C, S6A), it would not require clustering for activation. It could thus predominantly activate in the context of smaller complexes, or individual ligand-receptor pairs (Figure 1.5E, *bottom panel*). This would enable Dll4 ICD to generate sustained Notch signal in the receiver cell (Figure S1.6I), consisting of a relatively steady 'trickle' of receptor transendocytosis events, each generating a transendocytic vesicles containing a smaller number of receptor ECDs, leading to more dispersed staining in the sending cell.

Figure 1.6

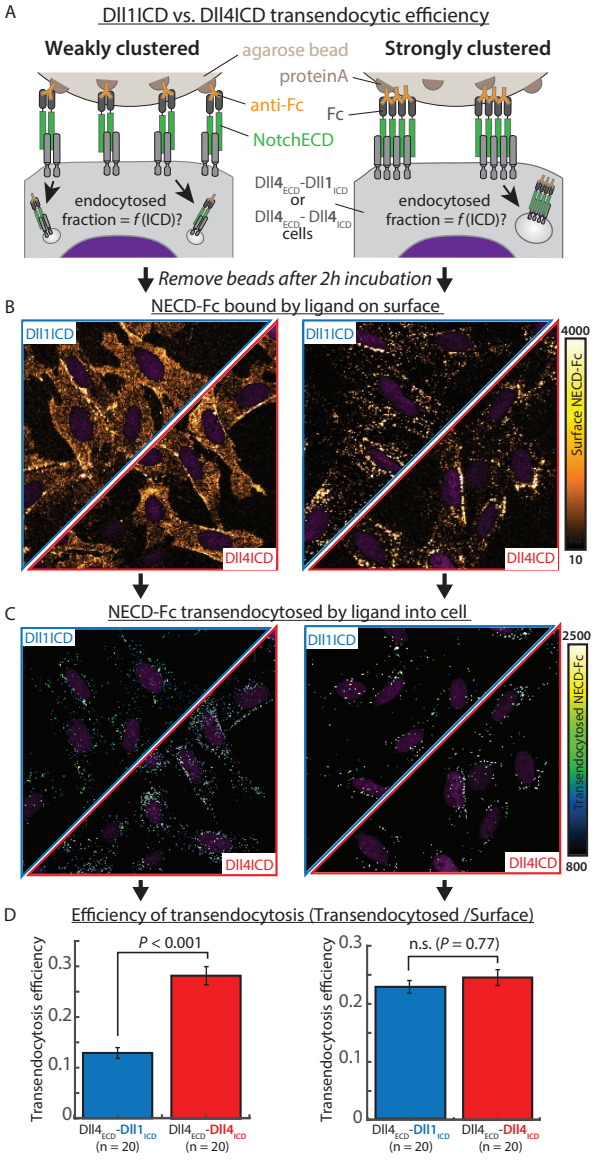

Ligand ICD identity affects the sensitivity of transendocytosis to cell-surface clustering. **A**, Recombinant NotchECD (green)-Fc (dark grey) is weakly (*left*) or strongly (*right*) pre-clustered using an Fc-targeting polyclonal antibody (orange, see Extended Data Fig. 6a), and adsorbed onto ProteinA (dark brown)-agarose beads through interactions between the anti-Fc and ProteinA (Schematic, see Methods). Cells (expressing $Dll4_{ECD}$-$Dll1_{ICD}$ or $Dll4_{ECD}$-$Dll4_{ICD}$ ligands shown in grey, co-expressing a nuclear H2B-mCherry fluorescent protein, indicated in purple) are then exposed to coated beads, leading to ligand-receptor binding and transendocytosis of a fraction of bound NECD-Fc:anti-Fc complexes ('endocytosed fraction') during the 2h experiment. Beads are removed from cells after 2h, and cells are immunostained for surface-bound and transendocytosed NECD-Fc:anti-Fc. **B-C,** Representative images of ligand-expressing cells immunostained for NECD-Fc:anti-Fc. Each panel shows Dll1ICD cells (top triangle, blue outline) and Dll4ICD cells (bottom triangle, red outline). Nuclear fluorescence reflects H2B-mCherry expression (purple pseudocolor). Each image represents the sum of 5 confocal Z-slices. **B,** Surface-bound NECD-Fc staining under weakly or strongly clustered conditions (*left* and right, respectively). **C**, Transendocytosed NECD-Fc staining under weakly or strongly clustered conditions (*left* and *right*, respectively; see Methods). **D**, Median value of transendocytosis efficiencies under weakly or strongly clustered conditions in $Dll4_{ECD}$-$Dll1_{ICD}$ cells (blue) and $Dll4_{ECD}$-$Dll4_{ICD}$ cells (red). Error bars represent standard error of the mean. *P*-value calculated using two-sided KS-test.

2.9 Discussion

The existence of multiple ligands in the Notch pathway suggests the possibility that they could function as distinct communication channels. However, Notch ligands have broad specificity; each one interacts with all Notch receptors. Therefore, such channels (if they exist) cannot be formed by orthogonal ligand-receptor pairs. In the prevailing Notch paradigm, ligand-receptor interactions are assumed to vary only quantitatively, in their activation strength. Thus, the Notch receiving cell appears to have no clear way to decipher the identity of an activating ligand. Here we find, unexpectedly, that Dll1 and Dll4 encode their signals in distinct dynamics (Figs. 1, 2), which are then decoded into distinct patterns of Hes and Hey target gene expression and, consequently, cell fate (Figs. 3, 4), indicating that these ligands do indeed represent distinct communication channels.

The use of dynamics to encode ligand identity differs from a simpler potential encoding scheme based on signaling amplitude. In such a scheme, downstream target gene activation would primarily be a function of the overall strength of signaling. While signaling amplitude is important, several lines of evidence show that dynamics plays a critical role in controlling downstream genetic programs. First, direct manipulation of signaling dynamics through the Notch1ΔECD system (Figure 1.3) demonstrates that even at pulse amplitudes larger than those occurring during intercellular signaling in co-cultures, the duration of NICD pulses strongly affect target gene activation patterns, with Hey1/L activation occurring only after a delay. This time-dependence cannot be explained by a slow ramp-up in NICD levels, as the instantaneous rate of expression of targets depend on the total time of Notch activation even when compared at the same NICD concentration

(Figure S1.3D-G). The role of dynamics is further supported by analysis of chimeric ligands that share the same extracellular domain, and therefore the same affinity for Notch1, but differ in their intracellular domains and signaling dynamics. At the same level of Hes1 activation, $Dll1_{ECD}$-$Dll4_{ICD}$ showed increased Hey1/L activation compared to Dll1, consistent with the more sustained signaling of the chimeric ligand (Figure 1.5B, S5E). Moreover, the Hey1 to Hes1 activation ratio of Dll1 could not be matched by tuning the expression level of this chimeric ligand. Overall, these results strongly argue against an exclusively amplitude-based scheme for controlling target gene expression in a ligand-dependent manner, but are consistent with a dynamic encoding scheme.

Our results support a simple model of dynamic encoding that builds on previous observations that Notch ligands and receptors spontaneously assemble into ligand-receptor clusters at cell-cell interfaces. In the model, a Dll1-mediated pulse occurs when receptors in the cluster activate in a coordinated manner, releasing a burst of Notch intracellular domains in the receiving cell (Figure 1.5E, Figure S1.6I). The key point is that the Dll1 ICD does not efficiently initiate transendocytosis until clusters reach a critical size, ensuring that most signaling occurs in pulses. By contrast, Dll4 may cluster, but it does not require strong clustering for activation, and therefore permits sustained signaling through a more steady rate of activation of individual ligand-receptor complexes or smaller clusters (Figure 1.5E, Figure S1.6I).

The stochastic and infrequent nature of the observed Dll1-mediated pulses could in principle emerge either at the step of cluster assembly or cluster activation. However, the observation that Dll1 expression level modulates pulse frequency more strongly than pulse amplitude (Figure 1.2) is more consistent with a process limited by cluster assembly. Amplitude modulation by Dll4 expression could similarly reflect changes in the rates of ligand-receptor complex formation, with the proteolytic nature of the Notch activation process being balanced by local protein replenishment in both types of signaling. Future studies should provide a more complete understanding of the molecular and biophysical basis of encoding by directly testing the sensitivity of transendocytosis to ligand-receptor clustering, and elucidating the mechanism and dynamics of the clustering process. Such a program would also complement recent efforts towards directly perturbing receptor clustering (Seo et al., 2017).

Decoding of Notch dynamics is evident in the distinct responses of Hes and Hey Notch target genes to different durations of Notch activation (Figure 1.3). Known features of the Hes/Hey system, including negative autoregulation and short half-life of Hes1, and negative cross-regulation of Hes1 and Hey1/L could play roles in decoding (Fischer and Gessler, 2007; Heisig et al., 2012; Kobayashi and Kageyama, 2014). Interestingly, previous work has reported similar reciprocal dynamics of the homologous *Drosophila* Hairy/E(spl) Notch target genes in response to Notch activation (Housden et al., 2013; Krejcí et al., 2009), raising the question of whether dynamic ligand discrimination existed ancestrally, and whether it is also utilized in species, such as *Drosophila*, that possess fewer ligands.

The Hes and Hey genes are widely utilized and could function as general dynamic decoding modules in other contexts. It would also be interesting to know whether there could be a relationship between the role of Hes1 in decoding and the phenomena of Hes1 oscillations that has now been observed in multiple contexts (Hirata et al., 2002; Kobayashi and Kageyama, 2014). Therefore, a more complete and quantitative understanding of the Hes/Hey decoding circuit, including measurements of homo- and hetero-dimerization patterns and cross-regulation, could provide insight into diverse developmental processes.

Despite their intrinsic differences, there are situations where Dll1 and Dll4 signaling appear qualitatively equivalent. For example, Dll4 can replace Dll1 in the retina (Preuße et al., 2015), possibly due to the expression of a distinct set of Hes/Hey genes (Rocha et al., 2009) that may not implement decoding. In addition, Dll1 may function more like Dll4 at high expression levels, when pulses from multiple sender cells effectively 'merge', and thereby become indistinguishable from sustained activation. This could explain why Dll1 can partially compensate for Dll4 when overexpressed in T-cell differentiation (Mohtashami et al., 2010).

The ability of the Notch pathway to either promote or inhibit somite myogenesis, depending on the activating ligand (Figure 1.4), challenges the conventional view that Notch activity promotes a single fate in any given context, and shows that a seemingly minor change in ligand usage, i.e. from Dll1 to Dll4, can have dramatic consequences. Such contrasting roles for Notch ligands have also been reported in other contexts (Gama-

Norton et al., 2015), where signaling dynamics remain uninvestigated. This importance of ligand-choice and Notch dynamics towards controlling cellular responses has implications for therapeutic interventions targeting Notch signaling and for directed differentiation applications that require control of Notch-dependent cell fate decisions (Andersson and Lendahl, 2014; Behar et al., 2013; Dahlberg et al., 2011; Mohtashami et al., 2010).

The use of dynamics to transmit multiple signals through the same pathway occurs in other systems (Purvis and Lahav, 2013) including p53 (Batchelor et al., 2011; Purvis et al., 2012), NFAT (Noren et al., 2016; Yissachar et al., 2013), NFκB (Cheong et al., 2008; Covert et al., 2005), growth factor signaling(Marshall, 1995; Santos et al., 2007), and yeast stress response (Hansen and O'Shea, 2016; Hao and O'Shea, 2012), suggesting it is a broadly useful strategy. Dynamic encoding could be particularly beneficial when the amplitude of signaling is difficult to control precisely, due to variability in expression or cell contact. Signaling pathways such as TGF-β, BMP, and Wnt, like Notch, also utilize multiple ligands capable of interacting with multiple receptors. This raises the question of whether these different ligands can be discriminated by signal-receiving cells, and, if so, whether this discrimination involves dynamics. Finally, pulsatile and sustained signaling could also provide different patterning capabilities in highly dynamic Notch-dependent patterning processes such as neurogenesis (Imayoshi and Kageyama, 2014), lateral inhibition (Barad et al., 2010; Cohen et al., 2010), and somitogenesis (Oates et al., 2012; Pourquié, 2011). Ultimately, the discovery that the Notch pathway can transmit more and

different types of information than previously suspected should help to explain how it enables such an extraordinary range of outcomes, in development and physiology.

2.10 References

Allan, A.L., Albanese, C., Pestell, R.G., and LaMarre, J. (2001). Activating transcription factor 3 induces DNA synthesis and expression of cyclin D1 in hepatocytes. J. Biol. Chem. *276*, 27272–27280.

Andersson, E.R., and Lendahl, U. (2014). Therapeutic modulation of Notch signalling [mdash] are we there yet? Nat. Rev. Drug Discov. *13*, 357–378.

Andrawes, M.B., Xu, X., Liu, H., Ficarro, S.B., Marto, J.A., Aster, J.C., and Blacklow, S.C. (2013). Intrinsic selectivity of Notch 1 for Delta-like 4 over Delta-like 1. J. Biol. Chem. *288*, 25477–25489.

Barad, O., Rosin, D., Hornstein, E., and Barkai, N. (2010). Error minimization in lateral inhibition circuits. Sci. Signal. *3*, ra51.

Bardot, B., Mok, L.-P., Thayer, T., Ahimou, F., and Wesley, C. (2005). The Notch amino terminus regulates protein levels and Delta-induced clustering of Drosophila Notch receptors. Exp. Cell Res. *304*, 202–223.

Batchelor, E., Loewer, A., Mock, C., and Lahav, G. (2011). Stimulus-dependent dynamics of p53 in single cells. Mol. Syst. Biol. *7*, 488.

Behar, M., Barken, D., Werner, S.L., and Hoffmann, A. (2013). The dynamics of signaling as a pharmacological target. Cell *155*, 448–461.

Bintu, L., Yong, J., Antebi, Y.E., McCue, K., Kazuki, Y., Uno, N., Oshimura, M., and Elowitz, M.B. (2016). Dynamics of epigenetic regulation at the single-cell level. Science *351*, 720–724.

Bray, S.J. (2016). Notch signalling in context. Nat. Rev. Mol. Cell Biol. *17*, 722–735.

Cappellari, O., Benedetti, S., Innocenzi, A., Tedesco, F.S., Moreno-Fortuny, A., Ugarte, G., Lampugnani, M.G., Messina, G., and Cossu, G. (2013). Dll4 and PDGF-BB convert committed skeletal myoblasts to pericytes without erasing their myogenic memory. Dev. Cell *24*, 586–599.

Castel, D., Mourikis, P., Bartels, S.J.J., Brinkman, A.B., Tajbakhsh, S., and Stunnenberg, H.G. (2013). Dynamic binding of RBPJ is determined by Notch signaling status. Genes Dev. *27*, 1059–1071.

Cheong, R., Hoffmann, A., and Levchenko, A. (2008). Understanding NF-kappaB signaling via mathematical modeling. Mol. Syst. Biol. *4*, 192.

Chitnis, A. (2006). Why is delta endocytosis required for effective activation of notch? Dev. Dyn. *235*, 886–894.

Choi, H.M.T., Chang, J.Y., Trinh, L.A., Padilla, J.E., Fraser, S.E., and Pierce, N.A. (2010). Programmable in situ amplification for multiplexed imaging of mRNA expression. Nat. Biotechnol. *28*, 1208–1212.

Choi, H.M.T., Calvert, C.R., Husain, N., Huss, D., Barsi, J.C., Deverman, B.E., Hunter, R.C., Kato, M., Lee, S.M., Abelin, A.C.T., et al. (2016). Mapping a multiplexed zoo of mRNA expression. Development *143*, 3632–3637.

Cohen, M., Georgiou, M., Stevenson, N.L., Miodownik, M., and Baum, B. (2010). Dynamic filopodia transmit intermittent Delta-Notch signaling to drive pattern refinement during lateral inhibition. Dev. Cell *19*, 78–89.

Covert, M.W., Leung, T.H., Gaston, J.E., and Baltimore, D. (2005). Achieving stability of lipopolysaccharide-induced NF-kappaB activation. Science *309*, 1854–1857.

Dahlberg, A., Delaney, C., and Bernstein, I.D. (2011). Ex vivo expansion of human hematopoietic stem and progenitor cells. Blood *117*, 6083–6090.

Elena de Bellard, M., and Bronner-Fraser, M. (2005). Neural crest migration methods in the chicken embryo. Methods Mol. Biol. *294*, 247–267.

Fischer, A., and Gessler, M. (2007). Delta–Notch—and then? Protein interactions and proposed modes of repression by Hes and Hey bHLH factors. Nucleic Acids Res. *35*, 4583–4596.

Fortini, M.E., Rebay, I., Caron, L.A., and Artavanis-Tsakonas, S. (1993). An activated Notch receptor blocks cell-fate commitment in the developing Drosophila eye. Nature *365*, 555–557.

Fryer, C.J., White, J.B., and Jones, K.A. (2004). Mastermind recruits CycC:CDK8 to phosphorylate the Notch ICD and coordinate activation with turnover. Mol. Cell *16*, 509–520.

Gama-Norton, L., Ferrando, E., Ruiz-Herguido, C., Liu, Z., Liu, Z., Guiu, J., Islam, A.B.M.M.K., Lee, S.-U., Yan, M., Guidos, C.J., et al. (2015). Notch signal strength controls cell fate in the haemogenic endothelium. Nat. Commun. *6*, 8510.

Guruharsha, K.G., Kankel, M.W., and Artavanis-Tsakonas, S. (2012). The Notch signalling system: recent insights into the complexity of a conserved pathway. Nat. Rev. Genet. *13*, 654–666.

Gururajan, M., Simmons, A., Dasu, T., Spear, B.T., Calulot, C., Robertson, D.A., Wiest, D.L., Monroe, J.G., and Bondada, S. (2008). Early growth response genes regulate B cell development, proliferation, and immune response. J. Immunol. *181*, 4590–4602.

Hansen, A.S., and O'Shea, E.K. (2016). Encoding four gene expression programs in the activation dynamics of a single transcription factor. Curr. Biol. *26*, R269–R271.

Hao, N., and O'Shea, E.K. (2012). Signal-dependent dynamics of transcription factor translocation controls gene expression. Nat. Struct. Mol. Biol. *19*, 31–39.

Heisig, J., Weber, D., Englberger, E., Winkler, A., Kneitz, S., Sung, W.-K., Wolf, E., Eilers, M., Wei, C.-L., and Gessler, M. (2012). Target gene analysis by microarrays and chromatin immunoprecipitation identifies HEY proteins as highly redundant bHLH repressors. PLoS Genet. *8*, e1002728.

Hirata, H., Yoshiura, S., Ohtsuka, T., Bessho, Y., Harada, T., Yoshikawa, K., and Kageyama, R. (2002). Oscillatory expression of the bHLH factor Hes1 regulated by a negative feedback loop. Science *298*, 840–843.

Housden, B.E., Fu, A.Q., Krejci, A., Bernard, F., Fischer, B., Tavaré, S., Russell, S., and Bray, S.J. (2013). Transcriptional dynamics elicited by a short pulse of notch activation involves feed-forward regulation by E(spl)/Hes genes. PLoS Genet. *9*, e1003162.

Ilagan, M.X.G., Lim, S., Fulbright, M., Piwnica-Worms, D., and Kopan, R. (2011). Real-time imaging of notch activation with a luciferase complementation-based reporter. Sci. Signal. *4*, rs7.

Imayoshi, I., and Kageyama, R. (2014). bHLH factors in self-renewal, multipotency, and fate choice of neural progenitor cells. Neuron *82*, 9–23.

Kesarwani, M., Kincaid, Z., Gomaa, A., Huber, E., Rohrabaugh, S., Siddiqui, Z., Bouso, M.F., Latif, T., Xu, M., Komurov, K., et al. (2017). Targeting c-FOS and DUSP1 abrogates intrinsic resistance to tyrosine-kinase inhibitor therapy in BCR-ABL-induced leukemia. Nat. Med. *23*, 472–482.

Kobayashi, T., and Kageyama, R. (2014). Expression dynamics and functions of Hes factors in development and diseases. Curr. Top. Dev. Biol. *110*, 263–283.

Kopan, R., Schroeter, E.H., Weintraub, H., and Nye, J.S. (1996). Signal transduction by activated mNotch: importance of proteolytic processing and its regulation by the extracellular domain. Proc. Natl. Acad. Sci. U. S. A. *93*, 1683–1688.

Krejcí, A., Bernard, F., Housden, B.E., Collins, S., and Bray, S.J. (2009). Direct response to Notch activation: signaling crosstalk and incoherent logic. Sci. Signal. *2*, ra1.

LeBon, L., Lee, T.V., Sprinzak, D., Jafar-Nejad, H., and Elowitz, M.B. (2014). Fringe proteins modulate Notch-ligand cis and trans interactions to specify signaling states. Elife *3*, e02950.

Lecourtois, M., and Schweisguth, F. (1998). Indirect evidence for Delta-dependent intracellular processing of notch in Drosophila embryos. Curr. Biol. *8*, 771–774.

Marshall, C.J. (1995). Specificity of receptor tyrosine kinase signaling: transient versus sustained extracellular signal-regulated kinase activation. Cell *80*, 179–185.

Meloty-Kapella, L., Shergill, B., Kuon, J., Botvinick, E., and Weinmaster, G. (2012). Notch ligand endocytosis generates mechanical pulling force dependent on dynamin, epsins, and actin. Dev. Cell *22*, 1299–1312.

Mohtashami, M., Shah, D.K., Nakase, H., Kianizad, K., Petrie, H.T., and Zúñiga-Pflücker, J.C. (2010). Direct comparison of Dll1- and Dll4-mediated Notch activation levels shows differential lymphomyeloid lineage commitment outcomes. J. Immunol. *185*, 867–876.

Nichols, J.T., Miyamoto, A., Olsen, S.L., D'Souza, B., Yao, C., and Weinmaster, G. (2007). DSL ligand endocytosis physically dissociates Notch1 heterodimers before activating proteolysis can occur. J. Cell Biol. *176*, 445–458.

Noren, D.P., Chou, W.H., Lee, S.H., Qutub, A.A., Warmflash, A., Wagner, D.S., Popel, A.S., and Levchenko, A. (2016). Endothelial cells decode VEGF-mediated Ca2+ signaling patterns to produce distinct functional responses. Sci. Signal. *9*, ra20.

Oates, A.C., Morelli, L.G., and Ares, S. (2012). Patterning embryos with oscillations: structure, function and dynamics of the vertebrate segmentation clock. Development *139*, 625–639.

Pourquié, O. (2011). Vertebrate segmentation: from cyclic gene networks to scoliosis. Cell *145*, 650–663.

Preuße, K., Tveriakhina, L., Schuster-Gossler, K., Gaspar, C., Rosa, A.I., Henrique, D., Gossler, A., and Stauber, M. (2015). Context-Dependent Functional Divergence of the Notch Ligands DLL1 and DLL4 In Vivo. PLoS Genet. *11*, e1005328.

Purvis, J.E., and Lahav, G. (2013). Encoding and decoding cellular information through signaling dynamics. Cell *152*, 945–956.

Purvis, J.E., Karhohs, K.W., Mock, C., Batchelor, E., Loewer, A., and Lahav, G. (2012). p53 dynamics control cell fate. Science *336*, 1440–1444.

Rios, A.C., Serralbo, O., Salgado, D., and Marcelle, C. (2011). Neural crest regulates myogenesis through the transient activation of NOTCH. Nature *473*, 532–535.

Rocha, S.F., Lopes, S.S., Gossler, A., and Henrique, D. (2009). Dll1 and Dll4 function sequentially in the retina and pV2 domain of the spinal cord to regulate neurogenesis and create cell diversity. Dev. Biol. *328*, 54–65.

Santos, S.D.M., Verveer, P.J., and Bastiaens, P.I.H. (2007). Growth factor-induced MAPK network topology shapes Erk response determining PC-12 cell fate. Nat. Cell Biol. *9*, 324–330.

Seo, D., Southard, K.M., Kim, J.-W., Lee, H.J., Farlow, J., Lee, J.-U., Litt, D.B., Haas, T., Alivisatos, A.P., Cheon, J., et al. (2017). A Mechanogenetic Toolkit for Interrogating Cell Signaling in Space and Time. Cell *169*, 1357.

Sprinzak, D., Lakhanpal, A., Lebon, L., Santat, L.A., Fontes, M.E., Anderson, G.A., Garcia-Ojalvo, J., and Elowitz, M.B. (2010). Cis-interactions between Notch and Delta generate mutually exclusive signalling states. Nature *465*, 86–90.

Struhl, G., and Adachi, A. (1998). Nuclear access and action of notch in vivo. Cell *93*, 649–660.

Weinmaster, G., and Fischer, J.A. (2011). Notch ligand ubiquitylation: what is it good for? Dev. Cell *21*, 134–144.

Yissachar, N., Sharar Fischler, T., Cohen, A.A., Reich-Zeliger, S., Russ, D., Shifrut, E., Porat, Z., and Friedman, N. (2013). Dynamic response diversity of NFAT isoforms in individual living cells. Mol. Cell *49*, 322–330.

2.11 Supplementary Figures

Figure S1.1

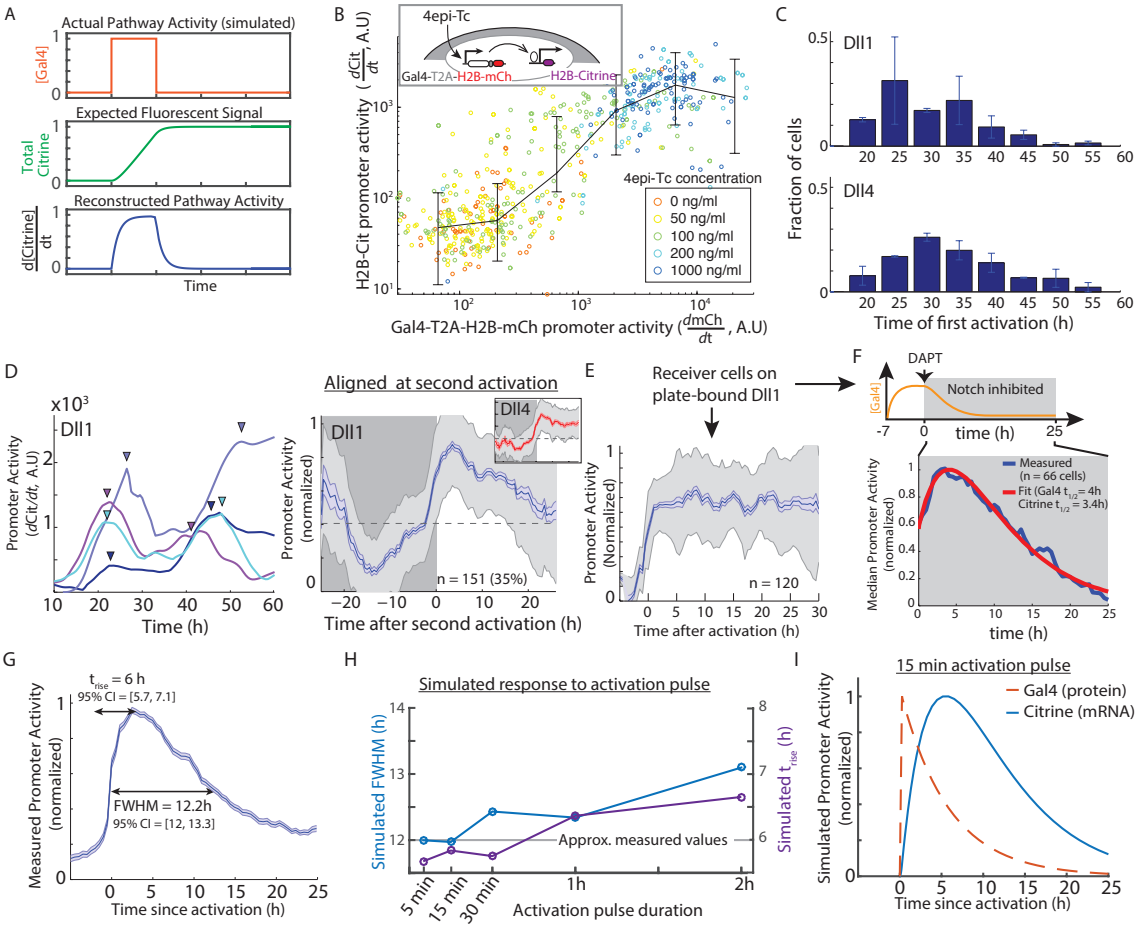

Characterization of diverted Notch reporter system and pulse features. **A**, Simulation showing how the derivative of total fluorescence (= 'Promoter Activity') can recover underlying Notch activation dynamics. In response to a simulated pulse of Gal4 (orange trace), H2B-Citrine reporter fluorescence increases ('Total Citrine', green). The first derivative of total Citrine fluorescence in an individual cell (blue trace) provides a reconstructed estimate of the active Gal4 concentration (compare 'Reconstructed Pathway Activity' and 'Actual Pathway Activity'). **B**, Correlation between Gal4 levels and promoter activity of the fluorescent reporter gene. (*Inset*) The cell line used for experiment expresses Gal4 (white, with a co-translationally expressed H2B-mCherry cassette, red) under control of a 4epi-Tetracycline ('4epi-Tc') inducible promoter. These cells also contain a fluorescent H2B-Citrine reporter gene (purple) that is responsive to Gal4 protein. (*Main plot*). Scatter plot of maximal (Gal4-T2A)-H2B-mCherry production rate (95th percentile value of promoter activity *d*mCherry/*d*t) vs. the maximal promoter activity of the H2B-Citrine reporter gene rate (95th percentile value of promoter activity *d*Citrine/*d*t), for

different levels of 4epi-Tc induction. Each circle represents the response in a single cell. The line indicates median values of promoter activity within equally-spaced bins of H2B-mCherry levels, and error bars indicate 25th to 75th percentile levels of the distribution of values within each bin. Cell-to-cell variability in induction of the reporter is partly due to extrinsic noise and can be observed in the promoter activity of a co-expressed constitutive H2B-Cerulean gene. Note that since the units of total fluorescence are arbitrary, the resulting derivatives also arbitrary units (A.U). **C**, Distribution of time points at which cells first activate during the Dll1 (*top*) or Dll4 (*bottom*) excess sender co-culture. Error bars indicate standard error of the mean (n = 2 experiments). **D**, (*Left*) Representative traces of cells displaying two pulses during co-culture with Dll1 (same dataset as in Figure 1D, E). Arrowheads indicate pulse peaks. See Supplementary Movie 3. (*Right*) Median response profile of receiver cells activated by Dll1 that could not be classified as single pulses (see Figure 1D caption, see Methods for alignment procedure), aligned *after* a period corresponding to the first pulse (7.5h). Each trace is aligned at a point when the promoter activity subsequent to the initial phase of activation (0-7.5h) again reaches the peak activity of the initial phase (n = 151 traces, 35% of all traces, cf. Dll1 response in Figure 1D). Each trace is individually normalized to the 90th percentile of promoter activity values between the alignment point and the end of the trace. Solid line indicates the median of the normalized promoter activity, light shaded areas show standard error of the mean, and the light gray shaded area indicates the standard deviation. The dark grey box indicates time period prior to the alignment time point, and the dashed horizontal line indicates the median level of (normalized) promoter activity at the alignment point. The median response in Dll1 returns to this level after 25h, consistent with a systematic second pulse of activity. (*Inset*) The same procedure applied to the Dll4 data (from Figure 1D) does not reveal a second pulse. **E**, Median promoter activity of receiver cells (same as Figure 1B) cultured on plate-bound Dll1ECD-Fc. Also shown are standard errors of the mean (light colored lines) and standard deviations (grey areas). See Methods for normalization and alignment procedure. **F**, (*Top, schematic*) Expected Gal4 response (orange trace) in cells allowed to activate for 7h, then inhibited (indicated by grey shading) by treatment with DAPT (t = 0h). (*Bottom*) Median promoter activity in receiver cells (blue line) after DAPT treatment. Red line shows simulated response using fitted parameters for Gal4 protein half life ('Gal4 $t_{1/2}$' = 4h, 95% bootstrapped confidence interval [3.8, 4]) and H2B-Citrine mRNA half life ('Citrine $t_{1/2}$' = 3.4h, 95% bootstrapped confidence interval [3.4, 3.5]). See Methods for fitting procedure and Supplementary Information for model. **G**, Median (blue line) and standard error of the mean (s.e.m., lighter blue region) of normalized Dll1 pulse promoter activities (same as Figure 1d). 't_{rise}' denotes time from 10% to 90% of the peak promoter activity, and FWHM denotes the full-width at half-maximum of the peak promoter value. '95% CI' indicates bootstrapped confidence intervals. **H**, Dependence of FWHM (blue circles) and t_{rise} (purple circles) values on duration of underlying Notch activation ('Activation pulse duration') based on a mathematical model for pulse-like activation, using values calculated in panel E (see Supplementary Information). The horizontal grey line indicates measured values for these quantities; the vertical grey line indicates a value for underlying pulse duration beyond which the simulated values differ systematically from the measured values. **I**, Simulated time-course of Gal4 protein (orange, dashed) and H2B-Citrine mRNA (blue) for

15 min Notch activation, using values for half-lives calculated in panel E. Note similarity with measured pulse shape in panel G.

Figure S1.2

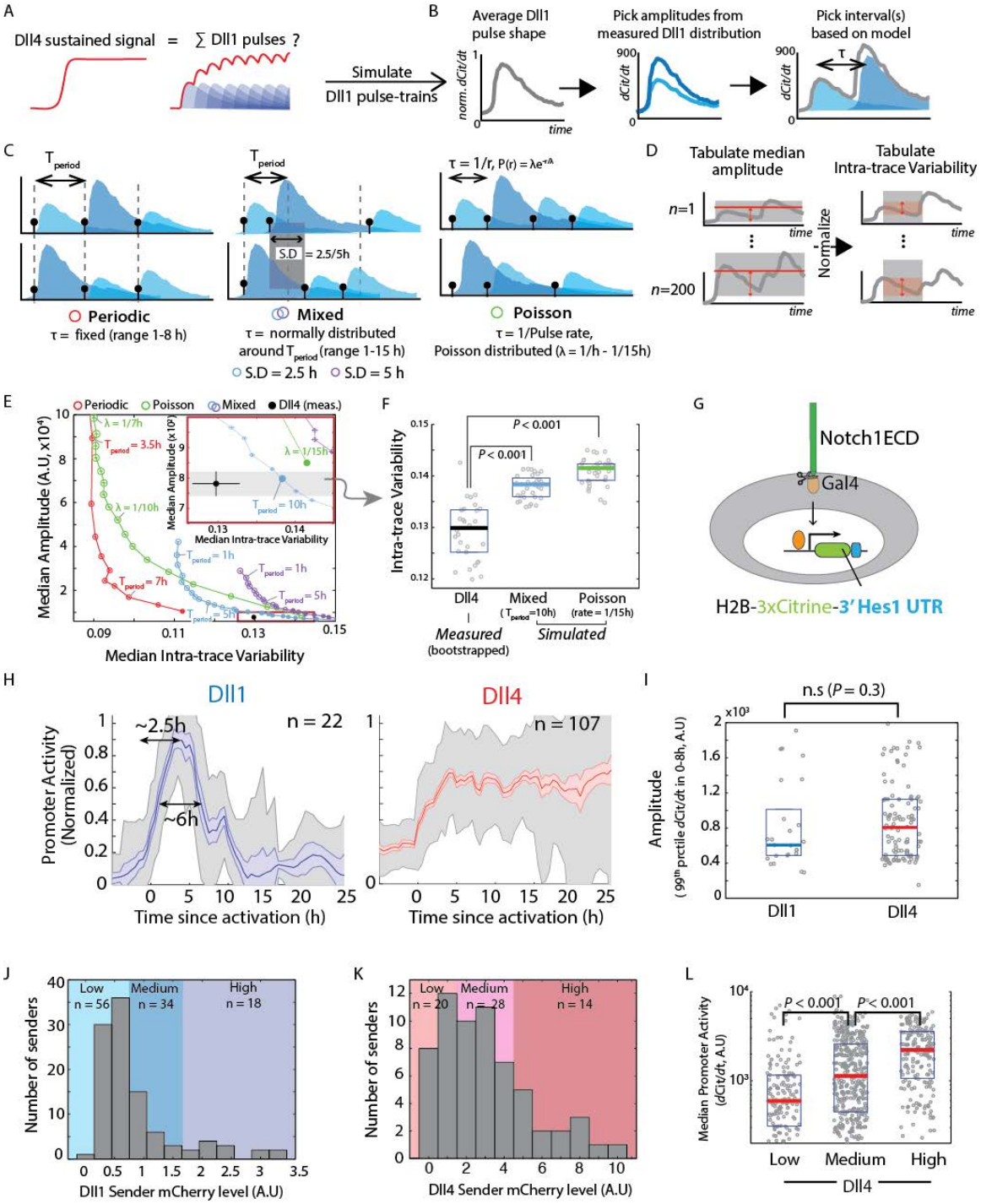

Pulse train model and analysis of increased time-resolution reporter. A-F Comparison of simulated Dll1 pulse trains to observed Dll4-induced responses. **A**, (*Schematic*) Can sustained Dll4 signal (red) be composed of a series of Dll1-like pulses (blue)? **B**, Schematic diagram illustrating the pulse train simulation procedure (see also Supplementary Information). Each pulse train is constructed from a series of pulses with the average Dll1 pulse shape (*Left schematic,* median of averaged traces in Figure 1D), scaled by an amplitude randomly sampled from the empirically measured distribution of Dll1 pulse amplitudes (*Center schematic*). Each pair of adjacent pulses (shades of blue) is temporally separated by an interval τ chosen based on one of the underlying pulse models shown in C, and combined to generate a particular pulse train (*Right schematic,* grey line). **C**, Schematics illustrating the underlying pulsing models. In each case two example traces are shown (top and bottom). (*Left*) In the Periodic model, the interval τ between adjacent pulses is fixed at a value T_{period}, that can range from 1h to 8h. Periods greater than 8h result in oscillating pulse trains in which the individual pulses can be clearly discerned. (*Right*) In the Poisson model, the interval between pulses i and i+1, τ_i, represents the inverse of a pulse rate, r_i, drawn from a Poisson distribution with parameter, λ, ranging from $1h^{-1}$-$15h^{-1}$. (*Center*) The mixed models interpolate between fixed and random intervals. In these models, the interval τ between adjacent pulses is drawn from a normal distribution with mean T_{period} (range 1- 15h) and standard deviation σ (= 2.5h or 5h). See Supplementary Information for further details. **D**, For each simulation, 200 pulse trains were simulated ('n' = 1 to 200). For each simulated trace, the median amplitude (*Left*) and the median temporal variability ('Intra-trace' variability, *Right*) were tabulated (see Supplementary Information). **E**, Relationship between median amplitude and median intra-trace variability for the different models. Each point corresponds to a different mean interval, and represents the median of 36 simulations. The black marker shows measured values of median amplitude and median intra-trace variability for Dll4 traces (using the data in Figure 1D, E). (*Inset*) Zoom into the region (red box) of the Dll4 data point (black). Error bars on Dll4 marker represent S.E.M (n = 200 traces). The grey shaded area delineates region of the plot that has median amplitude within the measured error in the Dll4 median amplitude. Filled circles are points in the mixed (σ = 2.5h, T_{period} = 10h) and poisson (λ = 1/15h) models closest to the experimental measurement. **F**, Boxplot comparison between median intra-trace variability in the simulations highlighted in E (inset) and the intra-trace variability measured for Dll4. For simulations, each point represents a single simulation (comprising 200 pulse trains). The colored horizontal lines (blue or green) represent the median value of these simulations (n = 36 simulations), while boxes delineate 25^{th} – 75^{th} percentile values. The black horizontal line represents a bootstrapped average of intra-trace variability values calculated from measured Dll4 data. See Supplementary Information for further details. *P*-value calculated by two-sided KS-test. **G**, (*Schematic*) Improved time-resolution reporter cell line, expressing the NotchECD (green)-Gal4 (orange) receptor and a Gal4-responsive H2B-3xCitrine (chartreuse) fused to 3'UTR (blue) derived from the mouse Hes1 gene (cf. Figure 1B, see Methods). **H**, Median normalized promoter activity of reporter cells co-cultured with either Dll1- (blue) or Dll4- (red) expressing sender cells. Also shown are standard errors of the mean (light colored lines) and standard deviations

(grey areas). See Methods for alignment and normalization procedure. Note the decreased values of rise time ('t_{rise}') and full width at half max ('FWHM') of the Dll1 pulse compared to S1G, which shows corresponding values for the original reporter cell line. **I**, Boxplots of maximal promoter activities of reporter cells in response to Dll1 (blue) or Dll4 (red), calculated for the traces averaged in b. Colored lines represent median values, and boxes delimit 25th to 75th percentile values. *P* value calculated using two-sided KS-test. **J**, Distribution of mCherry levels in Dll1-T2A-H2B-mCherry sender cells used in Figure 1.2B-C, with 'Low', 'Medium', and 'High' fractions delineated. 'n' values correspond to the number of sender cells in the experiment (cf. Figure 1.2B). **K**, Distribution of mCherry levels in Dll4-T2A-H2B-mCherry sender cells used in Figure 1.2B-C, with 'Low', 'Medium', and 'High' fractions delineated. 'n' values correspond to the number of sender cells in the experiment (cf. Figure 1.2B). **L**, Comparison of *median* promoter activities in activated receiver cells adjacent to sender cells expressing Low (light blue), Medium (navy blue), or High (dark blue) levels of Dll4 (same designations as used in Figure 1.2B). Grey circles represent individual responses, solid horizontal lines represent medians, while the boxes delineate 25th - 75th percentile values. *P*-values calculated by two-sided KS-test.

Figure S1.3

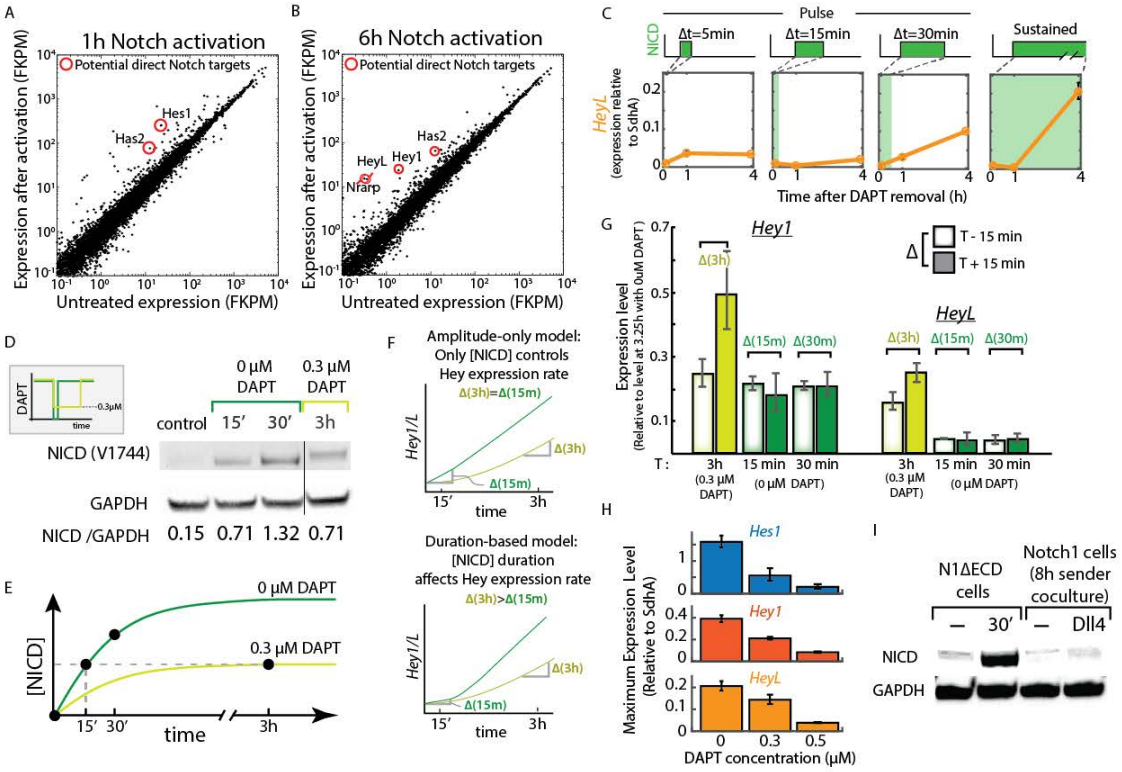

Duration dependence of gene expression in C2C12 cells. A, Transcript levels in C2C12-N1ΔECD cells in DMSO-treated cells vs. cells activated for 1h by DAPT removal. Circled genes are putative direct Notch targets, up-regulated by >5-fold (Supplementary Table 1.2).

B, Transcript levels in C2C12-N1ΔECD cells in DMSO-treated cells vs. cells activated for 6h by DAPT removal. Circled genes are putative direct Notch targets up-regulated by >5-fold (Supplementary Table 1.3). **C**, Response of HeyL (orange) to complete DAPT removal for 5 min, 15 min, or 30 min followed by replenishment ('Pulse'), or removal without replenishment ('Sustained'). Error bars represent S.E.M for duplicate experiments. **D**, (*Schematic*) For the experiment, DAPT is either washed out completely (final concentration 0 μM) for a brief period (15 min or 30 min, chartreuse line) or partially (final concentration 0.3 μM) for 3h (green line). (*Main panel*) Western blot analysis of cleaved NICD levels in cells after different DAPT washout treatments. NICD is detected using an antibody that detects the cleaved version (with N-terminal Val at amino acid position 1744, see Methods). GAPDH levels represent the loading control. Note similar levels of NICD at 15' and 3h samples. The vertical line indicates splicing together of two parts of the same western blot (removing intervening lanes) **E**, (*Schematic*) Expected time evolution of NICD concentration within cells for complete (green line) or partial (chartreuse line) DAPT washout. Black markers indicate points at which NICD levels are measured in D. **F**, Predictions from Amplitude-only model and Duration-based models for control of Hey expression. (*Top*) In the amplitude-only model, the rate of Hey1/L expression is determined by the concentration of NICD. Therefore, the 15' complete DAPT washout (green line) and 3h partial DAPT washout (chartreuse line), which result in comparable NICD levels, should result in similar increases in Hey1/L expression levels (Δ) during a given time window at the end of treatment. (*Bottom*) In the duration based model, the rate of Hey1/L expression depends on the duration of NICD activation. Specifically, a short period of Notch activation (15') leads to a smaller increase in Hey1/L levels (Δ) during a given time window than a longer period of Notch activation (3h), despite similar NICD levels at the two time points. **G**, Median expression level of Hey1 and HeyL (each normalized to its expression level at 3.25h with complete DAPT removal) 15 min prior to ('T-15 min', empty bars) or 15 min after ('T+15 min', filled bars) a 15 min, 30 min, or 3h period of Notch activation with complete (dark green) or partial (chartreuse) DAPT removal. Error bars represent S.E.M calculated from duplicate experiments. **H**, Maximum Hes1 (blue), Hey1 (burnt orange), and HeyL (orange) mRNA levels measured during the [0h, 1h, 4h] time-course, in response to sustained reduction of DAPT concentration to indicated levels (0, 0.3, or 0.5 μM). Error bars represent S.E.M calculated from duplicate experiments. **I**, Western blot analysis of cleaved NICD levels in N1ΔECD cells (see Figure 1.3A) and receiver cells expressing full-length human Notch1 (Figure S1.4D). N1ΔECD cells (co-cultured with CHO-K1 control cells to match total number of cells in co-culture) were maintained in DAPT (' – ') or DAPT was washed out completely for 30 min ('30 min'). Notch1 receiver cells were co-cultured with CHO-K1 control cells (' – ') or sender cells expressing maximal levels of Dll4 for 8h. NICD is detected using an antibody that detects the cleaved version (with N-terminal Val at amino acid position 1744, see Methods). GAPDH levels represent the loading control.

Figure S1.4

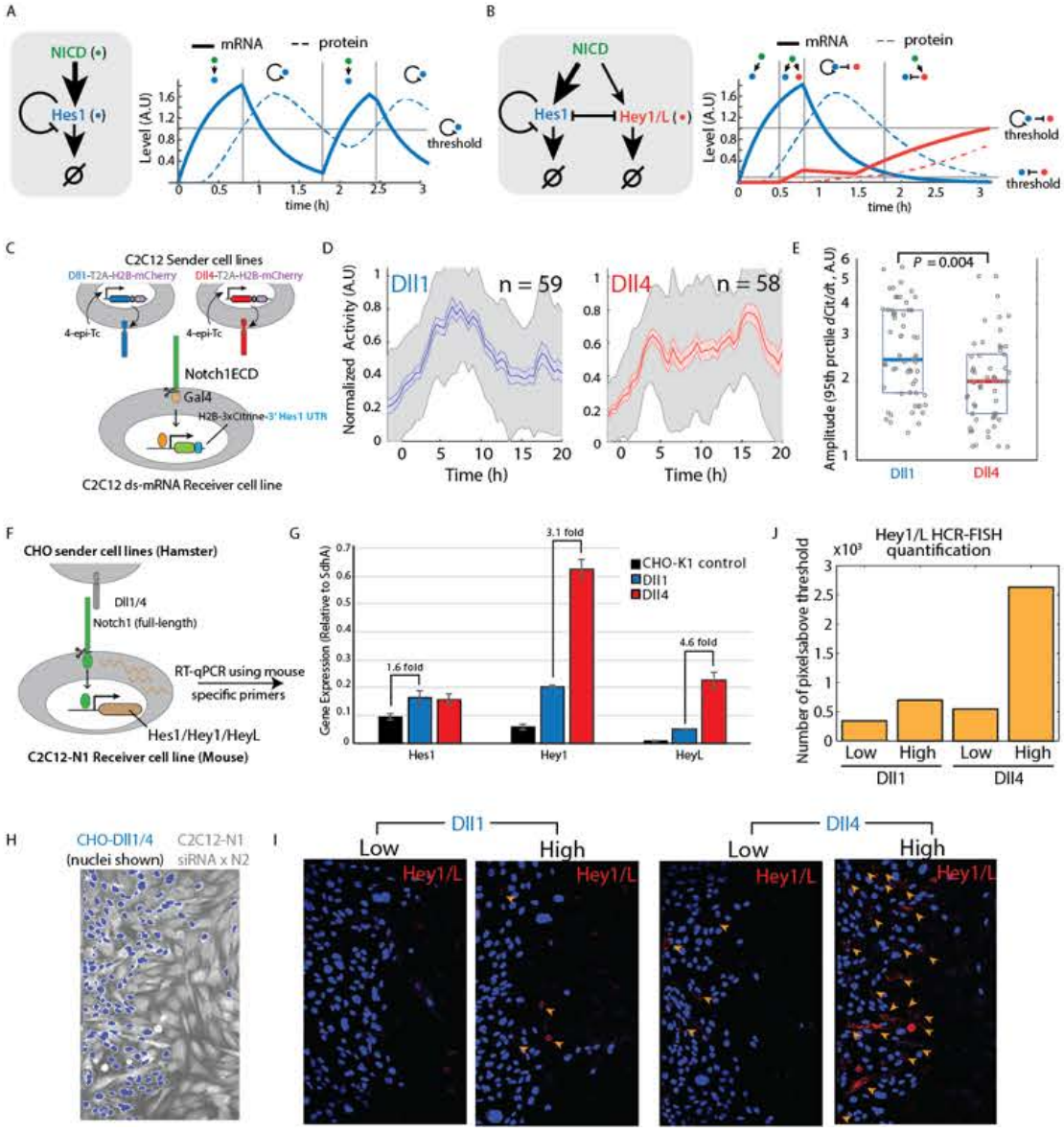

Decoding model and dynamic ligand discrimination in C2C12 cells. A, *(Left)* Circuit comprising only NICD and Hes1, corresponding to response shown in panel f. Hes1 (blue) is induced by Notch Intracellular Domain (NICD, green) and degraded. Hes1 also represses itself. *(Right)* In response to sustained NICD (*top*, green trace), Hes1 displays sustained oscillations (*bottom*) in mRNA (solid trace) and protein (dashed trace) levels. The glyphs (blue dot = Hes1, green dot = NICD) indicate the interactions predominant during each phase of the response. The horizontal line represents the threshold above which Hes1 auto-repression is active. **B**, *(Left)* Circuit with both Hes1 and Hey1, corresponding to response shown in panel h. Both Hes1 (blue) and Hey1 (red) are induced by NICD (green), and degraded, but Hes1 is induced more strongly. Hes1 represses its own production, and Hes1

and Hey1 can mutually repress each other. *(Right)* In response to sustained NICD (*top*, green trace), Hes1 displays a strong, but transient, early response, while Hey1 displays a delayed response. Solid and dashed traces represent mRNA and protein levels, respectively. The glyphs (blue dot = Hes1, red dot = Hey1, green dot = NICD) indicate the interactions most responsible for each phase of the response. The higher and lower horizontal lines represent the thresholds above which repression by Hes1 and repression by Hey1 are active, respectively. A-C, Dll1 and Dll4 activate Notch1 using pulsatile and sustained dynamics, respectively, in C2C12 cells. **C**, *(Top)* Engineered C2C12 sender cell lines contain stably integrated constructs expressing Dll1 (blue) or Dll4 (red), each with a co-translational (T2A, grey) H2B-mCh readout (purple). *(Bottom)* Receiver cell lines stably express a chimeric receptor combining the Notch1 extracellular domain (N1ECD, green) with a Gal4 transcription factor (orange) in place of the endogenous intracellular domain. Cells also contain a stably integrated H2B-3xCitrine fluorescent reporter (green), destabilized at the mRNA level by fusing it with a 3'UTR derived from the Hes1 cDNA (light blue, see Methods). **D**, Median normalized promoter activities in receiver cells co-cultured with an excess of Dll4 (red) or Dll1 (blue) senders. Traces were aligned (see Methods for special alignment procedure) and normalized to their 90^{th} percentile value prior to averaging. Also shown are standard error of the mean (light colored lines), and standard deviations (grey areas). **E**, Boxplots of maximal promoter activities of the responses averaged in panel B. Each grey circle represents the response of a single cell to Dll1 (blue) or Dll4 (red). Colored lines represent the median, while boxes delimit 25^{th} to 75^{th} percentile values. *P* value calculated using two-sided *KS*-test. **F**, (*Schematic*) RT-qPCR based measurement of Hes1/Hey1/HeyL response in C2C12-Notch1 + CHO-Dll1/4 co-cultures. C2C12-Notch1 receiver cells, expressing full length Notch1 (green) are co-cultured with CHO-K1 sender cells expressing either Dll1 or Dll4 (grey). The target genes (shown as brown gene target and corresponding brown mRNA) in C2C12-Notch1 receiver cells are specifically amplified using mouse-specific primers **G**, RT-qPCR expression levels of Hes1, Hey1, and HeyL in C2C12-Notch1 receiver cells co-cultured with CHO-K1 control cells (black), Dll1- (blue), or Dll4-expressing (red) sender cells for 8h. Error bars represent standard error of the mean (n=2 replicates). **H-J**, Characterization of Hey transcriptional response at the single-cell level using HCR-FISH. **H**, CHO sender cells (highlighted with blue nuclei) and C2C12-Notch1 receiver cells (grey cells) were co-cultured such that they interface along a line (see Methods). **I**, HCR-FISH detection of Hey1+HeyL mRNA (red) in C2C12-Notch1 cells co-cultured with sender cells (blue nuclei shown) expressing low or high levels of Dll1 (left panels) or Dll4 (right panels). Arrowheads indicate cells showing clear HCR-FISH signal. **J**, Quantification of panel G images. Values indicate number of pixels in the left half of images that lie above a threshold intensity value.

Figure S1.5

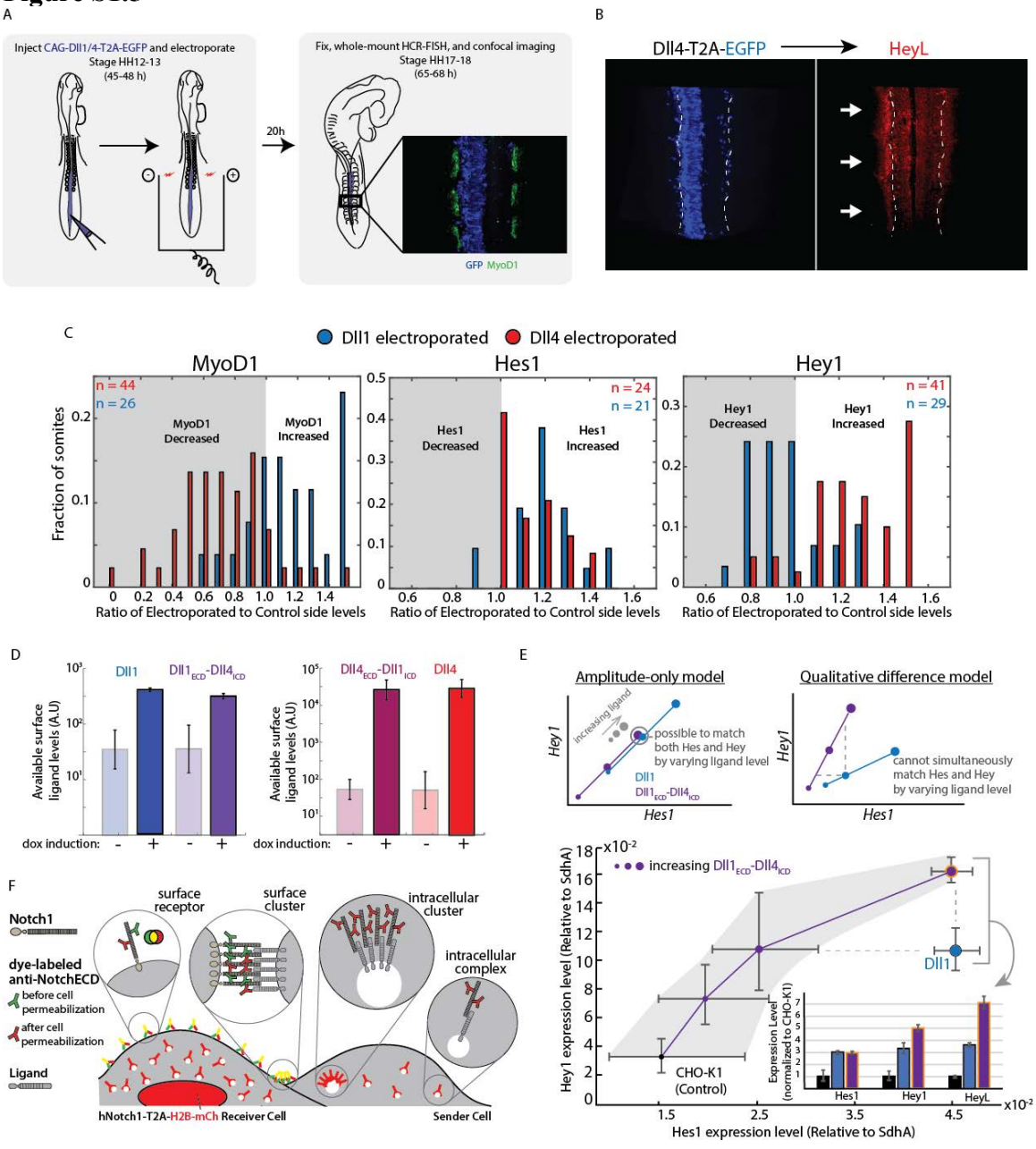

Quantitation of effects on MyoD1, Hes1, and Hey1 *in ovo*, and gene expression response to $Dll1_{ECD}$-$Dll4_{ICD}$ ligand. A, Schematic for chick electroporation experiments. The neural tubes of HH stage 12-13 embryos were injected *in ovo* with CAG-Dll1/4-T2A-EGFP plasmid and a rightward current was applied at the level of the pre-somitic mesoderm. 20h later embryos were dissected, fixed, and subjected to 3-color whole-mount HCR-FISH to detect GFP (blue), MyoD1 (green), and Hes1/Hey1/HeyL (not shown). Inter-limb somites were then imaged using scanning laser confocal microscopy. **B**, Representative image showing an increase in HeyL (red, *right panel*) in the DML of

somites when the neural tube and crest were electroporated with Dll4-T2A-EGFP (blue, *left panel*). Arrows indicate the electroporated side. **C**, Fold-changes in expression of MyoD1, Hes1, and Hey1 within somites (see Methods), in response to electroporation of Dll1 (blue bars) or Dll4 (red bars), calculated relative to the control side. 'n' values correspond to number of somites analyzed. **D**, Cell surface levels of natural and chimeric ligands, detected using soluble Notch1ECD-Fc (see Methods). (*Left*) Dll1 (blue bars) and $Dll1_{ECD}$-$Dll4_{ECD}$ (purple bars) are detected at similar surface levels before ('-', light shading) and after ('+', dark shading) maximal induction with doxycycline ('dox induction'). (*Right*) $Dll4_{ECD}$-$Dll1_{ICD}$ (magenta bars) and Dll4 (red bars) are detected at similar surface levels before (light shading) and after (dark shading) maximal induction. Error bars indicate standard deviation. Note that Notch1ECD has a higher affinity for the Dll4ECD than the Dll1ECD (Andrawes et al., 2013); hence ligand levels detected after induction in the *left* plot are higher than in the *right* plot. **E**, (*Top, schematics*) Expected dose-response behavior of Hes1 and Hey1 gene expression to varying Dll1 (blue) or $Dll1_{ECD}$-$Dll4_{ICD}$ (purple) ligand levels if (*Left*) ligands varied only in the amplitude of signaling ('Amplitude-only' model) and if (*Right*) ligands produced qualitatively different gene expression ('Qualitative-difference' model). In an amplitude-only model, it is possible to simultaneously match the Hes1 and Hey1 gene expression levels produced by one ligand by varying levels of the other. On the other hand, if ligands produced qualitatively different Hes1/Hey1 expression patterns, there exist Hes1/Hey1 expression levels induced by one ligand (for e.g. Dll1) that cannot be matched by varying the levels of the other ligand. (*Bottom*) Hes1 and Hey1 expression levels in N1 receiver cells co-cultured with CHO-K1 cells (control, black marker), Dll1 senders (blue marker), or sender cells expressing three different levels of $Dll1_{ECD}$-$Dll4_{ICD}$ (purple marker, increasing marker sizes indicate increase levels of level induction). Error bars represent S.E.M from duplicate experiments. (*Inset*) Comparison of fold-changes in Hes1, Hey1, and HeyL expression levels (relative to CHO-K1 control co-culture) in receiver cells co-cultured with Dll1 senders (blue bars, same experiment as indicated by blue marker) or $Dll1_{ECD}$-$Dll4_{ICD}$ senders (purple bars with orange outlines, same experiment as indicated by purple marker with orange outline). **F**, Schematic of types of staining observed in co-culture NotchECD immunostaining assay (see Methods) and the molecular species they are expected to represent. Intracellular Notch1 will only be labeled only after cell-permeabilization and should only be detected in a single channel (shown here as red). White circles within cells represent endosomes. All cell-surface Notch1, including unbound and ligand-bound forms, will be labeled both before and after cell-permeabilization; it should thus be detected in two channels (shown here as red + green = yellow). Receiver cells can be distinguished from sender cells based on expression of nuclear H2B-mCherry, which will also be detected in the red channel. Ligand-NotchECD complexes within the sender cell could exhibit two types of staining: large, bright puncta, corresponding to endocytosed ligand-receptor clusters, and low intensity staining, corresponding to individual or few endocytosed ligand-receptor complexes.

Figure S1.6

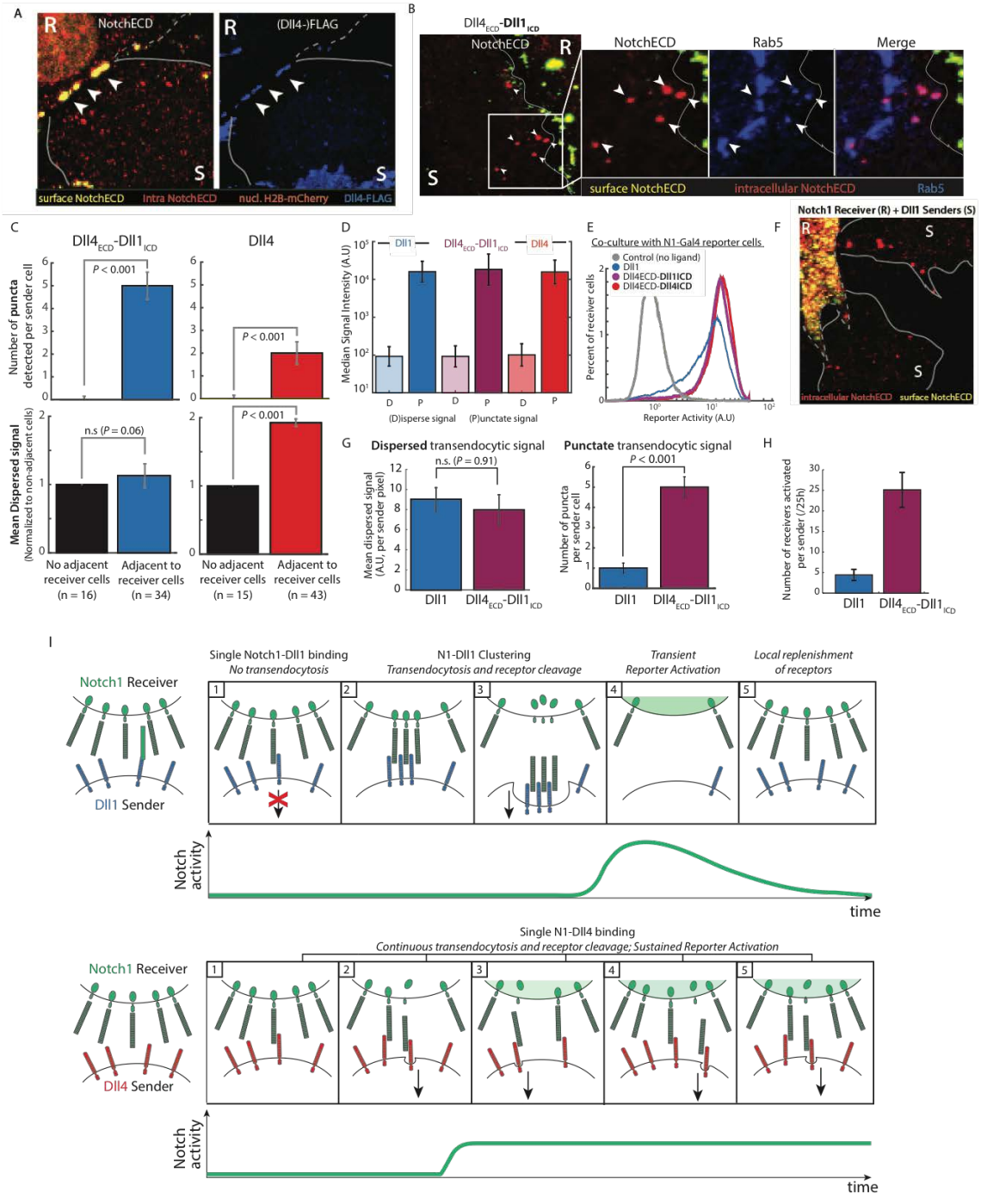

Role of ligand intracellular domains in receptor transendocytosis. A, Representative image showing Dll4 co-localization with Notch in clusters at the cell interface between the Notch1 receiver cell ('R') and a Dll4-FLAG expressing sender cell ('S') shown in Figure 1.5B. Cells are immunostained with antibodies for Notch1ECD (red, green, *left panels*,

same as Figure 1.5B) and FLAG (blue, *right* panels). Cell-surface receptors appear as yellow because they are labeled in two channels (red + green). White arrowheads indicated co-clustered ligands and receptors at the interface between the sender and receiver cell. **B**, Representative image showing co-localization of transendocytosed NotchECD puncta with the early endocytic marker Rab5 within a $Dll4_{ECD}$-$Dll1_{ICD}$ -expressing sender cell ('S') next to a Notch1 receiver cell ('R'). Cells are immunostained for Notch1ECD (red, green) and the early endocytic marker Rab5 (blue). Cell-surface receptors appear as yellow because they are labeled in two channels (red + green). **C**, Transendocytosis staining patterns in $Dll4_{ECD}$-$Dll1_{ICD}$ senders (*Left*) or Dll4 senders (*Right*) adjacent to or not adjacent to receiver cells within the same co-culture. (*Top Left*) Median values of the number of puncta detected (see Methods) in $Dll4_{ECD}$-$Dll1_{ICD}$ sender cells that are adjacent to (magenta bar) or not adjacent to (black bar) receiver cells (see Methods). Error bars represent standard error of the mean. *P* value calculated using the two-sided KS-test. 'n' indicates number of sender cells considered in the analysis. (*Top Right*) Corresponding median values of number of puncta detected in Dll4 cells. (*Bottom Left*) Median values of the mean pixel intensity of dispersed signal in $Dll4_{ECD}$-$Dll1_{ICD}$ sender cells that are adjacent to (magenta bar) or not adjacent to (black bar) receiver cells (see Methods). Error bars represent standard error of the mean. *P* value calculated using the two-sided KS-test. (*Bottom Right*) Corresponding median values of dispersed signal in Dll4 cells. **D**, Median values for intensities of pixels categorized as 'disperse' staining (light shading) and for cumulative intensities of 'puncta' (dark shading) in immunostained co-cultures of receiver cells with Dll1 (blue bars), $Dll4_{ECD}$-$Dll1_{ICD}$ (magenta bars), or Dll4 (red bars) sender cells. Error bars represent standard deviations from the mean. **E**, Flow cytometry histograms of activation levels in a Notch-Gal4 receiver cell line (same as used in Figure 1.1,2, 5A; background activity indicated by grey histogram) co-cultured with Dll1 (blue), $Dll4_{ECD}$-$Dll1_{ICD}$ (magenta) or Dll4 (red) cells expressing ligand levels similar to that used in Figure 1.5C, D. **F**, Representative image of an 'excess sender' co-culture of Notch1 receiver cells ('R') and Dll1 sender cells ('S'), immunostained for NotchECD. The red channel shows staining for intracellular receptors. Cell-surface receptors appear as yellow because they are labeled in two channels (red + green). **G**, (*Left*) Median values of the background subtracted mean pixel intensity of dispersed signal in Dll1 (blue) or $Dll4_{ECD}$-$Dll1_{ICD}$ (magenta) sender cells that abut receiver cells (see Methods). Error bars represent standard error of the mean. *P* value calculated using the two-sided KS-test. (*Right*) Median values of the number of puncta detected (see Methods) in Dll1 (blue) or $Dll4_{ECD}$-$Dll1_{ICD}$ (magenta) sender cells that abut receiver cells. Error bars represent standard error of the mean. *P* value calculated using the two-sided KS-test. **H**, Median values of the rate at which receiver cells are activated by $Dll4_{ECD}$-$Dll1_{ICD}$ (magenta) sender cells or Dll1 (blue) sender cells in excess receiver conditions. Error bars indicate standard error of the mean. **I**, (*Schematic*) Molecular basis of pulsatile and sustained signaling. *Top*, (1) Dll1 ligands (blue) do not activate Notch1 receptors (green) efficiently in single ligand-receptor complexes, but (2) ligand- receptor complexes can assemble into larger clusters, leading to (3) efficient transendocytosis and coordinated activation of constituent receptors in the receiver cell. (4) This releases a burst of NICD (green ovals) which is reflected in a strong pulse of downstream response in receiver cell (green shading, green trace in plot). (5) The system resets (locally) and awaits

another clustering event. *Bottom*, Dll4 ligands (red) transendocytose Notch1 (green) receptors efficiently even when bound in single ligand-receptor complexes (1, 2), or in small clusters (not shown). (3-5) This leads to a steady rate of NICD cleavage (green ovals), and a sustained downstream response in the receiver cell (green shading, green trace in plot).

Figure S1.7

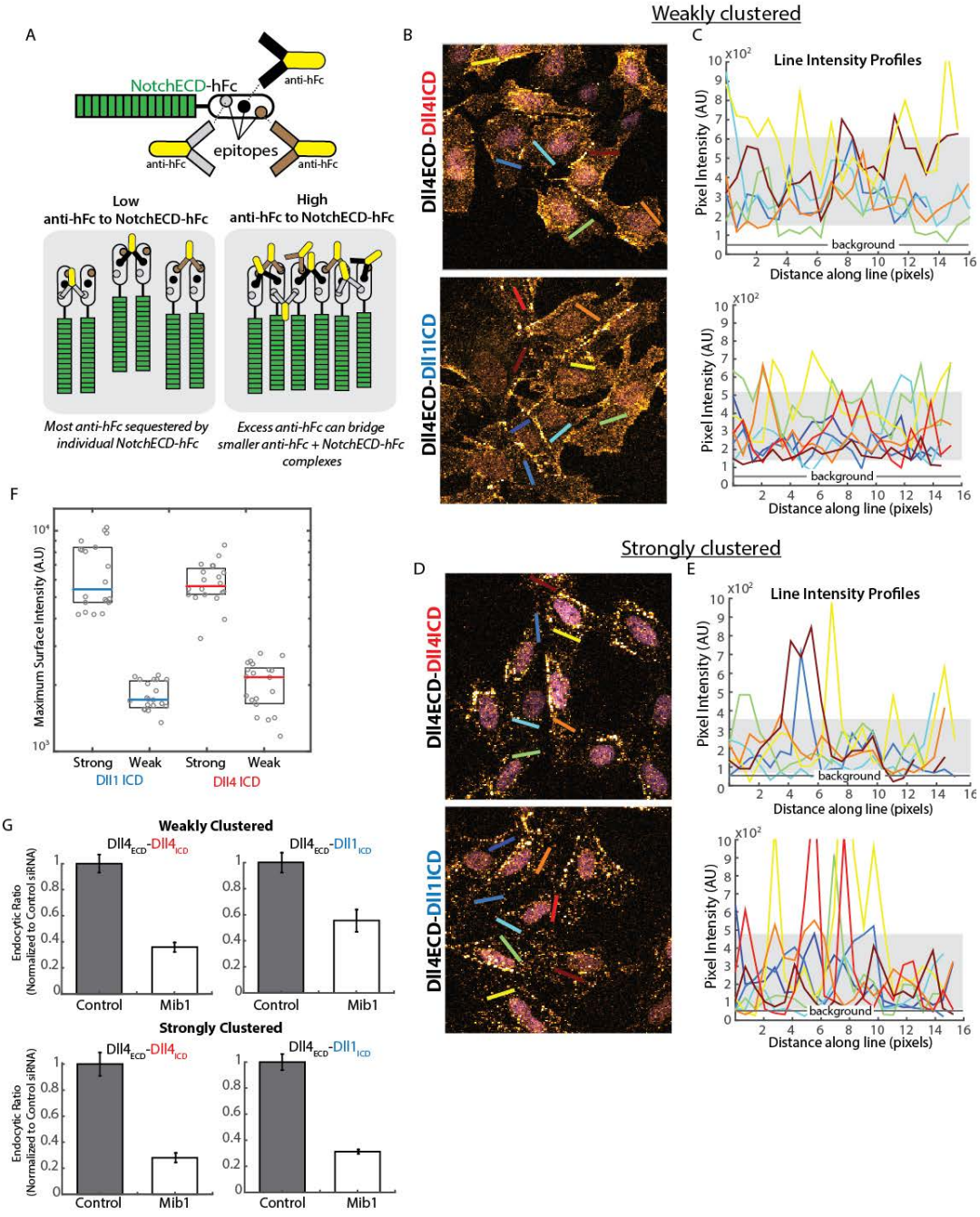

Characterization and validation of bead assay for controlling ligand-receptor clustering. A, Schematic relationship between NotchECD-hFc : anti-hFc ratio and (pre-) clustering levels. (*Top*) The polyclonal nature of the (goat) IgG antibody directed at the human Fc (hFc) domain implies the presence of multiple epitopes (black, grey, brown circles) within the hFc. These epitopes will be recognized by distinct isotypes of anti-hFc, which differ in their bivalent antigen-recognizing domains (black, grey, or brown Fab regions or 'arms'). (*Bottom, left*) When NotchECD-hFc is present in excess of anti-hFc, most antibodies are likely to bind to otherwise free NotchECD-hFc molecules. In the limit, individual complexes will be small, consisting of single anti-Fc molecules attached to two NotchECD-Fc molecules, due to IgG bivalency. Starting from this extreme, as the NotchECD-hFc concentration is reduced, (*bottom, right*) an increasing number of anti-hFc molecules are likely to bind to NotchECD-hFc molecules that are already attached to other anti-hFc molecules through other epitopes. These molecules can act as bridges between sets of NotchECD-Fc molecules, resulting in an increase in the size of individual complexes, each containing multiple NotchECDs located in close proximity to one another, thereby generating *clusters* of NotchECDs. **B**, Representative images of Dll4 ('$Dll4_{ECD}$-$Dll4_{ICD}$', *top*) and $Dll4_{ECD}$-$Dll1_{ICD}$ (*bottom*) cells, exposed to beads coated with weakly-clustered NotchECD-Fc:anti-Fc (2.5 ug/ml NotchECD-Fc + 1:2500 anti-Fc), and later immunostained for surface-bound anti-Fc (see Methods). The colored lines correspond to the line profiles shown in panel c. **C**, Representative profiles of staining intensities along the colored lines shown in the images in panel b. The light gray shaded area delimits the 10^{th} to 90^{th} percentile intensity values, calculated across all profiles. The grey 'background' line represents the median value of pixel intensities along lines chosen outside cells. **D**, Representative images (*left*) of Dll4 ('$Dll4_{ECD}$-$Dll4_{ICD}$', *top*) and $Dll4_{ECD}$-$Dll1_{ICD}$ (*bottom*) cells, exposed to beads coated with strongly-clustered NotchECD-Fc:anti-Fc (0.05 ug/ml NotchECD-Fc + 1:2500 anti-Fc), and later immunostained for surface-bound anti-Fc (see Methods). The colored lines correspond to the line profiles shown in panel e. **E**, Representative profiles of surface staining intensities along the colored lines shown in the images in panel d. The light gray shaded area delimits the 10^{th} to 90^{th} percentile intensity values, across all profiles. The grey 'background' line represents the median value of pixel intensities along lines chosen outside cells. **F**, Boxplots of maximal (99.9^{th} percentile) values of surface staining intensity in different fields of view (grey circles). Colored lines indicate median values, while boxes delimit 25^{th} to 75^{th} percentiles. **G**, Median endocytic ratios for cells that were treated with Mib1 siRNA (white bars) or control siRNA (grey bars), in the weakly (*top*) or strongly (*bottom*) clustered bead assay. Values are normalized to the control siRNA median values. Error bars represent (similarly normalized) standard errors of the mean.

2.13 Methods

Gene constructs

All constructs used in this paper (Supplementary Table 1.4) were assembled using standard restriction enzyme-based cloning and/or Gibson cloning (Gibson et al., 2010). pcDNA3-hNECD-Gal4 (Figure 1.1,2, 5) has been described previously (Sprinzak et al., 2010). The H2B-3xCitrine fluorescent reporter (Figure 1.1, 2, 5) was constructed by cloning 3 repeats of mCitrine in frame with H2B, downstream of a UAS promoter. The mRNA destabilized version of this reporter was constructed by fusing the 3'UTR of mouse Hes1 downstream of the STOP codon. Ligand constructs were cloned into pcDNA5 or *piggyBac* plasmids (System Biosciences Inc.) by fusing the complete rat Dll1 (kind gift from G.Weinmaster) or human Dll4 cDNA in frame with T2A-H2B-mCherry, downstream of a previously described inducible pCMV-TO promoter (Sprinzak et al., 2010) (Figure 1.1, 2, 5). We note that hDll1 shows the same pulsatile behavior described here for rDll1. Chimeric ligands (Figure 1.5) were constructed by exchanging the intracellular domains of rDll1 (aa 561 – 714) and hDll4 (aa 551 – 685). The hN1ΔECD gene (KOPAN et al., 1996) (Figure 1.3) was cloned from hN1 (kind gift from J. Aster) by removing residues 22-1716 and fused in frame with myc-T2A-H2B-mCherry, downstream of the CMV-TO promoter in a *piggyBac* construct. Constructs used for *in ovo* electroporation (Figure 1.4) were made by cloning rDll1 or hDll4 cDNA (minus stop) upstream of, and in frame with, T2A-EGFP in a pCI-CAGG plasmid.

Tissue culture

CHO-K1 (ATCC, No. CCL-61) or CHO-K1-TREx (Invitrogen) cells and their derivatives were grown on tissue-culture grade plastic plates (Thermo Scientific) in Alpha MEM Earle's

Salts (Life Technologies), supplemented with 10% Tet System Approved FBS (ClonTech), 100 U/ml penicillin, 100 ug/ml streptomycin, 0.292 mg/ml L-glutamine (Gibco). C2C12 cells (ATCC, No. CRL-1772) were grown in DMEM (Life Technologies), supplemented with 20% Tet System Approved FBS (ClonTech), 100 U/ml penicillin, 100 ug/ml streptomycin, 0.584 mg/ml L-glutamine (Gibco). C2C12 media was used for CHO-K1 + C2C12 co-culture assays (Figure S1.3). All cells were grown at 37 C in 5% CO2 in a humidified atmosphere. Cells were passaged every 2-3 days, depending on confluency, using 0.05% or 0.25% Trypsin-EDTA (Life Technologies).

Engineering Cell Lines

All cell lines used in this paper (Supplementary Table 1.5) were clonal populations containing stable integrations of all transgenes. To create each stable cell line, the following steps were followed: 1) Cells were first transfected with 800-1000 ng of plasmid DNA using Lipofectamine 2000 or Lipofectamine LTX. 2) 24 h later, cells were transferred to selection media containing 600 ug/ml Geneticin, 500 ug/ml Hygromycin, 400 ug/ml Zeocin, or 10 ug/ml Blasticidin as appropriate. 3) After selection for 1-2 weeks, the resulting multiclonal populations stably expressing the transgene were allowed to recover for ~1 week. 4) Single clones were isolated through the technique of limiting dilution. 5) Single clonal populations were screened for desired behavior, usually high expression (for constitutive genes) or low background expression of the transgene and large dynamic range (for inducible genes and reporter genes). Cell lines incorporating multiple transgenes were constructed by sequential rounds of this process. For *piggybac* constructs, the initial transfection comprised of the

target plasmid along with the construct expressing the *piggybac* transposase, typically in a 1:1 or 2:1 molar ratio.

Co-culture assays and time-lapse microscopy

Used in Figure 1.1,2, 5 and corresponding supplementary figures

Surface treatment: In preparation for plating of cells, glass-bottom multi-well plates (MatTek, No. 1.5 glass, 10 mm radius) were coated with 5 ug/ml Hamster Fibronectin (Oxford Biomedical Research) diluted in 1x phosphate-buffered saline (PBS) for 1h at room temperature.

Cell culture: After trypsinization, sender cells (pre-induced for >48h with 4-epiTc (Sigma)) or CHO-K1 cells were mixed in suspension with similarly trypsinized receiver cells at a ratio of 100:1 or 1:100, for excess sender or excess receiver assays, respectively. A total of $8x10^4$ cells (60% confluence) were plated for each experiment, with continued 4-epiTc induction when appropriate. Imaging commenced 2-4h post-plating.

Time-lapse microscopy: Movies were acquired at 20X (0.75 NA) on an Olympus IX81 inverted epi-fluoresence microscope equipped with hardware autofocus (ZDC2) and an environmental chamber maintaining cells at 37C, 5% CO2. Automated acquisition software (METAMORPH, Molecular Devices) was used to acquire images every 30 min in multiple colors (YFP, RFP, CFP) or differential interference contrast (DIC), from multiple stage positions.

Plate-bound Dll1 assay

Used in Figure S1.1D, E

Recombinant human Dll1IgG-Fc fusion proteins (kind gift from I. Bernstein) were diluted to 1 ug/ml in PBS, and the solution was used to coat the tissue-culture surface. After 1h incubation at room temperature, the solution was removed, and cells were plated for the experiment.

Image segmentation, tracking, and single-cell fluorescence calculation

Used in Figure 1.1,2, 5 and corresponding supplementary figures

Custom MATLAB code (2013a, MathWorks) was used to segment cell nuclei in images based on constitutive CFP/RFP fluorescence or background YFP fluorescence. The segmentation procedure uses edge detection, adaptive thresholds, and the Watershed algorithm to detect nuclear edges. Nuclear segments were then matched in pairs of images corresponding to consecutive time frames, and thus tracked through the duration of the movie. Single-cell tracks were subsequently curated manually. In particular, there were periods where any given cell could not be automatically segmented (typically due to high density) but could be visually followed. In such cases, the tracks corresponding to the cell prior to and after such timeframes were manually linked if fewer than ~5 frames were missing.

Fluorescence data was extracted from nuclear segments by calculating the integrated fluorescence within the segment and subtracting a background fluorescence level estimated from the local neighborhood of the segment. This fluorescence was linearly interpolated

across timeframes where nuclei could not be segmented automatically. Division events were detected automatically, and fluorescence traces were corrected for cell division by adding back fluorescence lost to sister cells. The resulting 'continuized' traces were smoothed and the difference in fluorescence between consecutive time frames was calculated. A smoothed version of this difference was used as the rate of change or promoter activity of the fluorescence.

Analysis of single-cell traces

Used in Figure 1.1,2, 5 and corresponding supplementary figures

Alignment: For each receiver cell trace, including those of cells in control conditions (showing background fluorescence levels) an average rate of fluorescence increase ('average slope') was calculated by dividing the change in total fluorescence of the reporter by the duration of the trace. Traces showing activation were automatically selected for further analysis based on their average slopes surpassing a threshold value, chosen to be higher than average slopes observed in receiver cells under control conditions. Activating traces were aligned at the point of activation, defined as the time point when their promoter activity crosses an absolute threshold level, chosen based on typical promoter activities corresponding to background activity. Note that activations occurring during the first 15h of the movie were typically not considered, to eliminate transient effects produced by cell transfer to imaging conditions.

The same thresholds were always used when direct comparisons were made between ligands or conditions, and we verified (by varying threshold levels) that qualitative results did not depend strongly on the choice of threshold.

For C2C12 dynamics (Figure S1.3) promoter activity could not be reliably used to align traces due to the low levels of reporter activity and resulting noise in the promoter activity data. These traces were instead aligned based on when the total fluorescence levels increased a threshold level.

Double-pulse alignment: In order to align traces showing two pulses in response to Dll1 (Figure S1.1D), *at the second pulse,* the following procedure was used: the first activation was determined using the usual procedure (see above). Traces were then normalized by the peak activity ('Peak1', 95th percentile) in the 0-7.5h window during which the first pulse is expected to reach maximum levels. Starting at 7.5h, i.e. after the peak of the first pulse, traces were re-aligned at the point when the subsequent promoter activity values cross Peak1, and re-normalized to the 90th percentile of values in the period from 7.5h (relative to the first activation point) to the end of the trace.

Normalization: When applied, the object of normalizing the response trace by its amplitude is to demonstrate its stereotyped features, such are *relative* rise time and duration. Un-normalized averaging would distort the shape of the response because higher-amplitude signals are also prolonged, since the timescales of the reporter are fixed by the half-lives of its components (Gal4 protein, H2B-3xCitrine mRNA) and do not scale with amplitude. Traces were typically normalized to the 90th percentile value during the analysis time

window, except in Figure S1.2H, where traces were normalized to the 90th percentile value occurring within 15h after activation.

Amplitudes: While normalized traces were used to make comparisons of the stereotyped shapes of responses (see above), absolute values of promoter activity, calculated from non-normalized promoter activity, are reported in all amplitude comparisons. Except in Figure 1.2C, this amplitude represents the 95th percentile of (absolute, non-normalized) promoter activity values between 0 and 7.5h (after alignment) in the traces. This time window is chosen to simultaneously estimate the promoter activity at the peak of pulses and at steady-state levels of sustained signaling. In Figure 1.2C, the amplitude represents the 95th percentile of promoter activity values during the 25h after activation (the period over which activities are averaged).

Trace filtering*:* In Figure 1D, traces were included in the Dll1 alignment if the median promoter activity between 20-25h fell below 50% of the peak activity (95th percentile) in the 0-7.5h period (after alignment). This criterion was designed to automatically detect single pulses in the data. In Figure 1.2B traces were only included in the Dll1 alignment if the normalized value at 20h fell below 0.7. This filter eliminates traces consisting of multiple pulses, especially in the high Dll1 cases. A similar filter applied to Dll4 traces reveals transiently activated cells, but with qualitatively different behavior, such as a systematic increase in duration and amplitude with increasing Dll4 levels in senders. For C2C12 experiments in Figure 1.3G-H, activating cells were identified based on an increase in total fluorescence levels above a threshold.

Sender cell categorization in excess receiver assays

Used in Figure 1.2 and corresponding supplementary figure

Dll1- and Dll4-T2A-H2B-mCherry sender cells were induced with different 4epi-Tc concentrations, to access their full dynamic range of ligand expression. Following co-culture with receiver cells and timelapse analysis, individual sender cell nuclei were automatically segmented, and mCherry levels were calculated. At the same time, each receiver cell response was automatically associated with the closest sender cell. All data, across 4epi-Tc induction levels, were then pooled, and sender cells re-categorized into 'low', 'medium', or 'high' expression along with their associated receiver cell responses. This process of pooling and recategorization was necessary because of the broad, overlapping distributions in mCherry expression produced by 4epi-Tc treatment.

Statistics

The non-parametric two-sided KS-test was used in Figure 1.2, 1.5 and corresponding supplementary figures to compare the distributions of receiver activation amplitudes in response to different sender cell lines. All pairwise comparisons between samples fulfilled the criterion $n1*n2/(n1 + n2) \geq 4$, where n1 and n2 represent the number of data points in two samples. Under this condition the KS-statistic is greater than the twice the inverse of the Kolmogorov statistic, and the calculated *P*-value is accurate. The non-parametric nature of the KS-test obviates the need to make assumptions regarding the shape of the distributions being compared. Furthermore, since the KS-test compares the distributions directly, and not the mean values, it is sensitive to differences in variance.

When the distribution itself is not shown, variance in the distribution is displayed as standard deviations or s.e.m.

Detection of surface ligand

Used in Figure S1.5D

Recombinant mouse Notch1^{ext}-Fc chimeric protein (R&D Systems) was used for surface-detection of ligands at a concentration of 10 ug/ml, based on a previously described protocol(Lebon et al., 2014).

C2C12 N1ΔECD activation assays

Used in Figure 1.3 and corresponding supplementary figure.

The procedure for activating the Notch pathway in C2C12-hN1ΔECD cells was as follows: Cells were cultured in 10 uM DAPT (Sigma-Aldrich) until the experiment. In order to wash out DAPT, cells were washed quickly twice and a third time for 5 min with media at room temperature. Finally, cells were incubated in medium containing the appropriate activating DAPT concentration (0, 0.3, or 0.5) at 37 C for the required activation duration (5 min, 15 min, 30 min, or until RNA extraction, i.e. sustained). In order to generate a pulse of activation, medium was then replaced with fresh 10 uM DAPT medium.

RNAseq

Used in Figure 1.3 and corresponding supplementary figure.

RNA was prepared using the RNeasy kit (QIAGEN) and submitted to the Caltech sequencing core facility, where cDNA libraries for RNAseq were prepared according to standard Illumina protocols. 100 base single-end read (100SR) sequencing was performed on a HiSeq2500 machine at the same facility. Reads were assembled, aligned, and mapped to the mouse genome (mm9 assembly) on a local instance of the Galaxy server, using Tophat. Cufflinks was used to calculate FPKM values. Raw sequencing reads and processed FKPM data were deposited in the Gene Expression Omnibus (GEO), under accession ID GSE72847. In the analysis, we focused first on genes that showed >5 fold-changes in their FKPM values (highlighted in Supplementary Table 1.2, 3). We further narrowed our subsequent analyses to the transcription factors Hes1, Hey1, and HeyL, because their promoters were shown to directly bind NICD by ChIP-Seq, they show early and strong (>10-fold) responses to NICD, and they are key factors mediating Notch responsive behaviors in many contexts. These are also the only Hes and Hey family genes that activate in response to Notch in C2C12 cells (Castel *et al*., 2013). The RNAseq experiment did show up-regulation of other genes, but we did not focus on them either because they were not transcription factors (such as Jag1 or Nrarp), or were not direct NICD targets based on the ChIP-Seq data.

RT-qPCR

Used in Figure 1.3 and corresponding supplementary figure.

RNA was prepared using the RNeasy kit (QIAGEN). cDNA was prepared from 500ng RNA using the iScript cDNA synthesis kit (Bio-Rad). 0.5 ul cDNA was used per 10 ul RT-qPCR reaction mix containing 1X iqSYBR Green Supermix (Bio-Rad) and 450 nM total forward

and reverse primers. Reactions were performed on a BioRad CFX Real-Time PCR Detection System using a 2-step amplification protocol, with the following thermocycling parameters: 95 C, 3 min followed by 40 cycles of 95 C, 10s (melting) and 55 C, 30s (annealing + extension). All reactions were performed in duplicate. The following primers were used:

Hes1

Forward, 5'-CAACACGACACCGGACAAAC-3' (Figure 1.3C)

5'-AAGAATAAATGAAAGTCTAAGCCAA-3' (Figure 1.3D, Figure S1.3C, D)

Reverse, 5'-AAGAATAAATGAAAGTCTAAGCCAA-3' (Figure 1.3C)

5'-TTCTTGCCCTTCGCCTCTTC-3' (Figure 1.3D, Figure S1.3C, D)

Hey1

Forward, 5'-GCCGAAGTTGCCCGTTATCT-3'

Reverse, 5'-CGCTGGGATGCGTAGTTGTT-3'

HeyL

Forward, 5'-GAGCTGACTTCCCACAACCA-3'

Reverse, 5'-GAGAGGTGCCTTTGCGTAGA-3'

SdhA

Forward, 5'-AGTGGGCTGTCTTCCTTAAC-3'

Reverse, 5'-GGATTGCTTCTGTTTGCTTGG-3'.

Western blot analysis of NICD

Used in Figure S1.3

For this analysis, 0.5e6 - 1e6 cells were trypsinized after treatment, spun down in excess PBS, and lysed using Lithium Dodecyl Sulfate (LDS) buffer also containing reducing agents (DTT + 2-Mercaptoethanol) and Protease Inhibitors (Roche). Standard procedure was used for LDS-PAGE gel electrophoresis and transfer to nitrocellulose (iBlot, Thermo Fisher Scientific). Cleaved NICD (1:1000, Cell Signaling Technology, Catalog # D3B8) and GAPDH (1:5000, Abcam, Catalog #6C5) were detected using monoclonal antibodies. The blots were subsequently stained using HRP-conjugated secondary antibodies and detected using the Enhanced ChemiLuminescence system (Pierce).

CHO-C2C12 co-culture assay

Used in Figure S1.4.

In preparation for the co-culture, C2C12-hN1 cells (4-6x10^4 cells in 12 well multi-well plate wells) were transfected with 60 pmol siRNA directed against mouse Notch2 (5'-UGAACUUGCAGGAUGGGUGAAGGUC-3'), using Lipofectamine RNAiMAX (Life Technologies). 24h later, 3x10^4 CHO-K1 based Dll1- and Dll4- sender cells (pre-induced for >48h) were plated within the two chambers of ibidi culture inserts (Ibidi USA) on hamster fibronectin-treated (5 μg/ml in PBS, incubated for 3-5h at RT) surfaces of 24-well glass bottom plate wells. Once cells had attached to the surface (<6h), inserts were removed and previously prepared C2C12-hN1 cells were plated, in 5 μM DAPT media, at high density so as to cover the gaps on the surface. After 12h, DAPT was washed out and cells were allowed to signal for 6h, after which the cultures were fixed in 4% formaldehyde at room temperature for 10 mins.

in ovo Electroporation

Used in Figure 1.4 and corresponding supplementary figure.

Fertile chicken (*Gallus gallus*) eggs, purchased from commercial sources, were incubated at in a humidified 37 C incubator, and staged by the criteria of Hamburger and Hamilton (HH)(Hamburger and Hamilton, 2005). Batches of eggs were selected at random for electroporation with either Dll1 or Dll4, and the final data represents experiments conducted on at least two separate batches. The neural tubes of HH stage 12-13 embryos were injected with plasmid DNA (5 mg/ml) and electroporated by applying a series of current pulses (25V, 5x, 30 ms pulses separated by 100 ms) at the level of the pre-somitic mesoderm. 20h post-electroporation, embryos were screened for GFP fluorescence. Healthy embryos showing strong fluorescence in the neural crest were dissected (to remove extra-embryonic tissue) in Ringer's solution and transferred to freshly prepared 4% paraformaldehyde, on ice. Embryos were fixed overnight at 4 C.

Hybridization Chain Reaction Fluorescence In Situ Hybridization (HCR-FISH)

Used in Figure S1.4, Figure 1.4 and corresponding supplementary figure.

The HCR-FISH protocol was based on a previously described protocol(Choi et al., 2014). Briefly, *in situ* HCR-FISH detection involves the following steps: 1. Dehydration and rehydration of embryos in MeOH, 2. Overnight hybridization with probes at 45 C, 3. Removal of unbound excess probes through washes at 45 C, 4. Overnight amplification at room temperature, and 5. Removal of excess amplifier. Each gene of interest was detected

using 6 probes. At most three genes were detected simultaneously, typically EGFP, MyoD1, and Hes1, Hey1, or HeyL. After HCR processing, portions of the embryos anterior to the forelimbs were removed. Embryos were then mounted on glass-bottom multiwell plates in 1% agarose, with the dorsal surface in contact with the glass.

Confocal laser-scanning microscopy of embryos

Used in Figure 1.4 and corresponding supplementary figure.

Samples were imaged on a Zeiss LSM700 or using a 20x (0.8 NA) dry objective. For embryos, Z-stacks were acquired using Zen software (ZEISS) and 3D-reconstructed in Imaris 8.0 (Bitplane). Optical slices in Imaris were used to remove obscuring auto-fluorescence from residual extra-embryonic tissue in the reconstructed images, without affecting signal in the areas of interest. For cell-culture Z-stacks, the sum was projected in 2D using ImageJ.

Quantitation of effect on MyoD1 and Notch targets

Blind scoring of embryos for changes in MyoD1 (*Used in Figure S1.4B)*

3D images of transverse optical sections of the interlimb region of the trunk (containing 3-5 pairs of somites per image), were sorted randomly, and then scored blindly for differences in somite MyoD1 levels between the electroporated and control sides of the embryo. The scoring procedure was as follows: any features that might reveal the specific experimental perturbation (Dll1 or Dll4 ectopic expression), such as image filenames, differences in pseudo-color attributes, or information from secondary channels, were removed before the

files were re-ordered using a pseudorandom sequence. Subsequently, images were scored blindly, comparing MyoD1 signal in somites on the electroporated side with signal in the corresponding somites on the control side, as long as the two somites were level with each other. This requirement minimizes imaging artifacts. Finally, sample images were re-matched with the perturbation type and scores were tallied. The number of embryos scored per condition (11 Dll1 expressing embryos, 10 Dll4 expressing embryos, 61 somites for each perturbation) is standard for this type of quantification(Rios et al., 2011).

Quantification of fold-changes in MyoD1, Hes1, and Hey1 gene-expression (*Used in Figure S1.4C)*

The DML regions of the somites on the electroporated and control sides were manually identified in Z-projections of 3D-reconstructed confocal images (see above), and the maximal HCR-FISH staining intensities (90^{th} percentile values within identically-sized areas on both sides) were calculated. The reported fold-changes represent the ratio of these values for electroporated vs. control DMLs.

Immunofluorescence detection of transendocytosed Notch in co-cultures

Used in Figure 1.5 and corresponding supplementary figure

Sender cells and receiver cells were co-cultured on glass-bottom dishes, in the excess sender configuration, as described above. After 24h of co-culture, cells were fixed in 4% formaldehyde (diluted in PBS). All subsequent steps were carried out in blocking solution (2% Bovine Serum Albumin (Sigma-Aldrich) diluted in PBS). Following 1h of incubation at room temperature, samples were incubated overnight at 4 C with 1:250 mouse anti-

hNotch1 (Biolegend Catalog No. 352014, RRID AB_10899408). Samples were then washed and incubated in an anti-mouse secondary antibody conjugated to Alexa-Fluor 488 (Life Technologies). After room temperature washes, samples were permeabilized in 0.3% Triton X-100 (Sigma-Aldrich) for 1h. Samples were then again incubated in 1:250 anti-hNotch1 overnight at 4C, following which they were incubated in Alexa-Fluor 647 conjugated anti-mouse antibody (Life Technologies).

Confocal imaging and quantification of transendocytosed Notch

Used in Figure 1.5 and corresponding supplementary figure

Immunostained cultures (see above) were imaged as Z-stacks (0.8um intervals) on an LSM800 inverted confocal microscope using a 100x (1.3 NA, oil-immersion) objective. Sender cells abutting receiver cells (or distant from them, for background estimation) were manually segmented in ImageJ software, and stacks composed of 5 slices each were exported to MATLAB. In MATLAB, pixels within the stacks were categorized as being either intracellular, or belonging to the cell surface, based on the intensity of pre-permeabilization stain. Only cells that showed mean dispersed staining intensities higher than the median of the background staining levels were included in further analysis. This selected cells that were likely to be active senders (especially in the Dll1 case); we verified that none of the cells eliminated at this step displayed puncta. Next, in order to identify puncta, the *bwconncomp* function in the Image Processing Toolbox was used to assess 3-D connectivities of intracellular pixels possessing intensities above a fixed threshold and to group them into puncta of sizes >6 pixels. Several threshold/puncta size combinations were tested; one pair

of values that returned puncta numbers most consistent with visual estimation was chosen. Qualitative conclusions remained the same for a range of threshold/size values. Pixels with intensities below the threshold, or failing to be included in such puncta were deemed part of the ‘dispersed’ staining.

2.14 Supplementary Information

Estimating Gal4 and mRNA half-lives (Figure S1.1F)

For this model, we assume that the free Gal4 protein produced due to cleavage of N1ECD-Gal4 degrades with first-order kinetics with rate γ_{Gal4} after inhibition of the pathway using DAPT, at time 0h.

$$\frac{d\text{Gal4}}{dt} = -\gamma_{\text{Gal4}}\text{Gal4}$$

Reporter mRNA m is produced through non-cooperative binding of Gal4 to the promoter, with dissociation constant K and maximum rate β_m. m is degraded with rate constant γ_m.

$$\frac{dm}{dt} = \beta_m \frac{\text{Gal4}}{K + \text{Gal4}} - \gamma_m m$$

The parameters γ_{Gal4}, K and γ_m were calculated by fitting the Citrine mRNA m to the experimentally measured decay in Citrine fluorescence rate using the *lsqnonlin* function in MATLAB. The fit was constrained using bounds for γ_{Gal4} and γ_m of log(2)/5h – log(2)/3h, based on (Sprinzak et al., 2010) and (Bintu et al., 2016). Bootstrapped 95% confidence intervals were computed from 100 iterations of fitting 30 points, chosen randomly with replacement, out of a total 50 measured timepoints.

Mathematical model for estimating duration of Notch activation (Figure S1.1H)

For this model, we assume that Gal4 is produced at a rate β_{Gal4} for a duration τ_{act}, and degrades with first-order kinetics with rate γ_{Gal4}.

$$\frac{d\text{Gal4}}{dt} = \begin{cases} \beta_{\text{Gal4}} - \gamma_{\text{Gal4}}\text{Gal4}, & t \le \tau_{\text{act}} \\ -\gamma_{\text{Gal4}}\text{Gal4}, & t > \tau_{\text{act}} \end{cases}$$

Reporter mRNA m is produced through non-cooperative binding of Gal4 to the promoter, with dissociation constant K and maximum rate β_m. m is degraded with rate constant γ_m.

$$\frac{dm}{dt} = \beta_m \frac{\text{Gal4}}{K + \text{Gal4}} - \gamma_m m$$

For the results of Figure S1.1, $\beta_{Gal4} = 1$, $\beta_m = 1$, and K = 6.6 (also fitted in Figure S1.1E), and estimated mean values from Figure S1.1E were used for the Gal4 and mRNA degradation rates.

Simulations of Dll1 pulse trains and analysis (Figure S1.2A-F)

This model constructs pulse-trains composed of Dll1-like pulses occurring at various frequencies and regularities based on each of three underlying pulse models, and analyzes the features of the resulting simulated signaling traces.

Pulse train construction (Figure S1.2B): For each simulation we construct 200 pulse trains. Each pulse train is constructed from a series of pulses with the average Dll1 promoter activity pulse shape (Figure S1.1D), scaled by an amplitude randomly sampled from the empirically measured distribution of Dll1 pulse amplitudes (from the Figure 1D dataset). The first pulse occurs at 0h, representing activation at time 0 in the aligned Dll4 traces. Subsequently, new pulses are introduced after successive time intervals τ chosen based on one of the underlying pulse models (see below), and the composite signal is constructed until it extends at least 10h beyond the 25h time period averaged in Figure 1D.

Feature analysis (Figure S1.2D): For each trace, two features are analyzed:

Amplitude: The amplitude of each constructed trace is its median value over 25h.

Intra-trace variability: After calculation of the amplitude, each trace is normalized to its 90th percentile value. For each point *t* in this trace, the local temporal variability is estimated by the standard deviation of values in a 10h window starting at *t*. The overall intra-trace variability calculated for each trace is the median of the local variability value at each point, calculated by moving a 10h time window through the trace.

For each simulation (200 constructed traces), the medians of the calculated amplitudes and intra-trace variability are tabulated, and the S.E.M calculated.

Pulse models (Figure S1.2C): Three models are considered for the underlying pulsing process:

Periodic model: In this model, the interval τ between adjacent pulses is fixed at a value T_{period}, that can range from 1h to 8h. Since the Dll1 pulse decay becomes apparent after 7.5 h (Figure 1D), intervals greater than 8h will result in pulse trains in which the individual pulses can be clearly discerned in each trace, and the average behavior will show oscillations. Since neither individual Dll4 traces, nor the average shape display overt oscillatory features, values for T_{period} greater than 8h are not considered in the simulation.

Poisson model: In this model, the interval between successive pulses *i* and *i*+1, τ_i, represents the inverse of a pulse rate, r_i, drawn from a Poisson distribution with parameter, λ, ranging from 1/h-1/15h.

Mixed model: In these models, the interval τ between adjacent pulses is drawn from a normal distribution with mean T_{period} (range 1h - 15h) and standard deviation σ (2.5h or 5h). This model therefore combines the regular pulsing inherent to the periodic model with the trace-

to-trace variability of the Poisson model (thus preventing 'constructive interference' of pulse peaks, which would lead to apparent oscillations in the average signal shape).

For every parameter value (T_{period}, λ, or σ, as appropriate) in each of the models, 36 simulations were run and the average of the median amplitudes and median intra-trace variabilities (see above) were calculated. These values are plotted in Figure S1.2E.

Bootstrapped analysis of variability in measured Dll4 signaling trace (Figure S1.2F): Finally, for direct comparison to simulation data, the Dll4 dataset of traces (200 traces in total) was subsampled 30 times (50 traces per sample) to generate a bootstrapped distribution of measured median intra-trace variability, and a corresponding median value was calculated. This bootstrapped median is compared to simulation data in Figure S1.2F.

Mathematical model of Hes-Hey decoding (Figure S1.4A, B)

The model attempts to account for the time-evolution of four entities – Hes1 mRNA, Hes1 protein, Hey mRNA, and Hey protein - in response to a step change in NICD ($0 \rightarrow 1$) applied at $t = 0$. In the absence of any repression, the dynamics of these components are determined by simple production and first-order degradation terms, with a brief delay between mRNA transcription and corresponding protein production. We also assume that Hey transcription in response to NICD commences after a brief delay.

$$\frac{d\mathrm{Hes1}_{\mathrm{mRNA}}}{dt} = \alpha_{\mathrm{Hes1,\,m}} * \frac{\mathrm{NICD}}{K_{\mathrm{Hes1,\,m}} + \mathrm{NICD}} - \gamma_{\mathrm{Hes1,\,m}} * \mathrm{Hes1}_{\mathrm{mRNA}}$$

$$\frac{d\mathrm{Hes1}_{\mathrm{protein}}}{dt} = \alpha_{\mathrm{Hes1,p}} * \mathrm{Hes1}_{\mathrm{mRNA}}(t - \Delta\tau) - \gamma_{\mathrm{Hes1,p}} * \mathrm{Hes1}_{\mathrm{protein}}$$

$$\frac{d\mathrm{Hey}_{\mathrm{mRNA}}}{dt} = \alpha_{\mathrm{Hey,m}} * \frac{\mathrm{NICD}}{K_{\mathrm{Hey,m}} + \mathrm{NICD}} - \gamma_{\mathrm{Hey,m}} * \mathrm{Hey}_{\mathrm{mRNA}}$$

$$\frac{d\mathrm{Hey}_{\mathrm{protein}}}{dt} = \alpha_{\mathrm{Hey,p}} * \mathrm{Hey}_{\mathrm{mRNA}}(t - \Delta\tau) - \gamma_{\mathrm{Hey,p}} * \mathrm{Hey}_{\mathrm{protein}}$$

$$\{\alpha_{\mathrm{Hey,m}} = 0 | \mathrm{t} < \tau_{\mathrm{Hey}}\}$$

For simplicity, we assume that repression by Hes1 and Hey1 proteins is complete, i.e. they eliminate NICD-mediated transcription, once their level exceeds a threshold. That is to say,

$$\begin{Bmatrix} \alpha_{\mathrm{Hes1,m}} = 0 \\ \alpha_{\mathrm{Hey,m}} = 0 \end{Bmatrix} \Big| \mathrm{Hes1}_{\mathrm{protein}} > T_{\mathrm{Hes1}} \Big\}$$

$$\{\alpha_{\mathrm{Hes1,m}} = 0 | \mathrm{Hey}_{\mathrm{protein}} > T_{\mathrm{Hey}}\}$$

Starting from an initial state in which all entities are zero, the MATLAB (R2015a) DDE solver dde23 was used to simulate the evolution of the system over 4h. The following parameter values were utilized for the plots shown in Figure S1.4.

Variable Name	**Value**
$\alpha_{\mathrm{Hes1,\,m}}$	10
$K_{\mathrm{Hes1,\,m}}$	1
$\gamma_{\mathrm{Hes1,\,m}}$	2.3 h^{-1} (half-life = 20 min[10])
$\alpha_{\mathrm{Hes1,p}}$	3

$\Delta\tau$	0.25 h
$\gamma_{\mathrm{Hes1,p}}$	2.3 h^{-1}
$\alpha_{\mathrm{Hey,m}}$	5
$K_{\mathrm{Hey,m}}$	5
$\gamma_{\mathrm{Hey,m}}$	0.5 h^{-1}
$\alpha_{\mathrm{Hey,p}}$	1
$\gamma_{\mathrm{Hey,p}}$	0.5 h^{-1}
τ_{Hey}	0.5 h
T_{Hes1}	1
T_{Hey}	0.1

2.15 Supplementary Tables

Supplementary Table 1.1
Expression of Notch-relevant genes in CHO-K1 cells. Highlighted genes show FKPM > 5.

Gene	Expression Level (FKPM)
Notch1	1.6
Notch2	10.8
Notch3	2
Notch4	0.02
Dll1	0
Dll3	0.04
Dll4	0.02
Jag1	1.5
Jag2	0
ADAM10	26.9
ADAM17	22.9
PSEN1	29.1
Mib1	23.8
Epn1	14.2
Dtx2	7.1
Pofut1	39.8
Poglut1	26.3
RFng	47
Lfng	3
MFng	0

Supplementary Table 1.2.
Genes up-regulated > 5-fold at 1h after DAPT washout, compared to untreated control. Highlighted genes are putative direct NICD targets (Castel et al., 2013).

Gene	Untreated (FKPM)	1h no DAPT (FKPM)
'8430408G22Rik'	0.351884	5.69606
'Atf3'	0.374606	14.59
'Btg2'	4.17528	84.4997
'Csrnp1'	4.6935	24.1845
'Ctgf'	212.877	1188.84

'Dalrd3'	0	5.15402
'Dusp1'	22.7818	254.212
'Dusp2'	2.37563	22.9875
'Egr1'	18.126	680.799
'Egr2'	1.58322	58.7534
'Egr3'	1.8697	49.0469
'Errfi1'	26.4629	162.512
'Fos'	0.475391	18.5828
'Fosb'	0.415128	16.8939
'Has2'	12.6329	76.5841
'Hes1'	22.4634	253.506
'Ier2'	32.603	196.579
'Klf2'	4.1184	25.6258
'Med19'	0	11.3654
'Mxd3'	0	31.4573
'Nr4a1'	1.87277	185.989
'Nt5c3l'	0	34.9025
'Pisd-ps3'	0	10.5308
'Polr3h'	0	15.0563
'Prickle3'	0	7.29054
'Rad54l'	0	6.94284
'Rfc4'	0	20.9275
'Rgs16'	1.99682	30.3236
'Rpl26'	0	111.215
'Sgk1'	51.0718	290.122
'Sync'	0	20.309
'Txnrd2'	0	10.2652
'Zfp36'	13.9853	102.737

Supplementary Table 1.3.
Genes up-regulated > 5-fold at 6h after DAPT washout, compared to untreated control.
Highlighted genes are putative direct NICD targets(Castel et al., 2013).

Gene	Untreated (FKPM)	6h no DAPT (FKPM)
'Alkbh1'	0	7.25156
'Gpbar1'	0	6.54794
'Has2'	12.6329	65.3957
'Hey1'	1.87305	23.8542
'Heyl'	0.315531	15.4937

'Hr'	1.40471	7.85818
'Il11'	0.10324	5.54274
'Il6'	0.487057	10.0101
'Inhba'	66.2761	493.125
'Med19'	0	10.9802
'Nrarp'	0.362193	15.0544
'Ntn4'	1.53885	8.07718
'Pkp1'	5.60393	39.8372
'Polr3h'	0	17.3167
'Rfc4'	0	19.8498
'Rgs16'	1.99682	15.6184
'Rpl26'	0	165.91
'Sco2'	0	29.3184
'Ttc19'	0	10.2361
'Ubald2'	0	5.50867

Supplementary Table 1.4.
Plasmid constructs utilized in this study.

Vector	**Promoter**	**Insert**	**Selection cassette**
pcDNA3	CMV	hN1ECD-Gal4esn	Neomycin
pEV	UAS	H2B-3xCitrine	Hygromycin
pcDNA5	CMV-TO	rDll1-T2A-H2B-mCh	Hygromycin
pcDNA5	CMV-TO	hDll4-T2A-H2B-mCh	Hygromycin
pb	CMV-TO	Gal4esn-T2A-H2B-mCh	Hygromycin
pEV	UAS	H2B-3xCitrine-3' Hes1 UTR	Hygromycin
pcDNA5	CMV-TO	$Dll1_{ECD}$-$Dll4_{ICD}$	Hygromycin
pcDNA5	CMV-TO	$Dll4_{ECD}$-$Dll1_{ICD}$	Hygromycin
pcDNA5	CMV-TO	Dll1-FLAG	Hygromycin
pcDNA5	CMV-TO	$Dll4_{ECD}$-$Dll1_{ICD}$-FLAG	Hygromycin
pcDNA5	CMV-TO	Dll4-FLAG	Hygromycin
pb	CMV-TO	hN1ΔECD-T2A-H2B-mCh	Hygromycin
pb	CMV7	hN1-myc-T2A-H2B-mCh	Neomycin

pCI	CAGG	rDll1-T2A-EGFP	None
pCI	CAGG	hDll4-T2A-EGFP	None

Supplementary Table 1.5.
Engineered cell lines used in this study.

Genotype	**Background**	**Selection (in ug/ml)** **G = Geneticin,** **H = Hygromycin** **Z = Zeocin** **B = Blasticidin** For e.g., B10 = 10 ug/ml Blasticidin	**First referred to in**
pcDNA3-CMV-hN1ECD-Gal4esn + pEV-UAS-H2B-3xCitrine	CHO-K1 TREx	B10/G600/H500	Figure 1
pcDNA3-CMV-hN1ECD-Gal4esn + pEV-UAS-H2B-3xCitrine + pGK-H2B-mCherry	CHO-K1 TREx	B10/G600/H500/Z400	Figure 1.2 (Dll1 excess receiver)
pcDNA5-CMV-TO-rDll1-T2A-H2B-mCherry	CHO-K1 TREx	B10/H500	Figure 1.1,2, 5
pcDNA5-CMV-TO-rDll1-T2A-H2B-mCherry + pLenti-CAG-H2B-Cerulean	CHO-K1 + CMV-tetR	B10/H500	Figure 1.2 (Dll1 excess receiver)
pcDNA5-CMV-TO-hDll4-T2A-H2B-mCherry	CHO-K1 TREx	B10/H500	Figure 1.1,2, 5
pb-CMV-TO-hDll4-T2A-H2B-mCherry + pb-CMV-H2B-Cerulean	CHO-K1 TREx	B10/H500	Figure 1.2 (Dll4 excess receiver)
pb-CMV-TO-Gal4esn-T2A-H2B-mCh + UAS-H2B-Citrine	CHO-K1 TREx	B10/H500/Z400	Figure S1.1B

pEF-hN1ECD-Gal4esn + UAS-H2B-3xCitrine-3'Hes1UTR	CHO-K1 TREx	B10/G600/H300	Figure S1.1G-H
pcDNA5-CMV-TO-rDll1$_{ECD}$-Dll4$_{ICD}$-T2A-H2B-mCherry	CHO-K1 TREx	B10/H500	Figure 1.5, S5
pcDNA5-CMV-TO-hDll4$_{ECD}$-Dll1$_{ICD}$-T2A-H2B-mCherry	CHO-K1 TREx	B10/H500	Figure 1.5, S5
pcDNA5-CMV-TO-rDll1-FLAG	CHO-K1 TREx	B10/H500	Figure 1.5, S5
pcDNA5-CMV-TO-hDll4-FLAG	CHO-K1 TREx	B10/H500	Figure 1.5, S5
pcDNA5-CMV-TO- hDll4$_{ECD}$-Dll1$_{ICD}$ -FLAG	CHO-K1 TREx	B10/H500	Figure 1.5, S5
pb/CMV7-hN1-myc-T2A-H2B-mCherry	CHO-K1 TREx	B10/G600	Figure 1.5, S5
pb-CMV-TO-hN1ΔECD-T2A-H2B-mCherry	C2C12	G600	Figure 1.3
pb-CMV-hN1-T2A-H2B-mCherry	C2C12	G600	Figure S1.3

2.16 Supplementary References

Bintu, L., Yong, J., Antebi, Y.E., McCue, K., Kazuki, Y., Uno, N., Oshimura, M., and Elowitz, M.B. (2016). Dynamics of epigenetic regulation at the single-cell level. Science *351*, 720–724.

Castel, D., Mourikis, P., Bartels, S.J.J., Brinkman, A.B., Tajbakhsh, S., and Stunnenberg, H.G. (2013). Dynamic binding of RBPJ is determined by Notch signaling status. Genes Dev *27*, 1059–1071.

Choi, H.M.T., Beck, V.A., and Pierce, N.A. (2014). Next-Generation in Situ Hybridization Chain Reaction: Higher Gain, Lower Cost, Greater Durability. ACS Nano *8*, 4284–4294.

Gibson, D.G., Glass, J.I., Lartigue, C., Noskov, V.N., Chuang, R.-Y., Algire, M.A., Benders,

G.A., Montague, M.G., Ma, L., Moodie, M.M., et al. (2010). Creation of a bacterial cell controlled by a chemically synthesized genome. Science *329*, 52–56.

Hamburger, V., and Hamilton, H.L. (2005). A series of normal stages in the development of the ... [Dev Dyn. 1992] - PubMed - NCBI. Dev Dyn *195*, 231–272.

KOPAN, R., SCHROETER, E.H., Weintraub, H., and Nye, J.S. (1996). Signal transduction by activated mNotch: importance of proteolytic processing and its regulation by the extracellular domain. *93*, 1683–1688.

Lebon, L., Lee, T.V., Sprinzak, D., Jafar-Nejad, H., Elowitz, M.B., and McNeill, H. (2014). Fringe proteins modulate Notch-ligand cis and trans interactions to specify signaling states. eLife Sciences *3*, e02950.

Rios, A.C., Serralbo, O., Salgado, D., and Marcelle, C. (2011). Neural crest regulates myogenesis through the transient activation of NOTCH. Nature *473*, 532–535.

Sprinzak, D., Lakhanpal, A., Lebon, L., Santat, L.A., Fontes, M.E., Anderson, G.A., Garcia-Ojalvo, J., and Elowitz, M.B. (2010). Cis-interactions between Notch and Delta generate mutually exclusive signalling states. Nature *465*, 86–90.

Chapter 3. Prevalent and functional *cis*-activation in the Notch pathway

Abstract

The Notch pathway consists of transmembrane ligands and receptors that are often co-expressed and can interact with each other both within the same cell (*cis*) and across cell boundaries (*trans*). *trans* activation of receptors by ligands has been studied extensively, but the possibility of *cis* activation has not been systematically investigated. Using an engineered cell-culture system in which the degree of intercellular contact - and thus *trans* signaling - could be controlled, we show that cells can *cis*-activate through the Notch pathway. The levels of *cis*-activation are comparable to that of *trans*-activation for a wide range of ligand expression, and this mode of cell-autonomous signaling shares several attributes of intercellular signaling, including inhibition at high ligand expression, sensitivity to receptor glycosylation, and requirement for ligand endocytosis. *Cis*-activation could be observed for all combinations of the receptors Notch1 and Notch2 and the ligands Dll1 and Dll4. Finally, we show that *cis*-activation occurs in self-renewing neural stem cells, where it could play a functional role in regulating cell survival and differentiation. Together, these results demonstrate the prevalence of *cis*-activation in the pathway, and its potential use in key Notch-dependent developmental and physiological processes.

3.1 Introduction

The Notch signaling pathway enables intercellular communication in animals and is widely used during development and homeostasis. Signaling occurs between cells that are in physical contact with each other, when ligands on one cell activate receptors on neighboring cells. However, there are several contexts in which ligands and receptors are co-expressed in the same cells, for example in the pre-somitic mesoderm and during neurogenesis. An interesting feature of the Notch pathway is that co-expressed ligands and receptors can directly interact with each other. Previous work has shown that this interaction can be mutually inhibitory, suppressing the ability of cis-interacting ligands and receptors to send signals to and receive them from other cells (Sprinzak et al. 2010; del Álamo and Schweisguth 2009; Fiuza et al. 2010).

Cis-activation, the ability of ligands to activate receptors within the same cell, has also been postulated (Formosa-Jordan and Ibañes 2014; Coumailleau et al. 2009; Pelullo et al. 2014), but this mode of signaling has not been investigated systematically in the pathway. Specifically, it remains unclear under what circumstances such signaling might occur, how it compares to trans-signaling in strength and other features, and how it relates to cis-inhibition. In this study, we investigated these questions by using a reconstituted cell-culture system in which cell-cell contacts and ligand/receptor levels and identity could be controlled. We find that cis-activation occurs readily in the Notch pathway, for multiple combinations of ligands and receptors. It is modulated by many of the same elements that determine trans-signaling levels, such as ligand-receptor affinity and relative levels of ligands and receptors. In stem-cell contexts where Notch signaling is often necessary for

cell survival, proliferation, and preventing differentiation, cis-activation could ensure maintenance of the stem-cell state, as we show here using neural stem cells.

Results:

3.2 Notch1-Dll1 cells show ligand-dependent cis-activation

Using CHO-K1 cells, we engineered cell lines that co-express the ligand Dll1 and a chimeric Notch1ECD-Gal4 receptor, along with the Gal4-activated H2B-Citrine reporter gene (Figure 2.1A). In these 'N1D1' cells, receptors are expressed constitutively, while ligand expression is under control of a promoter that could be induced using the small molecule 4-epitetracycline ('4epi'). Dll1 induction levels could be measured using a co-translational H2B-mCherry fluorescent protein. These cells also constitutively express a nuclear-localized H2B-Cerulean protein. A similar cell line design has previously been used to measure the strength of *cis*-inhibition between ligand and receptor (LeBon et al., 2014; Sprinzak et al., 2010).

We first sought to measure the ability of N1D1 cells to activate themselves (*cis*-activation) and to compare this mode of signaling to levels of *trans*-activation between cells. When a few N1D1 cells are co-cultured with an excess of control CHO cells that do not express ligands, each N1D1 cell is isolated from others. Under these conditions, any activation of the Citrine reporter observed in isolated N1D1 cells, before cell division, must reflect *cis*-activation. On the other hand, activation observed during the same period in N1D1 cultured by themselves, at high density so they can contact each other, should reflect a combination of *cis*- and *trans*-activation.

Figure 2.1

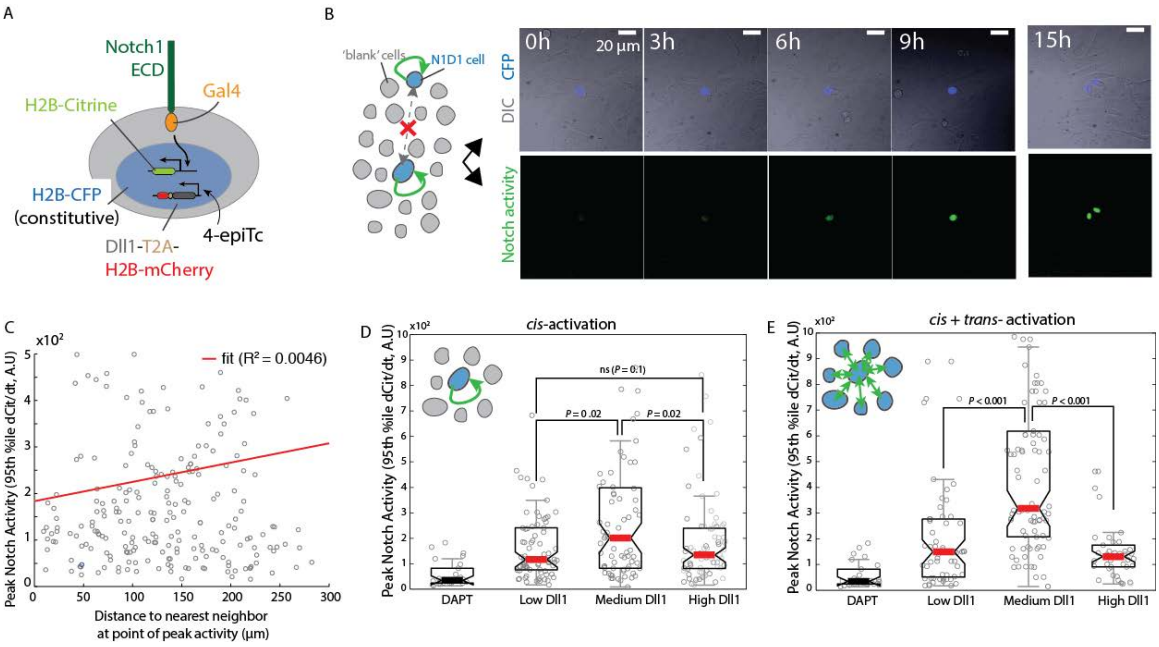

N1D1 cells show ligand-dependent *cis*-activation. A. Schematic of N1D1 cell line. CHO-K1 cells were engineered to express a chimeric receptor combining the Notch1 extracellular domain ('Notch1ECD') with a Gal4 transcription factor (orange) in place of the endogenous intracellular domain. When activated, Gal4 is released and activates a stably integrated fluorescent H2B-3xCitrine reporter gene (chartreuse). Cells additionally contain a stably integrated construct expressing Dll1 (grey) with a co-translational (T2A, brown) H2B-mCh readout (purple), from a 4epiTc-inducible promoter. Engineered cells also constitutively express a H2B-CFP protein, which localizes to the nucleus (blue). **B**, (*Left*) Schematic of cis-activation assay. A small minority (1%) of N1D1 cells (blue nuclei) are co-cultured with an excess of parental CHO-K1 cells (grey nuclei) that do not express ligand and therefore cannot signal to N1D1 cells. Activation in isolated cells under these conditions indicates *cis*-activation. (*Right*) Filmstrip showing the activation of a representative isolated N1D1 cell in this assay. **C,** Scatter plot of peak Notch activation rate in isolated N1D1 cells (y-axis) vs. distance of each to its closest neighboring cell (x-axis) at the point of maximum activity. **D,** Boxplots showing distribution of peak Notch activation rate in N1D1 cells prior to the first cell division, for three different mean Dll1 induction levels, in the *cis*-activation assay shown in panel B. **E**, Boxplots showing distribution of peak Notch activation rate in N1D1 cells prior to the first cell division, for three different mean Dll1 induction levels, in cultures that contain only N1D1 cells cultured at high density.

We used timelapse microscopy to assay the activation of N1D1 cells under these two conditions (see Methods). In cultures in which N1D1 cells constituted ~1% of cells, isolated N1D1 cells showed clear activation (Figure 2.1B). The strength of *cis*-activation, estimated by the peak Citrine production rate prior to the first cell division, showed no correlation with distance to the nearest neighbor, suggesting a cell-autonomous process (Figure 2.1C). Activation was ligand dependent and, interestingly, showed a non-monotonic trend with increasing levels of Dll1 induction (Figure 2.1D). Specifically, activation peaked at an intermediate level of Dll1 induction but decreased with further increases in Dll1 levels, suggesting *cis*-inhibition of receptor in this limit.

The same non-monotonic trend could be observed in N1D1 cells cultured by themselves (but at similar total density as in the *cis*-activation assay), where activation presumably reflected a combination of *cis*- and *trans*- signaling (Figure 2.1E). This trend, again, is consistent with a dominant role for *cis*-inhibition at high ligand levels. While it was not possible to directly measure the *trans* component of signaling, the level of activation observed under this condition (*cis* + *trans)* was < 2-fold increased relative to the *cis* component of activation, for all ligand induction levels, indicating that *cis*-activation strength is comparable to that of *trans*-activation.

To generalize these observations, we next used a flow-cytometry based assay that has increased throughput (see Methods). We measured total reporter Citrine levels for a range of Dll1 induction levels and varying degrees of intercellular N1D1 contact, achieved by

changing the fraction of N1D1 cells relative to parental CHO-K1 cells in the culture (while maintaining total cell density). Cells were cultured for 24h prior to measurement, during which cell division is limited. In these experiments, total activation levels showed the same non-monotonic dependence on ligand levels for all N1D1 fractions (Figure S2.1A). Interestingly, the relative contributions of *cis*- and *trans*- signaling to total observed activation also changed with ligand levels. *cis*-activation dominates at low and high levels of Dll1, while *trans*-activation makes its biggest contribution to total signaling at intermediate Dll1 induction levels (Figure S2.1B). It is also worth noting that both *cis*- and *trans*- signaling appeared to peak at the same ligand concentration.

To verify that this behavior was not specific to the chimeric Notch1ECD-Gal4 receptor, we measured activation in cells expressing Dll1 along with the full length Notch receptor and a 12xCSL-H2B-Citrine reporter (Sprinzak et al., 2010) that can activated by cleaved NICD through multimerized binding sites for the CSL complex in the promoter region (Figure S2.1C). These cells also showed *cis*-activation, comparable in strength to *trans*-activation, and the same non-monotonic dependence on ligand levels as described above for the N1ECD-Gal4 cells.

These results together show that cells co-expressing Notch and the ligand Dll1 are able to activate themselves in a ligand-dependent manner. This mode of activation is comparable in magnitude to *trans*-activation between cells. Moreover, like *trans*-activation it is subject to inhibition at high levels of ligand, and is strongest at intermediate ligand levels.

3.3 cis-activation increases with R-Fringe and Dll4

We next asked how factors that modify the interaction affinity between ligand and receptor affect *cis*-activation and inhibition. We first expressed Radical Fringe (R-Fringe), which enhances Notch1-Dll1 interaction through receptor glycosylation, in N1D1 cells (LeBon et al., 2014). R-Fringe increased cis-activation at intermediate levels of Dll1 expression, but also potentiated the inhibitory effect of ligand at higher expression levels (Figure 2.2A, B). This thus had the overall effect of accentuating the non-monotonic relationship between activation and ligand induction.

Figure 2.2

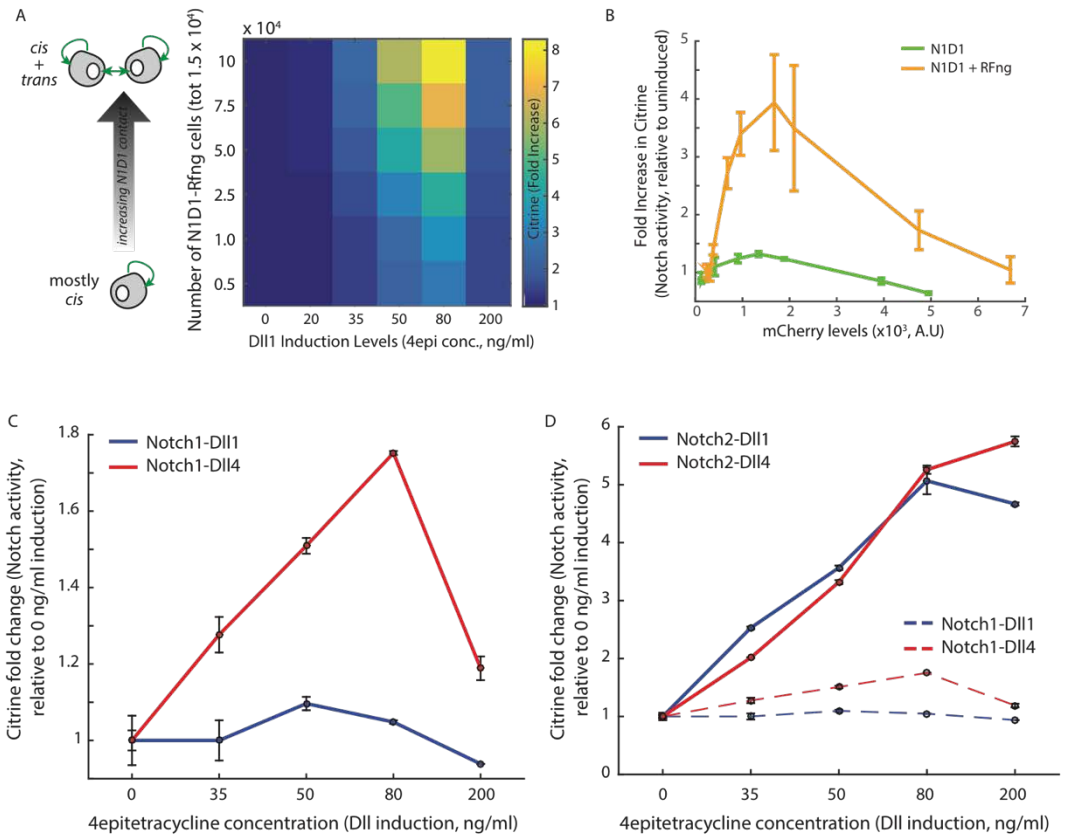

R-fringe, Dll4, and Notch2 enhance cis-activation. A, (*Right*) Heatmap matrix of mean Citrine levels in N1D1-Rfng cells co-cultured with control CHO-K1 cells at different ratios (rows of matrix) and induced with different levels of 4epi-Tetracycline (columns of matrix). (*Left, schematic*) Activation levels in the lowest row of the matrix (5k N1D1-Rfng cells + 150k CHO-K1 cells) represent *cis*-activating cells, since most N1D1 cells are isolated under these conditions. *Trans*-activation increases as the fraction of N1D1 cells in the culture increases, and activation levels at the highest row represent a combination of *cis*- activation and maximal *trans*-activation. **B**, Comparison of *cis*-activation in N1D1 and N1D1-Rfng cells. Error bars represent s.e.m (n = 3 replicate experiments). **C,** Comparison of *cis*-activation in Notch1 cells co-expressing Dll1 or Dll4. Error bars represent s.e.m (n = 3 replicate experiments). **D**, Comparison of cis-activation in Notch2 cells co-expressing Dll1 or Dll4. Error bars represent s.e.m (n = 3 replicate experiments).

Another factor that controls ligand-receptor interaction affinity is the identity of the ligand. Compared to Dll1, the ligand Dll4 has increased affinity for Notch1 (Andrawes et al., 2013). To measure the effect of Dll4 on cis-activation, we engineered CHO cells containing the Gal4-responsive reporter to stably express an inducible Dll4-T2A-H2B-mCherry gene and constitutive Notch1ECD-Gal4 (as in Figure 2.1A). To facilitate direct, quantitative, and general comparisons between two ligands, we compared the behavior of a multiclonal population of this cell line ('N1D4pop') with a corresponding N1D1 multiclonal line ('N1D1pop').

Compared to N1D1pop cells, N1D4pop cells showed enhanced *cis*-activation and inhibition (Figure 2.2C), showing higher maximal reporter activity at intermediate expression but comparable activity at the highest ligand expression levels. Like R-fringe, this again had the effect of accentuating the non-monotonic trend of activation as ligand expression changes. These results together show that *cis*-activation is not specific to Dll1, but occurs with Dll4 as well. Furthermore, they suggest that stronger ligand-receptor

interactions enhance inhibition at high ligand expression levels as shown previously (LeBon et al., 2014), but not without also increasing the tendency for *cis*-activation at lower ligand expression levels.

3.4 Notch2 shows strong cis-activation but decreased cis-inhibition compared to Notch1

Is *cis*-activation specific to Notch1? To check, we engineered cells to express a chimeric version of the paralogous receptor Notch2 (Notch2ECD-Gal4) in reporter cells, along with Dll1- or Dll4-T2A-H2B-mCherry as described above.

Both N2D1 and N2D4 cells showed a striking increase in *cis*-activation compared to their Notch1 counterparts, with 3-5 fold higher maximal activation across the same ligand expression levels (Figure 2.2D). Additionally, the non-monotonic trend in Notch activity with increasing ligand levels disappeared, suggesting that *cis*-inhibition no longer dominates at high ligand levels. Finally, unlike in the case of Notch1, Dll1 and Dll4 showed similar levels of activation with Notch2.

Therefore, Notch2 is also susceptible to cis-activation like Notch1. However, the relative activating and inhibitory effects of the Dll ligands are different for the two receptors. Specifically, Notch1 is strongly inhibited at high ligand expression levels, while Notch2 continues to be activated by *cis*-ligands at the same expression levels.

3.5 cis-activation occurs in neural stem cells

To test whether *cis*-activation occurs in a natural context, we used mouse neural stem cells (NSCs, see Methods), which self-renew and proliferate in the presence of the growth factors EGF and FGF, but can be induced to differentiate by withdrawal of growth factors (Bond *et al*., 2015; Homem *et al*., 2015). These cells express the receptors Notch1 and Notch2, and the ligand Dll1, and Notch signaling is known to play an important role in controlling NSC proliferation, self-renewal, and differentiation.

Figure 2.3

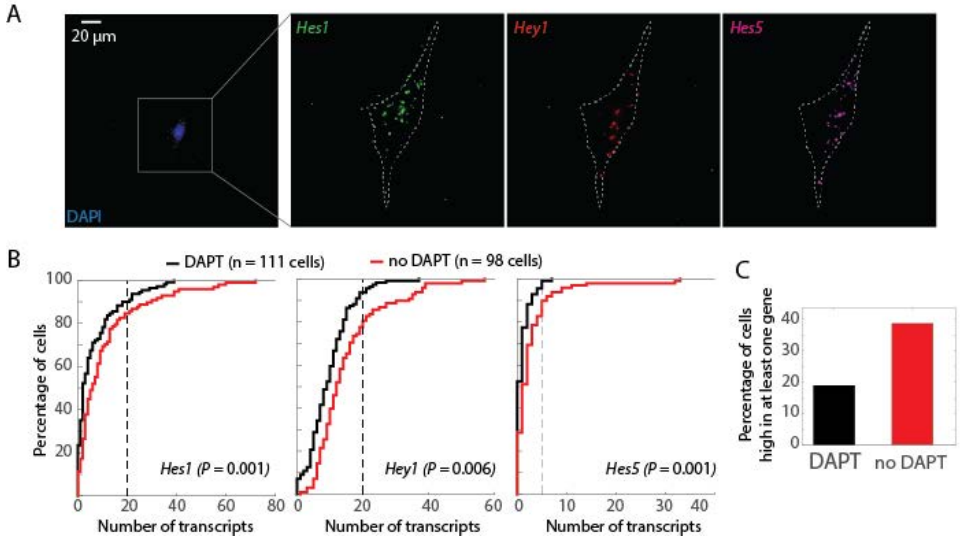

Isolated NSCs show Notch-dependent gene expression. A, Representative single-molecule HCR-FISH images showing expression of Hes1 (green), Hey1 (red), Hes5 (magenta) transcripts in an isolated cell. Cells are also stained with DAPI (blue). **B,** CDF plots showing expression of Hes1, Hey1, and Hes1 in the presence (black lines) or absence (red lines) of 10 µM DAPT. Dashed vertical lines indicate thresholds used for panel C. **C**, Percentage of cells expressing above threshold (see panel B) levels of at least one of the three genes.

We plated NSCs at low density (1000 cells/2.5 cm^2), such that cells were typically isolated (Figure 2.3A). Cells were plated either in the presence or absence of the inhibitor DAPT for a limited period of 12h, during which most isolated cells remain undivided. At the end

of this period, we performed single-molecule HCR-FISH (Choi et al., 2010, 2016) to detect mRNA transcripts of the Notch targets *Hes1*, *Hes5*, and *Hey1* in single cells (Figure 2.3A). Quantification of transcripts showed that although expression was generally heterogeneous, the levels of all three genes decreased significantly on treatment with DAPT (Figure 2.3B). Moreover, the fraction of cells showing higher expression of at least one of the genes decreased ~2-fold (Figure 2.3C). Together, these results show that neural stem cells show Notch-dependent gene expression even in isolation, suggesting that they perform cell-autonomous activation.

3.6 Discussion

The intercellular signaling capability of the Notch pathway is well appreciated and has been under study for several years. Here, we show that this pathway possesses an additional capability, *cis*-activation, which enables cell-autonomous signaling. The levels of *cis* signaling depend on the relative levels of ligands and receptors; this mode of signaling thus provides the cell with information regarding its own signaling components. Different ligand-receptor combinations show different degrees of cis-activation, which can further be modulated by R-Fringe. Together, this enables cells to tune the relative contributions of *cis* and *trans* signaling, and the choice of Notch component co-expression in any given context may be dictated by their *cis* signaling properties. In situations where Notch signaling is linked to cell survival and inhibition of differentiation, such as in many adult stem cells (Koch *et al.*, 2013), the ability to activate in a cell-autonomous manner might be crucial to the maintenance of a stable multipotent stem cell population. In this role, *cis*-activation may complement the niche and, especially in tissues where a clear niche is yet to be identified,

potentially compensate for one. Finally, *cis*-activation may play an important role in Notch-based patterning, for example in lateral inhibition, by providing cells with information regarding their own component levels. Combined with information about components in neighboring cells, received through *trans* activation, this could enable cells to make more informed fate choices using the Notch pathway. Generally, we expect that *cis*-activation operates in a wide variety of developmental and physiological contexts where, along with *trans*-activation, it helps define and determine the effects of Notch signaling.

3.7 Supplementary Figures

Figure S2.1

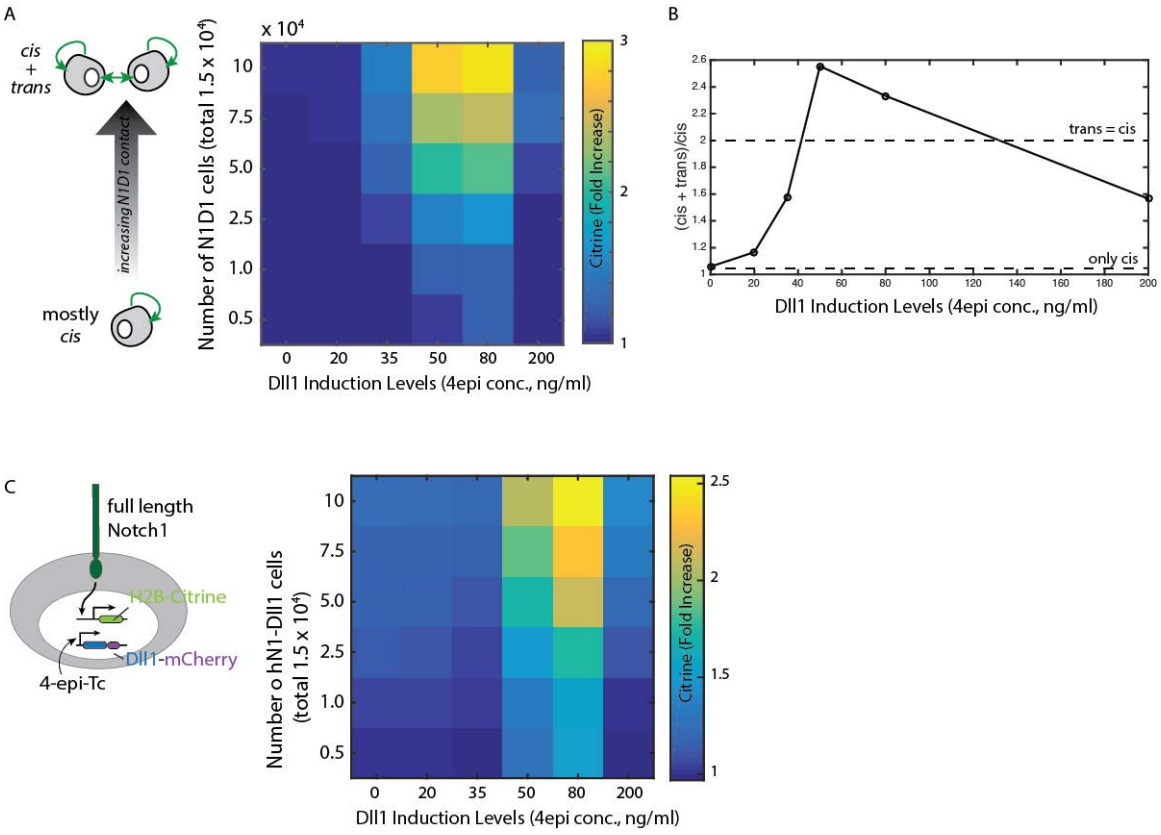

Further characterization of *cis*- and *trans*-activation in N1D1 cells. A, (*Right*) Heatmap matrix of mean Citrine levels in N1D1 cells co-cultured with control CHO-K1 cells at different ratios (rows of matrix) and induced with different levels of 4epi-Tetracycline (columns of matrix). (*Left, schematic*) Activation levels in the lowest row of the matrix (5k N1D1 cells + 150k CHO-K1 cells) represent *cis*-activating cells, since most N1D1 cells are isolated under these conditions. *Trans*-activation increases as the fraction of N1D1 cells in the culture increases, and activation levels at the highest row represent a combination of *cis*- activation and maximal *trans*-activation. **B**, Ratio of activation levels in *cis*+*trans* to *cis* conditions, at different levels of Dll1 induction. **C**, (*Left, schematic*) Schematic of flNotch1-Dll1 cell line. CHO-K1 cells were engineered to express the full-length Notch1 receptor. When activated, NICD is released and activates a stably integrated fluorescent 12xCSL-H2B-Citrine reporter gene (chartreuse). Cells also contain a stably integrated construct expressing Dll1 (blue) fused to mCherry, from a 4epiTc-inducible promoter. *(Right*) Heatmap matrix of mean Citrine levels in N1D1 cells co-cultured with control CHO-K1 cells at different ratios (rows of matrix) and induced with different levels of 4epi-Tetracycline (columns of matrix).

3.9 Methods

Cell culture

CHO-K1 cells and their derivatives were grown and maintained as described previously (section 2.13). Neural stem cells, derived from E14.5 mouse cortex, were purchased (EMD Millipore, Catalog No. SCR029) and cultured on tissue-culture grade plastic pre-coated with 10 μg/ml poly-L-ornithine (Sigma Catalog No. P3655) and 5 μg/ml Laminin (Sigma Catalog No. L-2020), in Neurobasal medium (EMD Millipore, Catalog No. SCM003) supplemented with 20 ng/ml EGF (EMD Millipore, Catalog No. GF003), 20 ng/ml FGF (EMD Millipore, Catalog No. GF001), and 5 μg/ml Heparin (Sigma Catalog H3149). Cells were passaged every 2-3 days using ESGRO Complete Accutase (EMD Millipore, Catalog No. SF006). Cells were typically used for experiments within six passages.

Flow cytometry assays

Cells of interest were typically induced with 4epi-Tetracycline, in the presence of 10 μM DAPT, for 48 h prior to the experiment. After induction, cells were co-cultured with parental CHO-K1 cells at defined ratios in the absence of DAPT. Cells were plated a high total surface density ($1.5x10^5/2.5$ cm^2) on plastic tissue-culture treated surfaces. 24h after plating, cells were analyzed on a MACSquant Flow Analyzer capable of measuring fluorescence in three channels, CFP, YFP, and RFP. The data was analyzed using custom MATLAB software.

Timelapse imaging

Cells were imaged and the data analyzed as described above (section 2.13). For the experiment, cells of interest (COI) were typically induced with 4epi-Tetracycline, in the

presence of 10 μM DAPT, for 48 h prior to the experiment. 1000 cells were co-cultured with $1.5x10^5$ CHO-K1 parental cells, or $1.5x10^5$ COI were plated by themselves, on fibronectin-coated glass surfaces (see section 2.13).

Neural stem cell *cis*-activation experiment and *in situ* HCR-FISH

Cells were plated on glass-surfaces pre-coated with 10 μg/ml poly-L-ornithine and 50 μg/ml Laminin and cultured in Neurobasal medium containing 0.5 ng/ml EGF and 5 μg/ml Heparin, with or without 10 μM DAPT. 12-15 after plating, cells were fixed in 4% Formaldehyde (diluted in PBS). Fixed cells were permeabilized with 70% ethanol, and washed once with solution containing 20% formamide, after which recommended HCR-FISH protocol was followed (Molecular Instruments). Bound probes were amplified for 45-60 min prior to final washes and imaging.

Quantification of *in situ* HCR-FISH gene expression

Cells were imaged using a 60X oil objective lens (NA 1.3) in a Nikon epi-fluorescence microscope equipped with continuous hardware auto-focus. 15 Z-slices 1 μm apart were acquired per field of view. These slices were centered around the optical plane in which cell nuclei (indicated by DAPI staining) were in optimal focus. In these images, cells were then automatically segmented, and local fluorescence maxima (‘dots’, corresponding to hybridized mRNA transcripts) possessing intensities above manually determined thresholds were detected within cell segments. The same threshold values were used for segmentation and dot detection in samples that were directly compared.

3.8 References

del Álamo, D., and Schweisguth, F. (2009). Notch Signalling: Receptor cis-Inhibition To Achieve Directionality. Curr. Biol. *19*, R683–R684.

Andrawes, M.B., Xu, X., Liu, H., Ficarro, S.B., Marto, J.A., Aster, J.C., and Blacklow, S.C. (2013). Intrinsic selectivity of Notch 1 for Delta-like 4 over Delta-like 1. J. Biol. Chem. *288*, 25477–25489.

Bond, A.M., Ming, G.-L., and Song, H. (2015). Adult Mammalian Neural Stem Cells and Neurogenesis: Five Decades Later. Cell Stem Cell *17*, 385–395.

Fiuza, U.-M., Klein, T., Martinez Arias, A., and Hayward, P. (2010). Mechanisms of ligand-mediated inhibition in Notch signaling activity in Drosophila. Dev. Dyn. *239*, 798–805.

Homem, C.C.F., Repic, M., and Knoblich, J.A. (2015). Proliferation control in neural stem and progenitor cells. Nat. Rev. Neurosci. *16*, 647–659.

Koch, U., Lehal, R., and Radtke, F. (2013). Stem cells living with a Notch. Development *140*, 689–704.

LeBon, L., Lee, T.V., Sprinzak, D., Jafar-Nejad, H., and Elowitz, M.B. (2014). Fringe proteins modulate Notch-ligand cis and trans interactions to specify signaling states. Elife *3*, e02950.

Sprinzak, D., Lakhanpal, A., Lebon, L., Santat, L.A., Fontes, M.E., Anderson, G.A., Garcia-Ojalvo, J., and Elowitz, M.B. (2010). Cis-interactions between Notch and Delta generate mutually exclusive signalling states. Nature *465*, 86–90.